Coherent Receiver Design and Analysis for Interleaved Division Multiple Access (IDMA)

Bathiya Senanayake
B.E (Hons I) and I.T
February 2012

A thesis submitted for the degree of Doctor of Philosophy
of the Australian National University

Australian
National
University

Department of Information Engineering
Research School of Information Sciences and Engineering
The Australian National University

Declaration

The work in this thesis is to the best of the candidate's knowledge and belief, his own work, original, except as acknowledged in the text, and the material has not been submitted, either whole or in part, for a degree at this or any other university.

Bathiya Senanayake

Acknowledgements

I would like to express my gratitude to everyone who has contributed to the production of this thesis. This thesis and the work it embodies was only possible through the continual help and support of a number of people. This research was funded through an Australian Postgraduate Award (APA) and through National ICT Australia. Without this financial supports this work wouldn't have happened.

I would like to thank my supervisor Dr. Mark C. Reed firstly for giving me the opportunity to undertake a Ph.D. and for his guidance throughout my studies. Thanks also go to Zhenning Shi, who has provided valuable advice when needed.

Finally, I would like to thank my family for their enduring love and support.

Abstract

This thesis discusses a new multiuser detection technique for cellular wireless communications. Multiuser communications is critical in cellular systems as multiple terminals (users) transmit to base stations (or wireless infrastructure). Efficient receiver methods are needed to maximise the performance of these links and maximise overall throughput and coverage while minimising inter-cell interference.

Recently a new technique, Interleave-Division Multiple Access (IDMA), was developed as a variant of direct-sequence code division multiple access (DS-CDMA). In this new scheme users are separated by user specific interleavers, and each user is allocated a low rate code. As a result, the bandwidth expansion is devoted to the low rate code and not weaker spreading codes. IDMA has shown to have significant performance gains over traditional DS-CDMA with a modest increase in complexity. The literature on IDMA primarily focuses on the design of low rate forward error correcting (FEC) codes, as well as channel estimation. However, the practical aspects of an IDMA receiver such as timing acquisition, tracking, block asynchronous detection, and cellular analysis are rarely studied in detail.

The objective of this thesis is to design and analyse practical synchronisation, detection and power optimisation techniques for IDMA systems. It also, for the first time, provides a novel analysis and design of a multi-cell system employing a general multiuser receiver. These tools can be used to optimise and evaluate the performance of an IDMA communication system. The techniques presented in this work can be easily employed for DS-CDMA or other multiuser receiver designs with slight modification.

Acquisition and synchronisation are essential processes that a base-station is required to perform before user's data can be detected and decoded. For high capacity IDMA systems, which can be heavily loaded and operate close to the channel capacity, the performance of acquisition and tracking can be severely

affected by multiple access interference as well as severe drift. This thesis develops acquisition and synchronisation algorithms which can cope with heavy multiple access interference as well as high levels of drift. Once the timing points have been estimated for an IDMA receiver the detection and decoding process can proceed.

An important issue with uplink systems is the alignment of frame boundaries for efficient detection. This thesis demonstrates how a fully asynchronous system can be modelled for detection. This thesis presents a model for the frame asynchronous IDMA system, and then develops a maximum likelihood receiver for the proposed system.

This thesis develops tools to analyse and optimise IDMA receivers. The tools developed are general enough to be applied to other multiuser receiver techniques. The conventional EXIT chart analysis of unequal power allocated multiuser systems use an averaged EXIT chart analysis for all users to reduce the complexity of the task. This thesis presents a multidimensional analysis for power allocated IDMA, and shows how it can be utilised in power profile optimisation. Finally, this work develops a novel power zoning technique for multicell multiuser receivers using the optimised power levels, and illustrates a particular example where there is a 50% capacity improvement using the proposed scheme.

Acronyms

Acronym	Description
3GPP	3rd generation partnership project
APP	A posteriori probability
AWGN	Additive white Gaussian noise
BCJR	Bahl, Cocke, Jelenick and Raviv
BEC	Binary erasure channel
BER	Bit error rate
BPSK	Binary phase shift keying
CC	Convolutional code
CDMA	Code division multiple access
CLL	Code locked loop
DLL	Delay locked loop
DS	Direct sequence
EL	Early-late
ESE	Elementary signal estimator
EXIT	Extrinsic information transfer
FEC	Forward error correcting
GEXIT	Generalized EXIT

IC	Interference canceller
IDMA	Interleave division multiple access
IMUD	Iterative multiuser detection
ISI	Intersymbol interference
LLR	Log likelihood ratio
MAC	Multiple access channel
MAI	Multiple access interference
MAP	Maximum *a posteriori*
MCRB	Modified Cramer-Rao bound
MI	Mutual information
MLSE	Maximum likelihood sequence estimator
MM	Mueller and Mueller
MMSE	Minimum mean square error
MRC	Maximal ratio combining
MSE	Mean square error
MUD	Multiuser detection
PDF	probability distribution function
PN	Pseudo noise
RSC	Recursive Systematic convolutional
RV	Random variable
SCM	Superposition Coded Modulation
SHO	Soft handover
SINR	Signal to interference-plus-noise ratio
SIR	Signal to interference ratio

SISO	Soft input soft output
SNR	Signal-to-noise ratio
SU	Single user
TED	Timing error discriminator
TD	Turbo decoder
UMTS	Universal Mobile Telecommunications System
VT	Variance Transfer

Notation

$\|a\|$	Euclidean Norm of variable X
$\hat{a}$	Estimate of random variable a
$\tilde{a}$	Soft information of random variable a.
$a(\cdot)$	Continuous function a
$a[\cdot]$	Discrete time function a
A	A *priori* log likelihood ratio
α	Pulse shaping filter roll-off factor
c_k	The coded bits for user k
$\mathbf{c}_k$	The block of coded bits for user k
C	Capacity
d_k	The data bits for user k
E	A *posteriori* log likelihood ratio
$\mathrm{E}\{X\}$	Expectation of random variable X
E_b	Energy per bit
E_s	Energy per symbol
E_d	Energy for a data bit
E_p	Energy for a pilot bit
$g(t)$	Square root raised cosine pulse shaping function
h_k	Channel coefficient for user k

$h_{k,l}$	Channel coefficient of the lth path for user k
i	Imaginary unit ($\sqrt{-1}$)
$J(\cdot)$	The J function
$J_s(\cdot)$	The J_s function
k	User identifier
K	Total number of users/ user groups
K_k	The number of users in user group k
$\mathbf{K}$	The set of user groups
K_T	Total number of users
$\Lambda_{A,k}^C$	*A priori* log-likelihood ratio of component C for user k
$\Lambda_{E,k}^C$	Extrinsic log-likelihood ratio of component C for user k
M	Over sampling rate
ν	Constraint length of a convolutional code
$\mathcal{N}(\mu, \sigma^2)$	Gaussian random variable with mean mu and variance σ^2
N_0	2-sided noise spectral density
N_s	Number of chips per symbol
$O(\cdot)$	Order of complexity
ω_n	Natural frequency
$\pi(\mathbf{x})$	Permutation function on the vector $\mathbf{x}$
$\pi^{-1}(\cdot)$	Inverse permutation of $\pi(\cdot)$
$p_k[j]$	The jth pilot bit for user k
P_k	Power level for user k
$P_{b,k}$	Probability of bit error for user k
r	Received signal

R_c	Code rate
R_g	Raised Cosine pulse shaping function
$R_{z,K}$	Radius of a cell
S	Spreading code length
σ_n^2	Additive white Gaussian noise variance
ς	Damping factor
T_c	Chip period
T_s	Symbol period
τ_k	Timing delay for user k
$x_k[j]$	The jth interleaved coded bit for user k
x^{Re}	The real component of random variable x
x^{Im}	The imaginary component of random variable x
$\mathrm{Var}\{X\}$	Variance of random variable X
$\zeta_k[j]$	The interference plus noise term of the jth chip for user k

Contents

List of Figures

List of Tables

Chapter 1

Introduction

The demand for high performance wireless networks is unrelenting, and has triggered the design and development of cellular standards and technologies, such as the Third Generation Partnership Project's (3GPP's) High Speed Packet Access (HSPA) and Long Term Evolution (LTE) standards, and 3GPP2's Evolution Data Optimised (EVDO) and Ultra Mobile Broadband (UMB). In the standardisation forums, the Wideband Code Division Multiple Access (WCDMA) technology has emerged as the most widely adopted third-generation air interface.

This thesis explores the physical layer aspects of wireless communications and specifically concentrates on a new multiple access technique called Interleave-Division Multiple Access (IDMA). Recently, IDMA was developed as a variant of DS-CDMA. In the new scheme users are separated by user specific interleavers, and each user is allocated a low rate code. As a result the bandwidth expansion is devoted to the low rate code and not weaker spreading codes. As a consequence IDMA receivers generally have higher spectral efficiency than DS-CDMA receivers, operating at the same loading. The other advantage of chip level interleaving is that larger block sizes lead to larger interleavers which improve the time diversity of the system. IDMA uses a simple chip-by-chip interference cancellation technique concatenated with single user forward error correcting (FEC) decoders for all users. IDMA inherits many advantages from Code Division Multiple Access (CDMA), in particular, diversity against fading and mitigation of the worst-case other-cell user interference problem. IDMA receivers are shown to have much higher capacity than single user CDMA receivers. Even when using much simpler sub-optimal interference cancellation (IC) techniques IDMA receivers support higher capacity than minimum mean squared error (MMSE) multiuser CDMA receivers.

When operating at higher capacity with higher loading the received signal for an IDMA receiver will have a very low signal-to-noise ratio (SNR) before interference cancellation. Under these circumstances it is envisaged that the necessary receiver functions such as timing, frequency and channel estimation and tracking will be much more challenging than in conventional spread spectrum receivers. It is also crucial to have efficient power allocation to maximise the performance of the multiuser receiver and minimise interference.

This thesis aims to design practical IDMA receivers with new and improved techniques for timing acquisition, tracking and asynchronous detection. Generally carrier frequency tracking can be combined with the timing tracking so we mainly focus on timing acquisition and tracking. We also aim to design and analyse frame asynchronous IDMA receivers, since frame asynchronous models are widely used in practical spread spectrum systems (such as the WCDMA air interface for HSPA). We then provide techniques and tools for analysis and power optimisation of IDMA systems. Finally, we aim to design and analyse a practical cellular system employing IDMA and develop a novel power zoning scheme, and show how it can improve system capacity.

1.1 Practical IDMA Receiver Design

Interleave Division Multiple Access is a multiple user communication scheme that uses interleavers as a means to separate users. By using low rate codes and large interleavers, IDMA can achieve near capacity performance with modest complexity. By using layering and low level modulation (typically BPSK or QPSK) high spectral efficiency can be achieved. IDMA has been proposed as a possible alternative future air interface wireless communications standard.

The primary advantage of IDMA over other multiple access techniques is its ability to devote the entire bandwidth expansion to FEC codes and then employ a low cost chip-by-chip interference canceller. A secondary advantage of the technique is the improved time diversity through chip interleaving of large blocks. Near capacity performance has been demonstrated for fully loaded and even overloaded systems, where traditional DS-CDMA multiuser detection fails. The IDMA receiver uses a simple interference canceller with complexity linearly proportional to the number of users. The cost complexity of the IDMA receiver is mainly dependent on the complexity of the outer FEC codes employed. It has been shown theoretically that weak repetition codes are near optimal for multiuser

receivers operating in the high noise region. Under these scenarios IDMA provides an ideal solution as it promises better performance than traditional DS-CDMA while having low complexity. IDMA has also been demonstrated in conjunction with orthogonal frequency division multiplexing (OFDM), orthogonal frequency division multiple access (OFDMA) as well as multiple-input multiple-output (MIMO) techniques incorporating the gains of these schemes as well as the performance benefits of IDMA. Due to the provision of low rate coding, as well as the detrimental effects of multipath interference, and timing and carrier frequency offsets, the practical design of IDMA systems is challenging.

1.2 Literature Review

1.2.1 Iterative Multi-user Detection

In cellular mobile communication systems with limited resources the division of access privileges is an ever increasing issue as the number and density of users and the data rates they demand increases. The basic approach to share resources is to divide the channel and multiplex the users such that only one user accesses a particular type of resource at any time. The channel can be divided in one of several ways: time division multiple access (TDMA), where all users transmit on the same frequency but users are assigned time slots during which they can share the same frequency; frequency division multiple access (FDMA) where each user is assigned a frequency band to use; and spatial division multiple access (SDMA), where smart antennae (phased array techniques) are used to direct transmissions at the mobile user to maximise the gain in that direction. In traditional code division multiple access (CDMA), users share frequency and time, that is they transmit over the same frequency band at the same time, but are separated using a spreading code. The spreading code is a pseudo-random sequence that is unique to each user and the transmitted sequence occupies a wider bandwidth so the technique is known as spread-spectrum signalling.

The conventional single-user CDMA receiver correlates the received signal with the spreading waveform of a particular user, treating the other users as noise. It is possible to remove the interference from other users if the interfering signals are orthogonal; in fact in this special case the conventional receiver is optimal. In reality, the spreading sequences are not orthogonal and in an asynchronous system there can be no guarantee that the codes are orthogonal. Therefore, in practice the conventional receiver suffers severe performance degradation. The

multiuser detector (MUD) was designed to cope with asynchronous transmission.

Since multi-access cellular networks were proposed, the problem of multiuser detection has been a subject of extensive research. In 1986, Verdu published the maximum likelihood sequence estimator (MLSE) [2]. This technique achieves optimum multiuser detection in an additive white Gaussian noise (AWGN) channel, but has prohibitively high complexity for even a small number of users.

Large improvements in MUD were realised following the discovery that CDMA could be combined with channel coding and the receiver could iterate between the MUD and the channel decoders (one for each user) in an analogous fashion to turbo codes. This is known as iterative MUD (IMUD) where an *a posteriori* probability (APP) CDMA detector and a bank of single-user (SU) decoders (separated by an interleaver) form an iterative loop and exchange soft information. Coded CDMA was first proposed in [3–6], where different approaches for interference suppression were used. In [4], Moher used a large interleaver with a conventional detector and FEC to show IMUD could achieve near single user performance. In [3], Reed *et al.* used a CDMA maximum *a posteriori* (MAP) detector with FEC, and Wang and Poor described a minimum mean-square error (MMSE) filter to perform interference suppression in [5]. Alexander *et al.* proposed the use of a simple interference canceller (IC) in [6] which subtracts an estimate of the interfering signals from the received (filtered) signal. Moher continued development for a synchronous and asynchronous IMUD in [7–9].

1.2.2 Interleaved Division Multiple Access

Interleaved-division multiple access (IDMA) is a recent iterative multiuser detection scheme proposed by Ping [10–13], where users are separated by user specific interleavers. Such a system is a development of earlier spread spectrum multiuser detection techniques by introducing chip-level interleaving as a means of mitigating burst impulsive noise disturbances, multiple access interference as well as intersymbol interference [14–16]. It is different from traditional division multiple access schemes as it is implicitly designed to be detected with an IMUD algorithm. IDMA differs from DS-CDMA since the entire bandwidth is devoted to a low rate code. Consequently IDMA was shown to be more bandwidth efficient than CDMA under similar operating conditions [17]. The low complexity iterative chip by chip (CBC) detection algorithm for IDMA in [18] has complexity linearly dependent on the number of users in the system. As a consequence,

the complexity cost for an IDMA receiver for K users is moderately higher than the total cost of K single-user receivers (assuming iterative decoders are involved in both cases). While having superior performance to DS-CDMA, IDMA also inherits the advantages of CDMA, in particular diversity against frequency selective fading and mitigation of the worst-case other-cell user interference problem. IDMA has been proposed as a possible future standard for 3GGP and LTE projects [19, 20].

The performance of multiuser code-division multiple access (MU-CDMA) systems is mainly limited by multiple access interference (MAI) and intersymbol interference (ISI). A conventional CDMA system involves separate coding and spreading operations. Theoretical analysis [21, 22] shows that optimal multiple access channel (MAC) capacity is achievable when the entire bandwidth is devoted to coding. This suggests that combining coding and spreading using low-rate codes maximises coding gain [21, 23]. Considering that spreading codes are no longer viable in this circumstance, interleavers can be employed to distinguish signals from different users. The principle has been studied previously and its potential advantages have been demonstrated [15, 16, 24–29]. Moher and Guinard in [15] showed the possibility of employing interleaving for user separation in coded systems for the first time. Brännström *et al.* [24] proposed narrow-band coded-modulation schemes in which trellis code structures are used for user separation and interleaving is considered as an option. For wideband systems, the performance improvement by assigning different interleavers to different users in CDMA has been demonstrated in [25, 26]. Mahadevappa and Proakis in [16] studied a chip interleaved CDMA scheme and a maximal-ratio-combining (MRC) technique for MACs with ISI. It demonstrated the advantages of chip-level interleavers. An interleaver based multiple access scheme was studied in [27–29] for high spectral efficiency for improved performance and low complexity. Interleave-division multiple access (IDMA) relies on user specific interleavers to distinguish signals for different users. IDMA inherits many advantages from CDMA, in particular, diversity against fading and mitigation of the worst-case other-cell user interference problem.

1.2.3 Acquisition

A necessary function in the receiver of a spread spectrum system is to determine the initial timing of the received replica of the transmitted signal. Before a receiver can begin detecting and tracking the user's data there must be an initial

estimate of the timing point to within half a chip. This process is generally termed acquisition. The acquisition process can be simplified to having two main processes: the searching strategy and the detector. The searching strategy is the procedure adopted by the receiver in its search through the uncertainty region. The detector evaluates multiple decision criteria at every step through the search, and deems whether the timing has been acquired. Once the initial timing has been acquired, the timing is continuously tracked by a tracking function such as a delay locked loop.

There are numerous acquisition search strategies for spread spectrum receivers, including serial search techniques [30–32], sequential-estimation techniques [33–35] and maximum *a posteriori* probability techniques [36, 37]. Serial searching techniques are generally believed to be superior in low signal to noise ratio (SNR) channels, to sequential algorithms which suffer from deteriorating performance with decreasing SNR, while the MAP techniques have prohibitive complexity. The performance parameter of greatest interest in evaluating the searching procedure is the total search time required to find the correct timing hypothesis. In order to determine whether the system is acquired (correct timing point), the detector must make a decision based on a specific statistical hypothesis test, i.e. Bayes [38], Neyman Pearson [39], or other. Minimising false alarms and missed detections is the primary goal of the detection process.

It has been shown that acquisition in the presence of MAI can significantly reduce the capacity of a spread spectrum system [40]. In [41], Madhow and Pursley defined the capacity of multiple user while maintaining acceptable acquisition performance. In [40], Corazza and Degli-Espoti suggested a multiple-dwell solution consisting of search mode and verification mode; in [40] the number of users was significantly fewer than the processing gain. Intuitively, the sensitivity of the acquisition unit is reduced to the MAI, which appears as noise like interference. In a highly loaded IDMA system with low rate coding, the MAI is expected to be quite severe, meaning that acquisition will be challenging. Therefore, it is necessary to study acquisition for low SNR environments.

Previous work on timing acquisition in the presence of MAI includes [42], which studied acquisition performance in the presence of MAI and the near-far problem. The authors compared the performance of approximate maximum likelihood (ML), MUSIC, and correlator performance, where the number of users was only one third of the spreading factor. In [43], a constant modulus algorithm was proposed. However, the number of users was also always less

than the processing gain. In [44], an investigation into parallel acquisition in DS-CDMA systems with MAI and other effects was performed. In [45], an improved acquisition technique was introduced, which is useful for channels with low SNR or MAI. Glisic *et al.* treated the MAI as noise. Moon *et al.* [35] studied the effect of MAI and an acquisition approach where multiple users exist. This only considered a small number of users where the ratio of users to spreading factor was far less than one.

In fully loaded systems with high levels of multiple access interference, poor acquisition performance can severely reduce the capacity of multiple user systems [46]. In [46, 47] the authors developed a model for acquisition using soft interference cancellation techniques for DS-CDMA. IDMA can be seen as a variant of DS-CDMA where the order of interleaving and spreading functions are swapped. Therefore we intend to apply acquisition techniques similar to those detailed in [46, 47] for the acquisition of IDMA users. In [48], we develop an acquisition technique for IDMA which uses interference cancellation and a correlating detection unit. This approach uses the soft estimates from the IDMA multiuser detector in order to acquire the timing of new users connecting to the base station. In [49] the authors show the performance degradation which sampling timing errors can cause in an IDMA system.

1.2.4 Tracking

Once receiver timing has been synchronised to within a fraction of a chip time, the estimate should be further refined to minimise timing errors. Furthermore, because of the relative motion of the transmitter and receiver and the instability of clocks, corrections must be made continuously [50]. This process is called tracking. Timing phase tracking consists of two distinct operations [51]: (i) estimation of the timing phase; (ii) utilisation of the timing estimate to correctly sample the received signal at the correct timing intervals. The former is referred to as timing error detection and the later as timing correction. Timing correction serves to provide the decision device with signal samples with minimum intersymbol interference. In the case of a digital implementation of timing tracking there are two broadly used configurations, namely, feedforward control, and feedback control. Oversampling is necessary in both schemes, where sampling is controlled by a fixed clock whose ticks are not locked to the incoming data. In practice the clocks sampling rate will be close but not equal to some rational multiple of the symbol rate.

Pulse shaping is generally performed by a combination of a transmit and receiver matched filter pair. A band limited pulse shaping filter which satisfies the Nyquist criterion for zero ISI, is commonly used in spread spectrum communications [52]. Bandlimited pulse shaping filters also have compact frequency spectrum thus they have better bandwidth efficiencies [53]. Based on both of these factors, a square root raised cosine (SRRC) pulse shaping filter is employed as the chip waveform of DS-CDMA signals in third generation (3G) wireless systems [54]. We adopt SRRC pulse shaped IDMA for the reasons stated above.

In the feedforward timing recovery scheme, the sampled received signal is matched filtered then timing estimation and correcting is performed before detection. In the feedback configuration, the timing error discriminator (TED) generates an error signal proportional to the difference between the actual chip timing and its current estimate. The error signal is then exploited to recursively update the timing estimates using feedback control. The central component of the timing recovery scheme is the TED. A variety of timing error detectors exist, either decision-directed (DD) or non-data-aided (NDA) [51, 55]. A synchroniser designed using a DD ML-based detector practically achieves the modified Cramer Rao bound (MCRB) [51]. Unfortunately an ML-based detector is complex to implement as it requires derivative matched filter in addition to the matched filter. Thus simpler solutions have been found. One of the most common TED is the early-late detector [56–58], which uses a simplistic approximation of the derivative matched filter. Some other timing error detectors of interest are the zero-crossing detector [59] and the Mueller and Muller (MM) detector [60].

Another prominent issue in timing recovery for an asynchronous multiuser receiver is the necessity for non synchronised sampling. In a fully digital implementation of the receiver, sampling is not locked to the incoming pulses. This is referred to as non-synchronous sampling. It is possible to have synchronous sampling for a single user receiver where a numerically controlled oscillator (NCO) can be used in conjunction with sampling such that the symbols are synchronous. However, for a multiuser receiver for IDMA this is not possible due to asynchronism, and the fact that multiple users must be resolved from the received signal. As such, it is most practical that non synchronous oversampling be employed and interpolation be used to correct the fractional timing error. It is then possible to employ an independent tracking loop for each user.

In this work, we mainly focus on decision directed feedback controlled tracking loops with non synchronous sampling and interpolation to estimate the

chip timing for an IDMA chip sequence. As previously discussed we consider SRRC pulse shaping, and user asynchronism as motivated by the 3G systems [54]. Conventional timing tracking/synchronisation techniques for DS-CDMA systems involve pilot aided timing recovery using code-locked loops which have been widely studied [50, 61]. It is conceivable that sever MAI can degrade the performance of conventional timing tracking algorithms, in a similar way that it affects conventional timing acquisition, as described in [46, 47]. This motivates us to study tracking algorithms operating in low SNR scenarios. In [62] the authors show that there is merit in maximum likelihood based iterative code-aided feedback phase tracking. A framework for iterative soft information based synchronisation techniques for turbo receivers is presented in [63]. Further developments in iterative synchronisation techniques, also referred to as turbo synchronisation, are presented in [64–72].

Although iterative timing synchronisation techniques have been studied for single user turbo-coded systems [62, 63, 70–72], they have not been applied to CDMA or IDMA systems, where they result in significant performance improvements for severe drift scenarios. The interference canceller in a heavily loaded IDMA system operates at a very low SNR due to the nature of the chip-by-chip processing required. It has been shown by experimentation that in fully loaded systems with high levels of multiple access interference, poor acquisition performance can severely reduce the capacity of multiple user systems [48]. The severity of the multiple access interference is increased by the fact that pilot channel has much lower power than the data channel in most practical systems (for example 3GPP [54]). We have simulated and analysed a multiuser turbo synchronisation algorithm for an IDMA receiver for the first time in [73].

1.2.5 Iterative Decoding Analysis

Hagenauer and Hoeher were the first to visualise the behavior of a soft-input soft-output (SISO) decoder in [74]. They considered the decoder as a filter which improves the SNR and derived a transfer function where the SNR of the decoder output is a function of the input SNR. This work was carried out before iterative, or turbo decoding was discovered. Several methods have since been derived to analyse the performance of convolutional and turbo codes.

The Variance Transfer (VT) method was first proposed by Alexander, *et al.* in [6] and developed further in [75]. The variance of the output of a decoder can be analysed as a function of the input SNR. The VT technique essentially

determines by simulation the input-output relationship of the constituent decoder by comparing the noise variance in the *a priori* input to the *a posteriori* output noise variance, for a fixed E_b/N_0. VT analysis assumes the noise has a Gaussian distribution and as such has been applied extensively in CDMA receivers as the interference plus noise in a CDMA channel is Gaussian-like. In [76] VT analysis was used to model unequal power CDMA. The same technique can be easily applied to IDMA for analysis.

A method known as density evolution (DE) was proposed independently by El Gamal and Hammons in [77, 78] and Divsalar *et al.* in [79]. The authors analysed iterative systems by tracking the density, or SNR, of the extrinsic information exchanged between constituent decoders. The technique considers each decoder as an SNR transfer device, the input is the SNR of the *a priori* input and the output is the SNR of the *a posteriori* output. The work by Richardson *et al.* in [80] and [81] was significant in DE analysis of LDPC codes. DE is useful for optimizing LDPC codes and as in VT analysis, requires the assumption that the input and output of the decoder is Gaussian [77, 78].

Both VT and DE analysis have been used extensively and have been found to exhibit properties that make them especially suitable to particular decoders or receivers. In 1999, ten Brink proposed the use of mutual information (MI) as a metric for tracking the convergence of iterative decoding in [82, 83]. The method is known as Extrinsic information transfer (EXIT) analysis and considers the decoder as a MI transfer device. The transfer function is obtained through simulation and describes the change in MI between the input and the output of the decoder. This technique typically assumes a Gaussian distributed input signal. However, it has the advantage that no assumption needs to be made on the output. EXIT analysis is generally considered to be a superior technique for modeling iterative decoding [84] and in recent years much work has been done in the field of EXIT analysis. The relationship between capacity, code rate and EXIT functions, now known as the Area Theorem, was proven in [85, 86] and [87]. In [88] it was shown that EXIT and Density Evolution are equivalent (and exact) in the BEC case. The Generalised EXIT (GEXIT) function was proposed in [89] which yielded a closed-form EXIT function for BEC case for simple codes and in [89] the authors derived a (tight) upper bound for the MAP threshold (threshold above which decoding can succeed). EXIT chart analysis was extended to parallel concatenated codes with three components by ten Brink in [90] and Brännström *et al.* proposed a method in [91].

Several other techniques have been proposed for convergence analysis of

iterative decoders and receivers. Belief propagation, otherwise known as the sum-product algorithm, was used to represent iterative multiuser joint decoding of CDMA signals by Boutras and Caire in [92] and [93]. They analysed the asymptotic performance of the decoding algorithms using DE. The convergence analysis tools mentioned previously assume a large (infinite) block length. In practice large block lengths are not suitable for communications as they suffer from high latency so block lengths typically less than 5000 are used. Transfer charts become less reliable with decreasing block lengths. Lee and Blahut proposed the SNR transfer characteristic band (TCB) in [94–96] which is useful for finite-length turbo codes. In [97] Lee and Blahut proposed an analogous EXIT band chart for finite-length turbo codes and derived lower bounds for the BER performance.

In [84], Tüchler *et al.* concluded that EXIT and fidelity transfer are most suitable for predicting the convergence behaviour of turbo codes. In consideration of the findings of [83] and [84] that EXIT charts are the most accurate tool for analysis of iterative receivers, they will be used exclusively in this thesis.

1.2.6 Power Optimisation

It is well understood that the maximum sum-capacity of a multiple access channel (MAC) can be achieved by either unequal power allocation (PA) or unequal rate allocation (RA), and using successive interference cancellation (SIC) [98, 99]. Recent results [100, 101] show that with rate or power control and group stripping decoding, the optimal spectral efficiency of a multiple access channel can be approached using low level modulation (e.g. BPSK or QPSK). The analysis and optimisation of IDMA has been studied in [102], where the authors use the large system approximation along with signal to interference plus noise ratio (SINR) evolution for performance evaluation, they also consider power profile optimisation of an IDMA system to maximise its spectral efficiency. The large-system approximation-based SINR analysis method provides less accurate performance evaluation than the Extrinsic information transfer (EXIT) chart analysis. This is because of the Gaussian approximation made in order compute the interference plus noise variance terms in the SINR estimation process.

Recently, it has been shown that for a system with equal power distribution, the capacity bound can also be achieved by adopting unequal rate allocation (RA) and successive cancellation, as long as the number of user rate groups is sufficiently large [103]. In a system with iterative soft onion peeling (SOP) and

unequal rate distribution, low-rate users converge faster than high-rate users and the operation of the iterative receiver is facilitated by using rate allocation.

Power optimisation of coded CDMA systems using EXIT chart analysis has been studied in [104, 105]. In [105] the capacity optimisation criterion is constructed by averaging the EXIT function of the outer codes across all the users in the system. The authors do not construct the optimal power/rate allocation scheme in order to achieve the sum-rate capacity given by the rate region constraint for multi access channel defined in [98].

Rate optimisation of repetition coded IDMA systems using conventional linear programming techniques has been studied in [101]. However, the results show that the performance is 5dB away from the ultimate sum-rate capacity of the channel. The LP criterion is not constructed in an optimal fashion.

1.2.7 Cellular analysis

Most of the literature that investigate multiuser receiver design omit the effects of out-of-cell (intercell) interference. Newson *et. al* in [106] showed that in a typical urban environment roughly 33% of the receiver interference comes from users in other cells (intercell interference), the other 67% coming from users within the cell (intracell interference). Alexander [107] shows how intracell interference on the uplink can be can be mitigated using MU receivers at the BS, and that intercell interference can be partially mitigated using soft hand over (SHO)[108]. As a result, huge signal to interference (SIR) gains with respect to conventional single user (SU) receivers can be observed. Dawy *et. al* in [109] propose relays at the edge of the cell to improve coverage and capacity while lowering the UL interference for cellular systems. In [110] the capacity and cell coverage by using successive interference cancelation along with service classes is used to show capacity and coverage gains over single user receivers. However, we believe that the average signal to interference ratio limitation due to intercell interference for the system in [110] must still conform to that given in [107], if the power levels are normalised.

1.3 Motivation of Research

The performance and complexity analysis of IDMA and its comparison with DS-CDMA has been evaluated in [1, 111, 112]. In [111] the authors evaluated both techniques by means of computer simulations in various scenarios such as

user asynchronism, multipath channel, near-far problem, and overloaded systems. In all the scenarios they evaluated IDMA performs better than or as good as CDMA despite its simplicity and lower complexity. In [1] the same authors provide a more comprehensive comparison of both detectors. The authors of [1] performed comprehensive comparisons of IDMA and CDMA systems using three iterative linear detectors: the MMSE, rake, and soft rake detectors from practical complexity concerns. The three detectors were analytically shown to be equivalent for IDMA over flat channels for asynchronous users. It was then pointed out that the equivalence guarantees the MMSE solution for IDMA over flat channels without computationally expensive matrix inversions and matrix vector multiplications. This is not the case for CDMA systems in general since CDMA is sensitive to user asynchronism.

In the case of CDMA, it was observed that the performance degradation is severe for the rake and soft rake detectors as compared to the MMSE detector in most scenarios. For IDMA, the simplest interference canceller (or soft rake detector) performs nearly as well as the most complex MMSE detector in many scenarios except highly user-loaded scenarios or for a channel with poor frequency characteristics. Table 1.1 presents the simulation parameters used in [1]. Figure 1.1 shows the performance for the IDMA receiver as given in [1]. It can be seen that the simplest interference canceller for IDMA performs as well as the more complex MMSE detector for CDMA. It should also be noted that when using low rate coding as in [10, 13, 113] the performance difference between the MMSE and simple IC for IDMA would be negligible. For this reason we opt to use the simpler IC for IDMA rather than the MMSE detector presented in [1].

	CDMA	IDMA
Information bits	1024	
Convolutional code	$R_c = 1/2$, mem 4, $[31, 27]_8$, trellis is terminated	
Repetition code	-	1/4
Bit interleavers	user-independent, uniform random	
Interleaver size	2056	8224
Modulation	QPSK (Gray labeling)	
Symbols	1028	4112
Spreading codes	length 4	-
Scrambling codes	UMTS uplink long codes	-

Table 1.1: Simulation parameters for IDMA system, from [1]

Recently in [19, 114] IDMA has been proposed as air interface for 3G

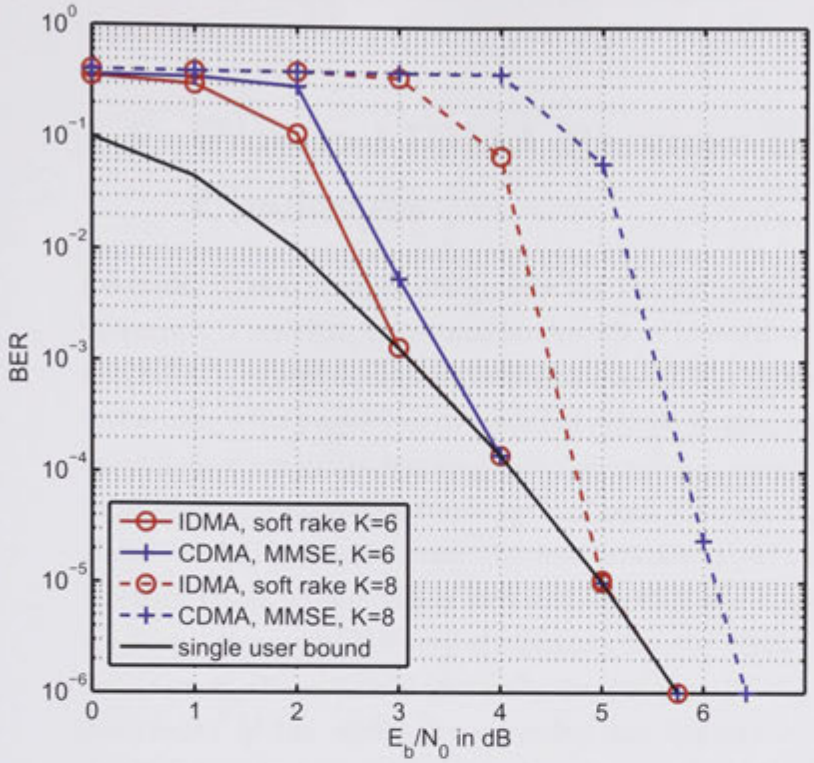

Figure 1.1: BER performance of highly loaded CDMA (MMSE) and IDMA systems with K = 6, 8 users after 10 iterations on an AWGN channel, for parameters in Table 1.1.

and 4G technologies. The literature shows that there are advantages of multi-layered, OFDM-IDMA systems whereby the systems can gain benefits from both non-orthogonal (IDMA) and orthogonal systems (OFDM). For example, in [17] the authors present the benefits of an asynchronous IDMA, being robustness in fading channels, inter-cell interference, and its flexibility in asynchronous transmissions, whereas OFDM has the main advantage of lower complexity equalisation for resolving multipath channels. OFDM-IDMA has been recently proposed as an alternative to plain IDMA in ISI channels [115, 116].

Spread spectrum communication techniques may have advantages over OFDM systems in ad hoc and self organizing networks. This is due to the robust, asynchronous nature of spread spectrum systems where users are uncoordinated. IDMA has been suggested as a practical system for ad hoc and self organizing networks in [112, 117, 118]. These properties of IDMA may deem it a

practical technology for femtocell [119] networks which are likely to rely on self organisation.

1.4 Practical IDMA Receiver Design Challenges

Practical IDMA receiver design has not been studied in any great detail in the literature. There has been considerable effort devoted to low rate coding, OFDM, and MIMO, as well as channel estimation for IDMA. However, the literature seems to be bare with respect to acquisition (initial timing and frequency estimation) as well as continuous tracking (timing and frequency). Most research on the topic of IDMA considers frame synchronous receiver models where all users are known to be connected with the base station *a priori*. Under heavily loaded systems with low rate coding and user layering, the operations of acquisition and tracking are potentially very challenging for the IDMA receiver. Asynchronous detection in the uplink is generally the norm in 3G standards as it reduces the complexity of the uplink by removing the requirement for closed loop timing synchronisation between users. Power allocation in practical cellular systems is important as it provides a number of benefits, being longer battery life in terminals, less interference onto the cell of interest enabling a combination of more connected users, higher data rates per user, connection robustness, and longer connection range. Cellular analysis of IDMA which incorporates inter-cell interference is important due to the reasons stated above. This thesis primarily focuses upon the practical implementation of an IDMA system operating in the uplink. We understand that the design of the IDMA base station receiver, will require asynchronism (as suggested above), as well as power control. As such the design of an IDMA receiver in the uplink provides a much more challenging problem to solve. It can also be envisaged that techniques pertaining to an uplink receiver could potentially be applied to a downlink receiver, however, this is out of scope of this thesis and isn't explored here. The design challenges we identify for an IDMA receiver in a base station are briefly summarised below;

Synchronisation Accurate synchronisation plays a central role in the efficient utilisation of any spread spectrum system. Typically the process of synchronising the incoming received chip timing with the source transmitted chip timing, is performed in two steps: first, timing acquisition, then tracking.

Acquisition The acquisition function is to determine the frame/symbol/chip timing to within a half a chip interval, such that the interleavers are synchronous with the user's data. Acquisition is necessary not only to determine the initial timing point of a user, but in-order to determine whether a user is attempting to connect to the base-station for the first time.

Tracking After the initial timing information for a user is known it is necessary to track the user's timing continuously in order to coherently detect the user's data.

Asynchronous Detection After the timing, carrier frequency and channel parameters have been estimated at the receiver it is still necessary to detect the users asynchronously. We use the term asynchronous to mean that different users have different initial timing offsets respectively.

Analysis and Optimisation Analysis of multiuser receivers allows for improved allocation of resources, namely, power or rate. Analysis is used to understand the convergence behaviour of the system and consequently allocate resources to users in an optimal manner. We mainly consider power allocation for the IDMA receiver (in the uplink), since it has the added benefit of reducing intercell interference (resulting in improved cellular capacity).

Cellular Analysis Cellular analysis is used to determine the capacity limits, we mainly focus upon the uplink capacity. Using the interference limits of multiuser receivers, and geometrical analysis the operating point of a cell can be determined analytically.

Figure 1.2 illustrates a simplified diagram of an IDMA receiver. The received signal is passed through an acquisition unit, which acquires users, as well as initial timing information. The timing synchronisation unit is used to track the timing and carrier frequency of all the users. The function of pulse-shape filtering and ADC down sampling is performed within the synchronisation unit, such that the output is the vector $\tau \triangleq \{\tau_1, \ldots, \tau_K\}$ where τ_k represents the timing point for user k. Note that all user's timing points are not necessarily the same, thus implying asynchronous detection. We do not investigate the channel estimation unit (as signified by the dotted line box) as this topic has been developed in the literature. However, we do assume that the channel parameters are passed

between the synchronisation, as well as interference canceller, such that both are coherent. The channel state information for all users is encapsulated in the vector, $\mathbf{h} \triangleq \{h_1, \ldots, h_K\}$. The interference canceller in the diagram is asynchronous in the sense that user's timings are not aligned. The output of the interference canceller is the vector of coded chips for all users denoted $\mathbf{x} \triangleq \{x_1, \ldots, x_K\}$.

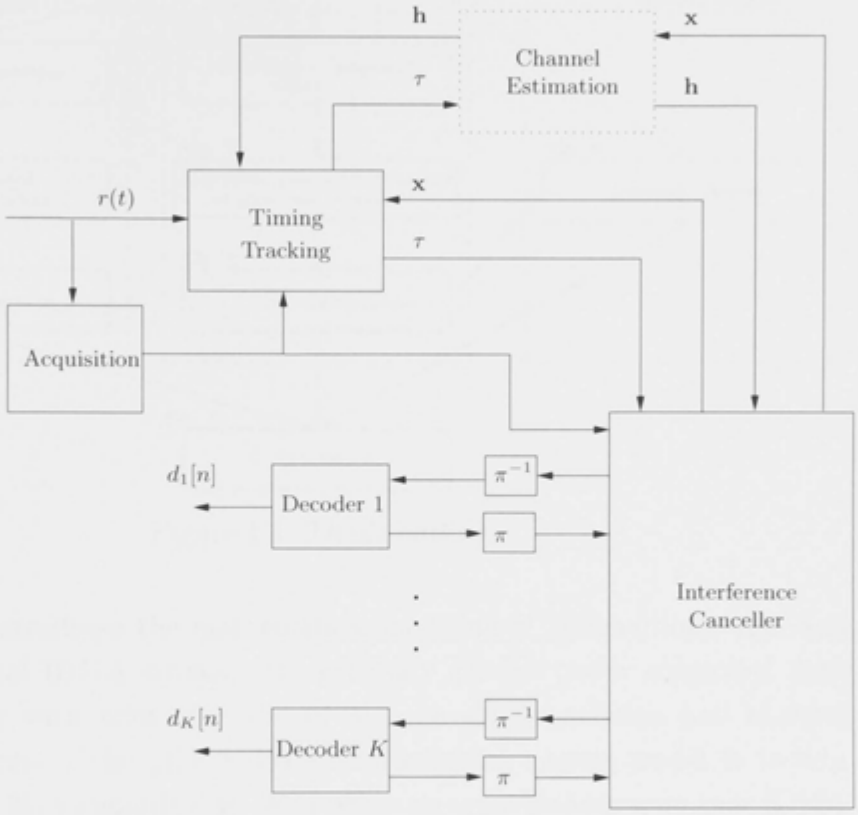

Figure 1.2: Practical IDMA receiver

1.5 Thesis Outline

The flow of this thesis reflects, to a large part, the procedures of a practical IDMA system. The initial synchronisation needs to be established in the uplink via the acquisition process. We then concentrate on tracking of multiple users. Once accurate chip timings are determined we study the frame asynchronous detection of IDMA. Then we introduce analysis and optimisation tools for the asynchronous multiuser IDMA receiver. Finally, we present a multicell analysis for the power optimised IDMA scheme using a novel power zoning technique. The outline of this thesis is shown in Figure 1.3.

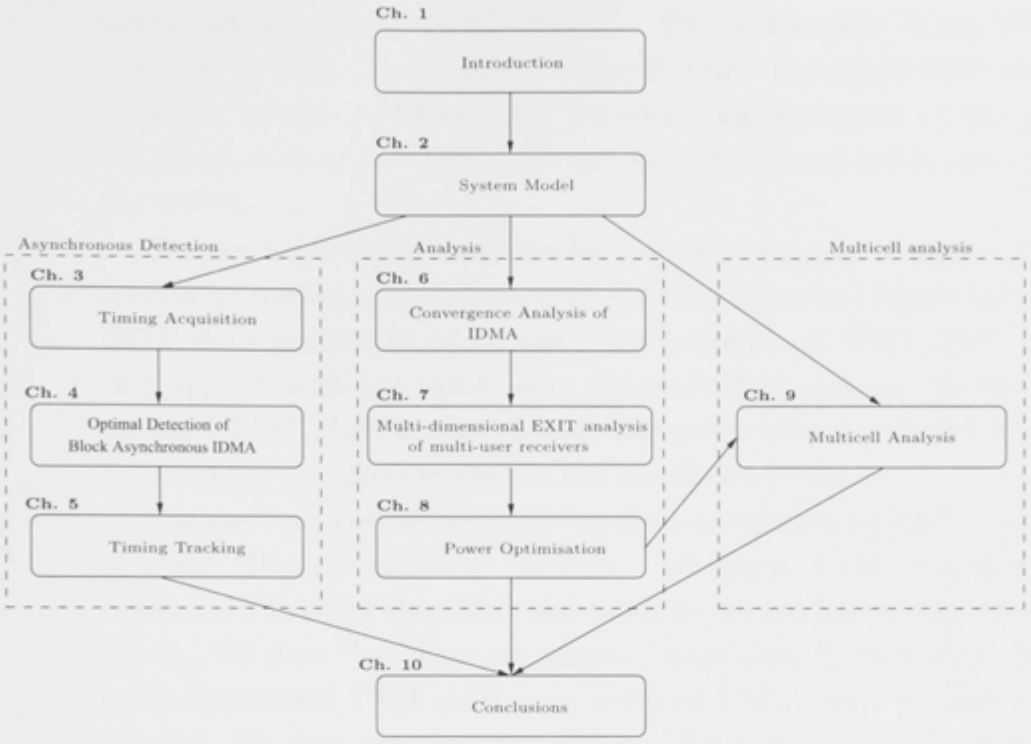

Figure 1.3: Thesis outline.

Chapter 2 introduces the mathematical modeling of the multiuser channels and the practical IDMA signals. We generally assume power controlled data channels, along with pilot channels to aid the synchronisation and channel estimation process. The pilot aided synchronisation system model is loosely based upon the 3G standards [54]. We assume an asynchronous multiuser IDMA receiver is implemented, where user frames have different initial timing points.

Chapter 3 describes a novel coarse timing acquisition algorithm. We propose an acquisition decision criterion which utilises soft information from the iterative multiuser detector in order to improve acquisition performance. Performance analysis and simulation results show that interference cancellation before acquisition result in lower false alarm and missed detection probabilities.

Chapter 4 investigates an iterative timing tracking algorithm for pilot aided IDMA. We develop a timing error detector which combines timing estimates from the pilot channel and the soft data channel. Analysis and simulation results show that under severe timing drift there are significant gains from iterative timing tracking.

Chapter 5 presents an optimal frame asynchronous IDMA receiver. We construct the maximum likelihood asynchronous IDMA receiver using a matrix

interpretation of the multiuser channel. The performance of the ML receiver is compared with a conventional approach which uses guard intervals between successive blocks. Although the practical implementation of the maximum likelihood receiver is not feasible, it does suggest ultimate performance bounds of the system.

Chapter 6 introduces methods for modeling iterative receivers. LLRs and metrics for tracking convergence, such as MI, variance and fidelity are explained. EXIT chart analysis is introduced. The conventional EXIT chart analysis is then applied to analyse equal power allocated IDMA systems. We then show an averaged EXIT chart analysis for unequal power allocated IDMA systems. In both scenarios we provide analysis and simulation results.

Chapter 7 presents a new multi-dimensional approach for EXIT chart analysis of power allocated multiuser receivers. We define a low complexity mutual information tracking algorithm, and use it to predict higher dimensional EXIT charts. We show that there are marginal improvements in analysis from using multi-dimensional EXIT charts over averaged EXIT charts for power allocated systems. We then use the new EXIT analysis technique to construct a power optimisation technique. A power optimisation problem is constructed to minimise sum transmit power while guaranteeing quality of service.

Chapter 8 presents a multi cellular analysis of IDMA systems. In this Chapter we develop a novel power zoning technique in which we incorporate the power allocation strategy designed in Chapter 7, along with geometrical zoning, in order to reduce intercell interference. We show that using power regions, where the higher power levels are allocated to zones closer to the base station, results in lower average intercell interference compared to uniform equal power allocation. We show that there is significant capacity gains from using this technique, even when employing soft handover strategies.

Chapter 9 concludes this thesis by summarizing the original contributions. It reviews the new techniques we have proposed and their importance in the design of practical IDMA systems. We also discuss future work and highlight the open areas in this subject.

1.6 Thesis Contributions

The motivation behind the work in this thesis is to design, analyse and optimise practical IDMA receivers in the uplink. We develop novel techniques for

acquisition, tracking and analysis of multiuser receivers and then construct a framework for the design of practical IDMA receivers and compare with conventional approaches. We show practical design methods for acquisition and tracking algorithms operating in severe interference scenarios. We then focus upon power optimisation for IDMA systems, developing new EXIT chart analysis techniques tailored for multiuser systems. Finally, we present analysis for multi-power multi cellular IDMA systems, showing that power allocation can significantly reduce intercell interference, resulting in increased cellular capacity.

- In Chapter 3, we develop an algorithm to improve the performance of acquisition in an IDMA system with significant MAI [48]. We show that by using soft information from already acquired users we can significantly improve the performance of the acquisition unit, by reducing the probability of false-alarms and missed-detections.

- In Chapter 4, we develop timing tracking algorithms specifically for heavily loaded IDMA systems [73]. We propose an iterative pilot-aided tracking algorithm which uses soft information from the data channel as well as the pilot channel in-order to estimate timing error. We show that in severe drift scenarios this algorithm has significant performance gain over the conventional pilot-aided tracking algorithm.

- In Chapter 5, we develop a frame asynchronous IDMA receiver. Frame asynchronism is the standard technique for 3G systems. We specifically construct a maximum likelihood IDMA receiver [120]. We compare the results with an IDMA receiver with a guard interval between successive blocks. Although the ML approach is computationally expensive it provides insight into the optimal asynchronous IDMA receiver performance for small block sizes and few users.

- In Chapter 7, we develop a new multi-dimensional EXIT chart analysis technique for IDMA systems [121, 122]. We show that the analysis developed is more accurate than the averaged EXIT chart analysis found in literature. We then show how the analytical tool can be incorporated into the power/rate optimisation problem for practical IDMA systems.

- In Chapter 8, a novel power zoning technique is proposed for multi-cellular, multi-power IDMA systems [123]. The analytical results show that by using power zones where stronger users are located in zones close to the base

station, results in significantly less inter-cell interference. As such there are two big advantages of such a power zoning scheme: (i) the optimal power optimisation with respect to intracell interference as described in Chapter 7; (ii) reduced inter-cell interference due to the geometry of the power zoning technique.

1.7 List of Publications

- B. Senanayake, M. C. Reed, and Z. Shi, Timing Acquisition for Multi-User IDMA, in *IEEE International Conference on Communications*, (Beijing, China), pp. 5077 5081, May 2008.

- B. Senanayake, M. C. Reed, and Z. Shi, Iterative timing recovery for IDMA receivers operating under severe timing drift, in *Australian Communications Theory Workshop (AusCTW)* , (Canberra, Australia), pp. 71 76, February 2010.

- B. Senanayake, M. C. Reed, and Z. Shi, An Optimal Asynchronous IDMA Receiver, in *Australian Communications Theory Workshop (AusCTW)*, (Sydney, Australia), pp. 28 32, February 2009.

- B. Senanayake and M. C. Reed, Multi-dimensional EXIT analysis for iterative multi-user detection with unequal power allocation, in *6th International Symposium on Turbo Codes and Iterative Information Processing (ISTC)*, (Brest, France), pp. 409 413, September 2010.

- B. Senanayake and M. C. Reed, "Multi-Dimensional EXIT Analysis and Optimization for Multi-User Receivers," *conditionally accepted by IEEE Transactions on Wireless Communications*, December 2011.

- B. Senanayake and M. C. Reed, "Analysis of the Capacity Enhancement of Cellular Systems using Multiuser Receivers and Multiple Power Zones," in *the 7th IEEE Workshop on Broadband Wireless Access*, (Houston, USA), pp. 1490-1494 , December 2011.

Chapter 2

System Model

2.1 Introduction

Since iterative decoding was first presented in 1993 [124, 125], a focus in the literature has been on understanding how the technique achieves near optimal performance using a concatenation of suboptimal components. The turbo-principle can be successfully applied to many detection/decoding problems such as serial concatenated decoding, equalisation, coded modulation, multiuser detection and joint source and channel decoding [126]. In particular, a Turbo equalisation scheme is proposed in [127] for convolutionally coded digital transmission over an intersymbol interference channel. Using a similar paradigm, turbo-type iterative multiuser detection (IMUD) schemes have been extensively studied [3–6, 15, 75, 92, 128–133]. A framework describing the general multiuser receiver is first introduced in this Chapter. We then proceed to describe the Interleave Division Multiple Access (IDMA) scheme and define assumptions regarding channel parameters and system configuration.

A discrete time mathematical model of multiuser DS/CDMA and IDMA systems is introduced. A baseband discrete time model is used (without loss of generality) to avoid more complicated notation due to asynchronism. This thesis considers asynchronous models for IDMA in Chapter 3, Chapter 4 and Chapter 5 , when necessary we provide an amended system model. As a method of introduction we provide details about the synchronous detection of IDMA [13] using the chip-by-chip (CBC) detector. We contrast the IDMA technique with the more popular multiuser CDMA schemes [5, 6, 128]. Details of the forward error correcting (FEC) codes used with IDMA are given. Finally, we provide simulated performance results for the FEC coded IDMA systems described.

2.2 Iterative Multi-user Detection

The traditional system model for a multiuser detection scheme is shown in Figure 2.1. The transmitter scheme shown in Figure 2.2 is natural when DS/CDMA is used as the mechanism for user separation. In [134], it is shown that the optimal decoding scheme for an asynchronous convolutionally coded CDMA system combines the trellises of both the asynchronous multiuser detector and the convolutional code, resulting in prohibitive computational complexity ($O(2^{K\nu})$), where K is the number of users in the channel, and ν is the code constraint length. In [3, 4, 135] the respective authors show how a MAP multiuser detector can be constructed, and how soft information can be iterated between the MUD and the single user decoders. Note that the posteriori distribution ($\Pr\left\{\underline{y}_t|\underline{d}_t\right\}$ in [3]) is a multivariate Gaussian distribution, due to the cross correlation of users spreading sequences. Consequently, the proposed MAP detection scheme has exponential complexity in the number of users ($O(2^{K+\nu})$). In [5] the authors present iterative soft interference cancellation and decoding for coded CDMA in a manner similar to turbo decoding where the single user decoders and the CDMA multiuser channel are separated by interleavers (as shown in Figure 2.3). In [5] a moderate complexity suboptimal SISO MUD is developed which is based upon soft interference cancellation and linear MMSE filtering. The complexity of the IMUD proposed is in the order of $O(K^2 + 2^{\nu})$. Alexander *et al.* proposed the use of a simple interference canceller (IC) in [6] which subtracts an estimate of the interfering signals from the received signal. The suboptimal simple IC proposed in [6] exhibits close to SU performance even in highly-loaded systems with significantly lower complexity (in the order $O(K)$) over the MMSE and MAP detectors.

2.3 IDMA for multiple users

The performance of multiuser code-division multiple-access (MU-CDMA) systems is mainly limited by multiple access interference (MAI) and intersymbol interference (ISI). A conventional CDMA system (as shown in Figure 2.3) involves separate coding and spreading operations. Theoretical analysis [21, 22] shows that optimal multiple access channel (MAC) capacity is achievable when the entire bandwidth is devoted to coding. This suggests that combining coding and spreading using low-rate codes should maximise coding gain [21, 23]. Considering that spreading codes are no longer viable in this circumstance,

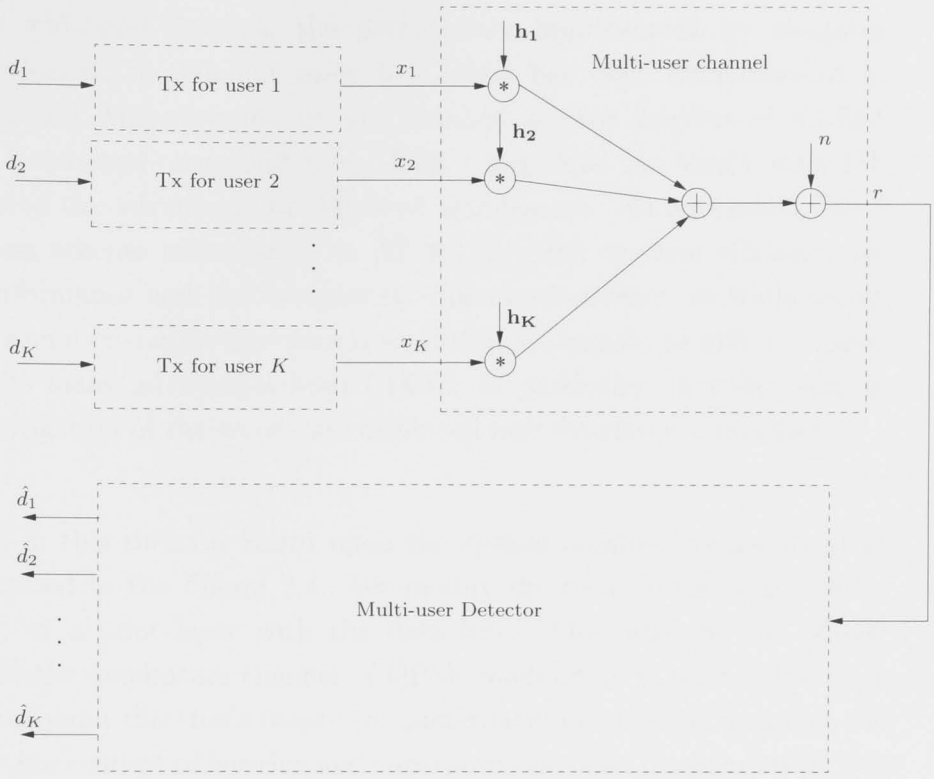

Figure 2.1: A general system model for K user Multiuser detection scheme.

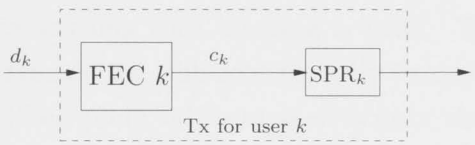

Figure 2.2: The transmitter structure for user k in a DS/CDMA system.

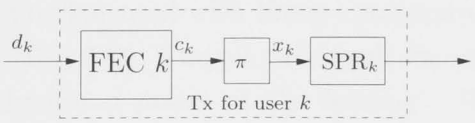

Figure 2.3: The transmitter structure for user k in a DS/CDMA system with interleaving.

interleavers can be employed to distinguish signals from different users. The principle has been studied previously and its potential advantages have been demonstrated [15, 16, 24–29]. In [15] Moher *et al.* showed the possibility of employing interleaving for user separation in coded systems. In [24] Brännström *et al.* proposed narrow-band coded-modulation schemes in which trellis code structures are used for user separation and interleaving is considered as an

option. For wideband systems, the performance improvement by assigning different interleavers to different users in CDMA has been demonstrated in [25, 26]. In [16] Mahadevappa *et al.* studied a chip interleaved CDMA scheme and a maximal-ratio-combining (MRC) technique for MACs with ISI. It demonstrated the advantages of chip-level interleavers. An interleaver based multiple access scheme was studied in [27–29] for high spectral efficiency for improved performance and low complexity. Interleave-division multiple access (IDMA) relies on user specific interleavers to distinguish signals for different users. IDMA inherits many advantages from CDMA, in particular, diversity against fading and mitigation of the worst-case other-cell user interference problem.

The work in this thesis is based upon the system architecture proposed in [27–29] illustrated in the Figure 2.4. We modify the transmitter structure by superposition of a pilot layer with the data bits. Motivated by the 3GGP standard [136] the quadrature channel of QPSK modulation is used as the pilot channel. Throughout this thesis binary (or quaternary) modulation is used and is motivated by the concept of layering and superposition coded modulation (SCM) [19, 20, 137–140]. Hoeher *et al.* has published numerous papers suggesting IDMA as a possible standard for 4G wireless communications [19, 114, 141, 142], in all of these references binary data streams with layering is used. The authors of [20] suggest that binary data streams are sufficient in order to approach channel capacity (Section 5 in [20]). The main advantage of binary data streams is real-valued processing at the receiver side. Binary data streams are less vulnerable with respect to linear and nonlinear interference, phase jitter, fast fading, etc. The detection of SCM can be implemented with linear complexity with respect to the number of layers (users) [137, 140]. The pilot channels for all users employ pseudo-noise (PN) sequences known *a priori* at the receiver. The Figure 2.5 illustrates the pilot aided IDMA transmitter for user k. The pilot aided IDMA system is used in Chapter 3 for timing acquisition and Chapter 4 for timing synchronisation. Pilot aided channel estimation for IDMA using a similar system model has been illustrated in [143, 144].

The proceeding subsection of this Chapter provides a brief overview of the basic IDMA scheme developed in [27–29]. Several low-cost detection algorithms for the interference canceler (IC) are presented for different channel conditions, namely, real-single-path and complex-multi-path channels.

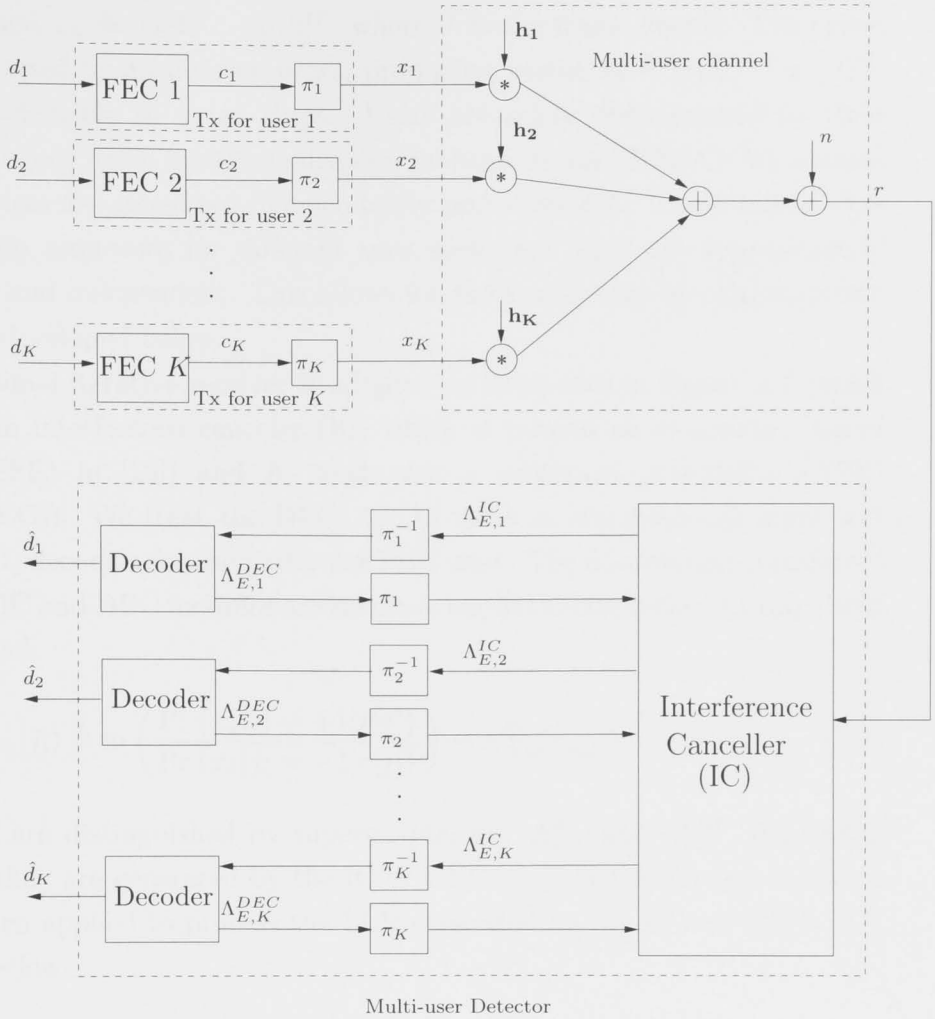

Figure 2.4: The architecture of an IDMA system for K users

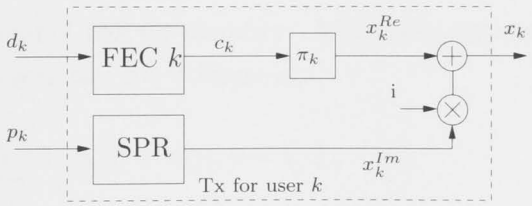

Figure 2.5: IDMA transmitter structure with pilot layer

2.4 IDMA Transmitter and Receiver Principles

The upper part of Figure 2.4 shows the transmitter structure of the multiple-access scheme under consideration with K simultaneous users. The data bits for user k, d_k, are encoded with a low rate code C, generating a

coded sequence, $\mathbf{c}_k \triangleq [c_k[1] \dots c_k[J]]^T$, where J is the frame length. The coded bits are permuted by an interleaver π_k, producing vector $\mathbf{x}_k \triangleq [x_k[1] \dots x_k[J]]^T$. We refer to elements in x_k as chips. Users are solely distinguished by their interleavers, hence name interleave-division multiple access (IDMA). We assume that interleavers are generated independently and randomly. These interleavers make the chip sequences for different uses such that they are approximately uncorrelated and independent. This allows for the simple chip-by-chip detection mechanisms developed below.

A suboptimal iterative receiver is adopted as illustrated in Figure 2.4, which consists of an interference canceler (IC, which is termed an elementary signal estimator (ESE) in [13]) and K single-user a posteriori probability (APP) decoders (DECs). We treat the DECs for all users as standard soft input soft output (SISO) decoders for the particular FEC used. The information transferred between the IC and DEC modules are extrinsic log-likelihood ratios (LLRs) about $\{x_k[j]\}$ defined,

$$\Lambda_{E,k}^{\mathrm{IC}}(x_k[j]) \triangleq \ln\left(\frac{\Pr\{x_k[j]=+1|r[j]\}}{\Pr\{x_k[j]=-1|r[j]\}}\right) - \Lambda_{A,k}^{\mathrm{IC}}(x_k[j]) \qquad \forall k,j \tag{2.1}$$

These LLRs are distinguished by superscripts, i.e. $\Lambda_{E,k}^{\mathrm{IC}}$ and $\Lambda_{E,k}^{\mathrm{DEC}}$, depending on whether they are generated by the IC or DEC. A global turbo-type iterative process is then applied to process the LLR generated by the IC and DECs [27], as detailed below.

2.4.1 The Basic IC Function

We first assume that the channel has no memory. After chip-matched filtering, the received signal from K users can be written as,

$$r[j] = \sum_k h_k x_k[j] + n[j], j = 1, 2, \dots, J, \tag{2.2}$$

where h_k is the channel coefficient for user-k and $\{n[j]\}$ are samples of an AWGN process with variance $\sigma_n^2 = \frac{N_0}{2}$, where N_0 is the power spectral density of the noise. We assume that the channel coefficients are known *a priori* at the receiver. Due to the use of random interleavers $\{\pi_k\}$ the IC operation can be carried out in a chip-by-chip manner, with only one sample $r[j]$ used at a time. Rewrite (2.2) as,

$$r[j] = h_k x_k[j] + \zeta_k[j], \tag{2.3}$$

where

$$\zeta_k[j] = r[j] - h_k x_k[j], \tag{2.4}$$

$$= \sum_{k' \neq k} h_{k'} x_k[j] + n[j], \tag{2.5}$$

is the interference plus noise in $r[j]$ for user-k. Using the central limit theorem, ζ_k, can be approximated as a Gaussian random variable, and $r[j]$ can be characterised by a conditional Gaussian probability density function (PDF) conditioned on the kth user,

$$\Pr\{r[j]|x_k[j] = \pm 1\} = \frac{1}{\sqrt{2\pi \mathrm{Var}\{\zeta_k[j]\}}} \exp\left(-\frac{(r[j] - (\pm h_k + \mathrm{E}\{\zeta_k[j]\}))^2}{2\mathrm{Var}\{\zeta_k[j]\}} \right), \tag{2.6}$$

where $\mathrm{E}\{\cdot\}$ and $\mathrm{Var}\{\cdot\}$ are the mean and variance functions respectively.

The goal of the IC is to cancel interference for user k from all users $k' \neq k$ based on estimates from previous iteration of x_k. We can determine the average of the noise plus interference term $\zeta_k[j]$,

$$\mathrm{E}\{\zeta_k[j]\} = \sum_{k' \neq k} h_{k'} \mathrm{E}\{x_{k'}[j]\}. \tag{2.7}$$

The variance of the interference term can be calculated in a similar manner,

$$\mathrm{Var}\{\zeta_k[j]\} = \sum_{k' \neq k} \|h_{k'}\|^2 \mathrm{Var}\{x_k[j]\} + \sigma_n^2. \tag{2.8}$$

We can simplify the IC by computing $\mathrm{E}\{r[j]\}$ and $\mathrm{Var}\{r[j]\}$ and then subtracting the contributing terms for user k. Since $\mathrm{E}\{r[j]\}$ and $\mathrm{Var}\{r[j]\}$ is user independent this process reduces the number of computations significantly,

$$\mathrm{E}\{r[j]\} = \sum_i h_i \mathrm{E}\{x_i[j]\},$$

$$\mathrm{Var}\{r[j]\} = \sum_i \|h_i\|^2 \mathrm{Var}\{x_i[j]\} + \sigma_n^2. \tag{2.9}$$

The terms (2.7) and (2.8) can be rewritten,

$$\mathrm{E}\{\zeta_k[j]\} = \mathrm{E}\{r[j]\} - h_k \mathrm{E}\{x_k[j]\}, \tag{2.10}$$

$$\mathrm{Var}\{\zeta_k[j]\} = \mathrm{Var}\{r[j]\} - \|h_k\|^2 \mathrm{Var}\{x_k[j]\}. \tag{2.11}$$

In order to treat the IC as a SISO module it needs to output an extrinsic LLR of $x_k[j]$, using the Gaussian approximation, it is easy to determine LLR of $x_k[j]$,

$$\Lambda_{E,k}^{IC}(x_k[j]) = 2h_k \frac{(r[j] - \mathrm{E}\{\zeta_k[j]\})}{\mathrm{Var}\{\zeta_k[j]\}}. \tag{2.12}$$

The cost of computing $\mathrm{E}\{r[j]\}$ and $\mathrm{Var}\{r[j]\}$, are shared by all users and costs $3KN$ multiplications and $(2K-1)N$ additions, where N is the block length and K is the total number of users. Overall the IC uses $7KN$ multiplications and $(5K-1)N$ additions to process a block, thus having linear complexity ($O(K)$). The cost per information bit is linearly dependent on the number of user K. This is considerably lower than that of other alternatives. For example the well-known MMSE in [5] has complexity of $O(K^2)$.

2.4.2 The IC for complex multipath channels

We now extend our description to complex multipath channels. We will user either the superscripts "^{Re}" and "^{Im}" or function notations $\mathrm{Re}\{\cdot\}$ and $\mathrm{Im}\{\cdot\}$ to indicate real and imaginary parts respectively. We primarily consider QPSK signaling in this thesis as,

$$x_k[j] = x_k^{Re}[j] + \mathrm{i}x_k^{Im}[j], \tag{2.13}$$

where $\mathrm{i} = \sqrt{-1}$, $x_k^{Re}[j]$ and $x_k^{Im}[j]$ are two coded bits from $\mathbf{c}_k$. We now adopt a multipath complex channel which is L chips long,

$$r[j] = \sum_{k=1}^{K} \sum_{l=0}^{L-1} h_{k,l} x_k[j-l] + n[j] \quad j = 1, \ldots, N+L-1. \tag{2.14}$$

We write,

$$r[j+l] = h_{k,l} x_k[j] + \zeta_{k,l}[j], \tag{2.15}$$

where,

$$\zeta_{k,l}[j] = r[j+l] - h_{k,l} x_k[j]. \tag{2.16}$$

We expand (2.14),

$$r[j] = \sum_{k=1}^{K}\sum_{l=1}^{L}\left(h_{k,l}^{\mathrm{Re}}x_k^{Re}[j-l] - h_{k,l}^{\mathrm{Im}}x_k^{Im}[j-l]\right) + i\sum_{k=1}^{K}\sum_{l=1}^{L}\left(h_{k,l}^{\mathrm{Re}}x_k^{Im}[j-l] + h_{k,l}^{\mathrm{Im}}x_k^{Re}[j-l]\right) + n[j], \tag{2.17}$$

where samples of $\{n[j]\}$ are samples of a complex AWGN process with variance σ_n^2 per dimension. Denote $h_{k,l}{}^*$ the conjugate $h_{k,l}$. The phase shift due to $h_{k,l}$ is canceled out in $h_{k,l}{}^* r[j+l]$, which means that $\mathrm{Im}\{h_{k,l}{}^* r[j+l]\}$ is not a function of $x_k^{Re}[j]$. Therefore the detection of $x_k^{Re}[j]$ only requires,

$$\mathrm{Re}\{h_{k,l}{}^* r[j+l]\} = \|h_{k,l}\|^2 x_k^{Re}[j] + \mathrm{Re}\{h_{k,l}{}^* \zeta_{k,l}[j]\}. \tag{2.18}$$

Algorithm 1 below outlines the procedure to estimate $x_k^{Re}\{\cdots\}$ based on (2.18).

It can be verified that $\Psi[j]$ in (2.20) is the covariance of $r^{Re}[j]$ and $r^{Im}[j]$. It is introduced for cost saving since it is shared by all users, costing $2LKN$ multiplications and $(L-1)(K-1)N$ additions. If the cost of $\Psi[j]$ is ignored, the complexity of the Algorithm 1 is approximately, $2L(7KN)$ multiplications and $2L(5KN)$ additions, giving linear complexity ($O(K)$). A similar procedure to Algorithm 1 can be used to estimate $x_k^{Im}[j]$ based on $\{\mathrm{Im}\left(h_{k,l}{}^* r[j+l]\right), l = 0, \ldots, L-1\}$.

2.5 Forward Error Correcting Codes

In [13] low rate turbo Hadamard codes [145] and in [146] low rate turbo codes have been applied in order to illustrate near capacity achieving performance of IDMA systems. The approach that was taken in both cases was to design the best possible single user code and apply it to multiple IDMA users. The optimal code design for concatenation with soft IC receivers such as IDMA, is still an open problem [147, 148]. However, in [147, 148] the authors show that in the high noise region the weak repetition code has close to optimal performance. In [149] the authors compare low rate turbo codes for IDMA [146] with a number of LDPC coding schemes. The results of [149] show that the extremely weak single-user codes perform much better under heavily loaded scenarios. This observation conforms with the theory developed in [147] since a heavily loaded IDMA system

Algorithm 1 Chip-by-Chip Detection in a Complex Multi-Path Channel

Step(i): Estimation of Interference Mean and Variance

$$\mathrm{E}\left\{r^{Re}[j]\right\} = \sum_{k,l}\left(h_{k,l}^{\mathrm{Re}}\mathrm{E}\left\{x_k^{Re}[j-l]\right\} - h_{k,l}^{\mathrm{Im}}\mathrm{E}\left\{x_k^{Im}[j-l]\right\}\right), \tag{2.19a}$$

$$\mathrm{E}\left\{r^{Im}[j]\right\} = \sum_{k,l}\left(h_{k,l}^{\mathrm{Re}}\mathrm{E}\left\{x_k^{Im}[j-l]\right\} + h_{k,l}^{\mathrm{Im}}\mathrm{E}\left\{x_k^{Re}[j-l]\right\}\right), \tag{2.19b}$$

$$\begin{aligned}\mathrm{Var}\left\{r^{Re}[j]\right\} = \sum_{k,l}\big(\,&(h_{k,l}^{\mathrm{Re}})^2\mathrm{Var}\left\{x_k^{Re}[j-l]\right\} \\ &+ (h_{k,l}^{\mathrm{Im}})^2\mathrm{Var}\left\{x_k^{Im}[j-l]\right\}\,\big) + \sigma_n^2,\end{aligned} \tag{2.19c}$$

$$\begin{aligned}\mathrm{Var}\left\{r^{Im}[j]\right\} = \sum_{k,l}\big(&(h_{k,l}^{\mathrm{Re}})^2\mathrm{Var}\left\{x_k^{Im}[j-l]\right\} \\ &+ (h_{k,l}^{\mathrm{Im}})^2\mathrm{Var}\left\{x_k^{Re}[j-l]\right\}\,\big) + \sigma_n^2.\end{aligned} \tag{2.19d}$$

$$\Psi[j] = \sum_{k,l} h_{k,l}^{Re}h_{k,l}^{Im}\left(\mathrm{Var}\left\{x_k^{Re}[j-l]\right\} - \mathrm{Var}\left\{x_k^{Im}[j-l]\right\}\right). \tag{2.20}$$

$$\begin{aligned}\mathrm{E}\left\{Re\{h_{k,l}{}^{*}\zeta_{k,l}[j]\}\right\} = {}& h_{k,l}^{\mathrm{Re}}\mathrm{E}\left\{r^{Re}[j+l]\right\} \\ &+ h_{k,l}^{\mathrm{Im}}\mathrm{E}\left\{r^{Im}[j+l]\right\} - \|h_k\|^2\mathrm{E}\left\{x_k^{Re}[j]\right\},\end{aligned} \tag{2.21a}$$

$$\begin{aligned}\mathrm{Var}\left\{Re\{h_{k,l}{}^{*}\zeta_{k,l}[j]\}\right\} = {}& (h_{k,l}^{\mathrm{Re}})^2\mathrm{Var}\left\{r^{Re}[j]\right\} + (h_{k,l}^{\mathrm{Im}})^2\mathrm{Var}\left\{r^{Im}[j]\right\} \\ &+ 2h_{k,l}^{\mathrm{Re}}h_{k,l}^{\mathrm{Im}}\Psi[j+l] - \|h_k\|^4\mathrm{Var}\left\{x_k^{Re}[j]\right\}.\end{aligned} \tag{2.21b}$$

Step(ii): LLR Generation and Combining

$$\Lambda_{E,l}^{IC}(x_k^{Re}[j]) = 2\|h_{k,l}\|^2\frac{\mathrm{Re}\left(h_{k,l}{}^{*}r[j+l]\right) - \mathrm{E}\left\{\mathrm{Re}\left(h_{k,l}{}^{*}\zeta_{k,l}[j]\right)\right\}}{\mathrm{Var}\left\{\mathrm{Re}\left(h_{k,l}{}^{*}\zeta_{k,l}[j]\right)\right\}}, \tag{2.22a}$$

$$\Lambda_{E}^{IC}(x_k^{Re}[j]) = \sum_{l=0}^{L-1}\Lambda_{E,l}^{IC}\left(x_k^{Re}[j]\right). \tag{2.22b}$$

is effectively equivalent to operation of the IC in the high noise region. In [150] the authors show how using FEC allocation to different user groups along with an VT chart based optimisation can be used to improve the performance of IDMA.

Throughout the work in this thesis we avoid the issue of designing optimal FEC codes for IDMA. we mainly focus on practical implementation issues of IDMA which are essentially independent of the choice of FEC code. For this reason we choose the simplest FEC codes for IDMA, being, convolutional or turbo

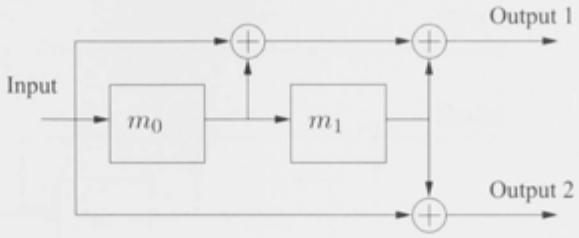

Figure 2.6: A rate 1/2, constraint length 3, non-recursive, non-systematic convolutional encoder (07,05).

codes concatenated with repetition codes as commonly used in [12, 13, 28, 151], or just the repetition codes. One advantage of using FEC concatenation with repetition codes is the ability to lower complexity by dynamic scheduling of the soft information transfer between the soft repetition decoder and FEC decoder [105, 152].

2.5.1 Convolutional Codes

In a CC the information sequence d is fed sequentially into a shift register with m memory registers. The constraint length of a code is defined as $m + 1$ and the memory elements (shift registers) are usually initialised to zero. The encoder has a number of modulo-2 adders and their configuration determines the characteristics of the code. The configuration of the adders is described by the generator polynomial of the code, which is usually expressed in octal notation. The generator polynomial is $G = (\mathbf{g}_1, \mathbf{g}_2, \ldots, \mathbf{g}_r)$, where the encoder has r outputs. Each $m + 1$ bit vector $\mathbf{g_i}$ represents the binary coefficients of a modulo 2 convolution operation. The ith bit of the output sequence is calculated by modulo 2 convolution of $\mathbf{g_i}$ and the $m+1$ information bits in the memory shift registers. Figure 2.6 shows a $(07, 05)_8$ code where $\mathbf{g_1} = [1, 1, 1]$ and $\mathbf{g_2} = [1, 0, 1]$. The code rate is defined as $R_c = 1/r$.

If the input is included in the output, a CC is said to be systematic, and one of the outputs in the generator polynomial is equal to one. Furthermore, if one of the outputs is fed back to the input, the code is named a recursive systematic convolutional (RSC) code. In recursive codes the generator polynomial has a fractional element (g_f/g_b) where g_f and g_b are feed-forward and feed-back connections respectively. Figure 2.7 shows a RSC with generator polynomial $G = (1, 07/05)$.

The data is encoded by passing the input sequence x sequentially into the

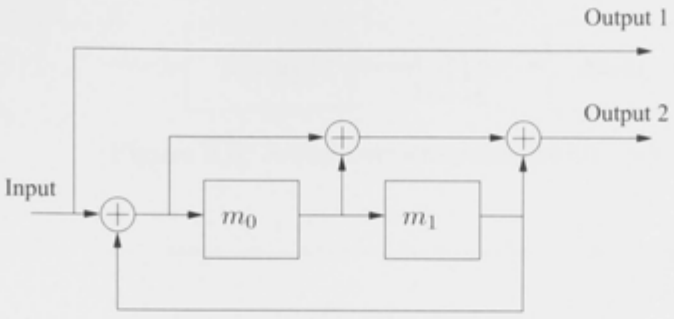

Figure 2.7: A rate $\frac{1}{2}$, constraint length 3, recursive systematic convolutional encoder (1,07/05)

encoder. The adders specify which elements of the shift register are modulo-2 added, and the result of the additions for each generator vector g_i become the output of the encoder, and for the recursive encoder the output of the feedback vector g_f is fed back as illustrated in Figure 2.7. The registers are then right shifted by one bit and the next information bit is passed through the same process again. If there are no more information bits then encoding can be finished by terminating the trellis, where the memory registers are all returned to the zero state.

2.5.2 Turbo Codes

Turbo codes were first described by Berrou *et al.* in [124] and have achieved performance within a fraction of a decibel of the fundamental limits of communications described by Shannon [153]. A turbo code is constructed by the concatenation of two or more CCs and separating them with an interleaver. The concept is that the interleaver spreads the coded bit errors between the constituent decoders[154, 155], thus allowing for a coding diversity gain. One of the major results of this is that two relatively weak codes can be combined in order to construct a very strong code, in a "divide and conquer" type approach. CC encoders can be concatenated serially or in parallel [124, 156]. A serially concatenated turbo code encoder is shown in Figure 2.8 and Figure 2.9 shows a parallel concatenation of two RSC encoders. The code rate for a serial concatenation is $R_c = \prod_{j=1}^{J} R_j$ and for the parallel case $R_c = \left(1 - \left(\sum_j (1 - R_j^{-1})\right)\right)^{-1}$ where R_j is the code rate of code j.

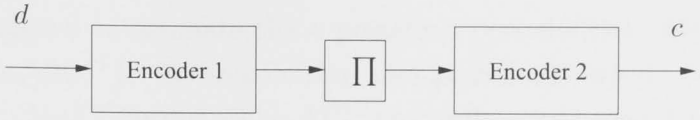

Figure 2.8: Serial concatenated turbo code encoder

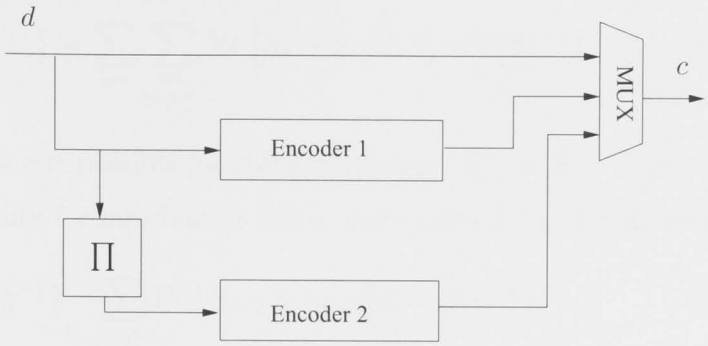

Figure 2.9: Parallel concatenated turbo code encoder.

2.6 Decoder

In this thesis we mainly consider performance of either a CC or a turbo code concatenated with a repetition code. The use of repetition codes is required in order to make a low rate outer code. IDMA can be shown to have poor performance when low rate FECs are employed due to unresolvable multiuser interference. In the proceeding subsections we present the decoding algorithms for the soft repetition code, convolutional code and the turbo code, respectively.

We assume perfect bit synchronisation and we let $c_{n,j} \triangleq \mathbf{c}[jN+n]$ represent the n-th coded bit at uncoded bit time index j, where $N = 1/R_c$. The uncoded bit at time index j is $d[j]$. The received sequence is $\mathbf{r}_0^{\mathcal{L}-1} = [\mathbf{r}_0, \ldots, \mathbf{r}_{\mathcal{L}-1}]^T$, where $\mathbf{r}_j = [\mathbf{c}[jN], \ldots, \mathbf{c}[jN+N-1]] + \mathbf{n_j}$ and the information block length is $\mathcal{L}$. The elements of the noise vector $\mathbf{n_j}$ are i.i.d and normally distributed with mean 0 and variance σ^2.

2.6.1 Convolutional Decoder

The BCJR algorithm [157] is commonly used in modern digital communications systems as it is the optimal convolutional decoder which minimises the BER. However, the cost is high complexity, which is why the Viterbi [158] algorithm is used where the complexity of the BCJR algorithm is too high or close-to-capacity performance is not required. All work in this thesis utilises the BCJR algorithm, which will be briefly described below.

The decoder is designed to estimate the a posteriori probabilities (APP) of the channel bits $\Pr\left\{c_{n,j}|\mathbf{r}_0^{\mathcal{L}-1}\right\}$. By maximising this probability we produce a maximum a posterior (MAP) output. The APP probability for coded bit n at time index j can be expressed,

$$\Pr\left\{c_{n,j}=c|\mathbf{r}_0^{\mathcal{L}-1}\right\}=\sum_{m'}\sum_{\substack{m\\c_{n,j}=c}}\Pr\left\{S_{j-1}=m',S_j=m|\mathbf{r}_0^{\mathcal{L}-1}\right\}, \tag{2.23}$$

where coded bit $c_{n,j}=c$ is possible for state transition $(S_{j-1}=m')\rightarrow(S_j=m)$.

The APP probability for information bit at time index j can be expressed

$$\Pr\left\{d[j]=d|\mathbf{r}_0^{\mathcal{L}-1}\right\}=\sum_{m'}\Pr\left\{S_{j-1}=m',d[j]=d|\mathbf{r}_0^{\mathcal{L}-1}\right\}, \tag{2.24}$$

$$=\sum_{m'}\sum_{m}\Pr\left\{S_{j-1}=m',S_j=m|\mathbf{r}_0^{\mathcal{L}-1}\right\}, \tag{2.25}$$

where $d[j]=d$ is the information bit hypothesis which may cause state the transition $m'\rightarrow m$.

The decoder calculates the APP probability (2.24) by evaluating the joint probabilities using Bayes theorem,

$$\Pr\left\{S_{j-1}=m',S_j=m|\mathbf{r}_0^{\mathcal{L}-1}\right\}=\frac{\Pr\left\{S_{j-1}=m',S_j=m,\mathbf{r}_0^{\mathcal{L}-1}\right\}}{\Pr\left\{\mathbf{r}_0^{\mathcal{L}-1}\right\}}, \tag{2.26}$$

where $\Pr\left\{\mathbf{r}_0^{\mathcal{L}-1}\right\}$ is independent of $d[j]$ and can be dropped. It can be shown that the joint probability $\Pr\left\{S_{j-1}=m',S_j=m,\mathbf{r}_0^{\mathcal{L}-1}\right\}$ can be rewritten,

$$\begin{aligned}\Pr\left\{S_{j-1}=m',S_j=m,\mathbf{r}_0^{\mathcal{L}-1}\right\}&=\Pr\left\{S_{j-1}=m',\mathbf{r}_0^{j-1}\right\}\Pr\left\{S_j=m,\mathbf{r}_j|S_{j-1}=m'\right\}\\&\quad\times\Pr\left\{\mathbf{r}_{j+1}^{\mathcal{L}-1}|S_j=m\right\},\end{aligned} \tag{2.27}$$

where simplification is possible due to the Markov property of the state of the convolutional decoder.

We can define the forward state probability function,

$$\alpha_j(m)=\Pr\left\{S_j,\mathbf{r}_0^j\right\}, \tag{2.28}$$

and the reverse state probability function,

$$\beta_j(m)=\Pr\left\{\mathbf{r}_{j+1}^{\mathcal{L}-1}|S_j=m\right\}. \tag{2.29}$$

The state transition probabilities are defined as,

$$\gamma_j(m', m) = \Pr\{S_j = m, \mathbf{r}_j | S_{j-1} = m'\}. \tag{2.30}$$

Now (2.27) can be rewritten,

$$\Pr\left\{S_{j-1} = m', S_j = m, \mathbf{r}_0^{\mathcal{L}-1}\right\} = \alpha_{j-1}(m')\gamma_j(m', m)\beta_j(m). \tag{2.31}$$

Due to the Markov property, the forward and reverse state probabilities can be derived recursively, where the initial and final states of the trellis are known due to termination. The state transition probability can be rewritten as,

$$\gamma_j(m', m) = \Pr\{S_j = m | S_{j-1} = m'\} \Pr\{\mathbf{r}_j | \mathbf{c}[j]\}, \tag{2.32}$$

where $\Pr\{S_j = m | S_{j-1} = m'\}$ is the state transition probability. The transition metric can be rewritten,

$$\gamma_j(m', m) = \Pr\{S_j = m | S_{j-1} = m'\} \prod_{n=1}^{\mathcal{N}} \Pr\{r_{n,j} | c_{n,j}\}, \tag{2.33}$$

For a Gaussian channel the conditional probability metric equals,

$$\Pr\{r_{n,j} | c_{n,j}\} = \frac{1}{\sqrt{2\pi\sigma^2}} \exp\left(-\frac{(r_{n,j} - c_{n,j})^2}{2\sigma^2}\right), \tag{2.34}$$

With *a priori* input $\Lambda_A(d[j])$, the transition probability is,

$$p_i = \Pr\{S_j = m | S_{j-1} = m'\} = \frac{\exp\left(\frac{(i+1)}{2}\Lambda_A(d[j])\right)}{1 + \exp\left(\Lambda_A(d[j])\right)}, \tag{2.35}$$

for $i \in \{-1, +1\}$. Using (2.35) and (2.34), (2.33) becomes,

$$\gamma_j^i(m', m) = p_i \exp\left(-\frac{\sum_{n=1}^{\mathcal{N}} (r_{n,j} - c_{n,j})}{2\sigma^2}\right), \tag{2.36}$$

where the i superscripts represents the information bit hypothesis for the transition from m' to m on bit j. The APP LLR of bit $d[j]$ can be computed,

$$\Lambda_D(d[j]) = \ln\left(\frac{\sum_{m=1}^{N_s}\sum_{m'=1}^{N_s} \gamma_j^1(m', m)\alpha_{j-1}(m')\beta_j(m)}{\sum_{m=1}^{N_s}\sum_{m'=1}^{N_s} \gamma_j^{-1}(m', m)\alpha_{j-1}(m')\beta_j(m)}\right). \tag{2.37}$$

Substituting (2.36) into (2.37) it is possible to break down the APP information into,

$$\Lambda_D(d[j]) = \ln\left(\frac{p_1}{p_{-1}}\right) + \ln\left(\frac{\exp\left(-\frac{(r_{1,j}-c_{1,j})}{2\sigma^2}\right)}{\exp\left(-\frac{(r_{1,j}+c_{1,j})}{2\sigma^2}\right)}\right) + \ln\left(\frac{\sum_{m=1}^{N_s}\sum_{m'=1}^{N_s}\exp\left(-\frac{\sum_{n=2}^{N}(r_{n,j}-c_{n,j})}{2\sigma^2}\right)\alpha_{j-1}(m')\beta_j(m)}{\sum_{m=1}^{N_s}\sum_{m'=1}^{N_s}\exp\left(-\frac{\sum_{n=2}^{N}(r_{n,j}-c_{n,j})}{2\sigma^2}\right)\alpha_{j-1}(m')\beta_j(m)}\right). \tag{2.38}$$

where the first term on the right hand side is the *a priori* input Λ_A, the second term is the channel input Λ_C since the coded bit $c_{1,j}$ is the systematic bit ($c_{1,j} = d[j]$), and the third term to extrinsic information Λ_E. Therefore (2.38) can be rewritten as,

$$\Lambda_D(d[j]) = \Lambda_A(d[j]) + \Lambda_C(d[j]) + \Lambda_E(d[j]), \tag{2.39}$$

which is the common representation for the output of a soft input soft output (SISO) decoder.

2.6.2 Turbo Decoder

As discussed in Section 2.5.2, turbo codes can be constructed with a serial or parallel concatenation of CCs. In a parallel turbo code decoder, all decoders have two inputs - a channel input and an *a priori* input from the other decoder as in (2.39). In a serial turbo decoder, only the inner decoders have two inputs, the outer decoder has a single input form the connecting decoder. In this case the *a priori* input can be considered to be zero and therefore, $\Lambda_D(d[j]) = \Lambda_C(d[j]) + \Lambda_E(d[j])$. The IMUD receiver scheme illustrated in Figure 2.4 can be considered to be a serial concatenation of a FEC code and the multiuser channel.

Parallel Concatenated Turbo Code

A TD with two parallel concatenated CC codes is shown in Figure 2.9. Since the encoders/decoders are separated by an interleaver the constituent decoders in the TD share information only on the systematic bits which are the same as the information bits. In the TD the *a priori* ($\Lambda_A(d[j])$) input contains soft

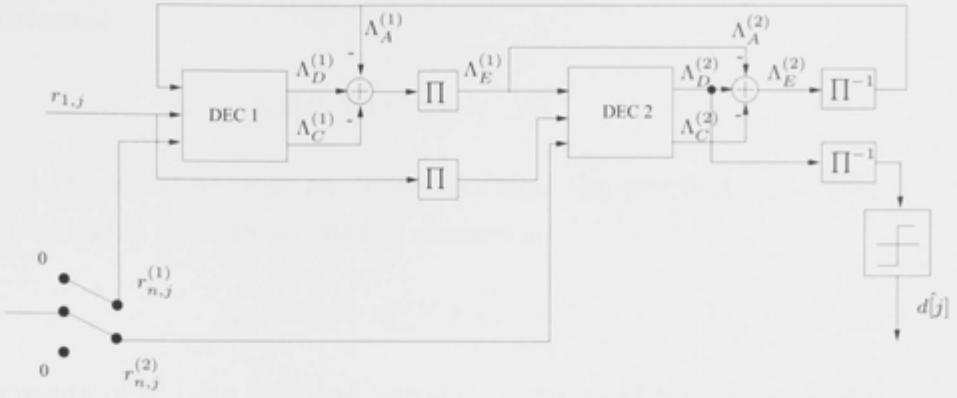

Figure 2.10: Parallel concatenated turbo decoder.

information on the systematic bits. The parity check bits are input separately for both constituent decoders using a multiplexer. The systematic bits $r_{1,j}$ are shared by both decoders whereas when $n > 1$, $r_{n,j}^{(1)}$ represent the parity bits for decoder 1 and $r_{n,j}^{(2)}$ represent the parity bits for decoder 2. The extrinsic information output from Decoder 1 (DEC 1) is interleaved and passed to Decoder 2 as *a priori* information for the systematic bits. Similarly Decoder 2 (DEC 2) passes extrinsic information as *a priori* information for Decoder 1. In this way both decoders enhance extrinsic information on each iteration and thus improve the performance of both decoders. After a predetermined number of iterations the LLR of the outer decoder (DEC 2) is passed through a hard decision unit in order to estimate the original uncoded bit sequence ($\hat{d}[j]$).

2.6.3 Soft Output Repetition Decoder

A low rate repetition code is commonly used in concatenation with a more powerful FEC in IDMA systems [10] in order to achieve low rate coding which is necessary to separate different users. It has also been shown that the use of repetition codes along with optimal power allocation for IDMA can achieve channel capacity at high E_b/N_0 [159]. Another advantage of concatenation of repetition codes with a stronger code is the ability to have a dynamic activation ordering of the decoder components which allow for complexity saving. It has been shown recently that for interference cancellation systems, that the low rate repetition code approaches the limit of the optimal symbol estimator in the high-noise regime [147].

We consider the rate $1/N$ repetition code which uses a masking sequence $s_i = \pm 1$, for $i = 1 \ldots N$. Mathematically the repetition coded bit for data bit

$d[j]$, can be surmised,

$$c_{i,j} = s_n d[j], \text{ for } i = 1, \ldots, N, \tag{2.40}$$

where we adopt the same notation for coded bits from the previous subsection. Now the received signal through an AWGN channel is,

$$r_{i,j} = c_{i,j} + n[jN + i], \tag{2.41}$$

where the elements of $n[\cdot]$ are i.i.d and normally distributed with mean 0 and variance σ^2.

The APP of the soft output repetition decoder can be formulated,

$$\begin{aligned} \ln\left(\frac{\Pr\{d[j]=+1|\mathbf{r}\}}{\Pr\{d[j]=-1|\mathbf{r}\}}\right) &= \ln\left(\frac{\Pr\{\mathbf{r}|d[j]=+1\}}{\Pr\{\mathbf{r}|d[j]=-1\}}\right) \\ &\quad + \ln\left(\frac{\Pr\{d[j]=+1\}}{\Pr\{d[j]=-1\}}\right), \end{aligned} \tag{2.42}$$

Now assuming that $\Pr\{d[j]=+1\} = \Pr\{d[j]=-1\} = \frac{1}{2}$, and since the samples of $\mathbf{r}$ are i.i.d Gaussian distributed, i.e;

$$\Pr\{r_{i,j}|d[j]=1\} = \frac{1}{\sqrt{2\pi\sigma^2}} \exp\left(-\frac{(r_{i,j}-s_i)^2}{2\sigma^2}\right), \tag{2.43}$$

where $\{r_{i,j}|d[j]=1\}$ is normally distributed such that $r_{i,j} \sim \mathcal{N}(s_i, \sigma^2)$. The LLR output of the CBC detector derived in (2.12) and (2.22) make the Gaussian approximation due to the law of large numbers validating the assumption that input into the repetition decoder is approximately Gaussian distributed. It can be shown that (2.42) can be computed as,

$$\begin{aligned} \Lambda_D(d[j]) &= \sum_{i=1}^{N} s_i \frac{2r_{i,j}}{\sigma^2}, \\ &= \sum_{i=1}^{N} s_i \Lambda_D(c_{i,j}). \end{aligned} \tag{2.44}$$

In the IDMA scheme shown in Figure 2.4 the decoder passes the extrinsic LLR of the coded bits (Λ_E^{DEC}) back to the IC in the next iteration. Therefore it is necessary to compute the extrinsic information of the coded bits, $\Lambda_E(c_{i,j})$. The

extrinsic LLR for a coded bit $c_{n,j}$ within $s_i d[j]$ is defined by,

$$\Lambda_E(c_{i,j}) \equiv \ln\left(\frac{\Pr\{c_{i,j}=+1|\mathbf{r}\}}{\Pr\{c_{i,j}=-1|\mathbf{r}\}}\right) - \Lambda_A(c_{i,j}). \tag{2.45}$$

We notice that $c_{i,j} = +1$ if $s_i = d[j]$ and $c_{i,j} = -1$ otherwise. Therefore we have [16],

$$\Lambda_E(c_{i,j}) = s_i \Lambda_D(d[j]) - \Lambda_A(c_{i,j}). \tag{2.46}$$

2.7 Coded System

In this Section we show simulation results of the described IDMA system, operating with two different FEC coding schemes, namely, a repetition code and a convolutional code concatenated with a repetition code. The performance results are demonstrated on an AWGN channel where the total number of users is $K = 16$ and the outer code rate is 1/16 in each case. The performance of an IDMA receiver using a rate 1/16 repetition code is shown in Figure 2.11. The BER result for the rate 1/8 repetition code concatenated with a rate 1/2 $(7,5)_8$ CC code is shown in Figure 2.12. The bit error rate (BER) performance after one, five and ten iterations is shown in each case. The power of the IDMA receiver is evident from the figure, the fully loaded multiuser scheme is compared to the single-user bound (where $K = 1$). Thus the principle of IDMA is demonstrated. The results show that users are able to share cellular system resources without performance degradation.

2.8 Summary

This Chapter described in detail the general system model used in this thesis. We first described the basic model for iterative multiuser detection. Interleave-division multiple-access was introduced and contrasted with the traditional multiuser DS/CDMA receiver technique. The receiver technique for IDMA was developed in detail. The FEC coding schemes utilised with IDMA in this thesis were described in detail. We mainly focused upon the CC and turbo codes concatenated with repetition codes. Finally, the performance results for IDMA receiver utilising the afore-mentioned codes were presented.

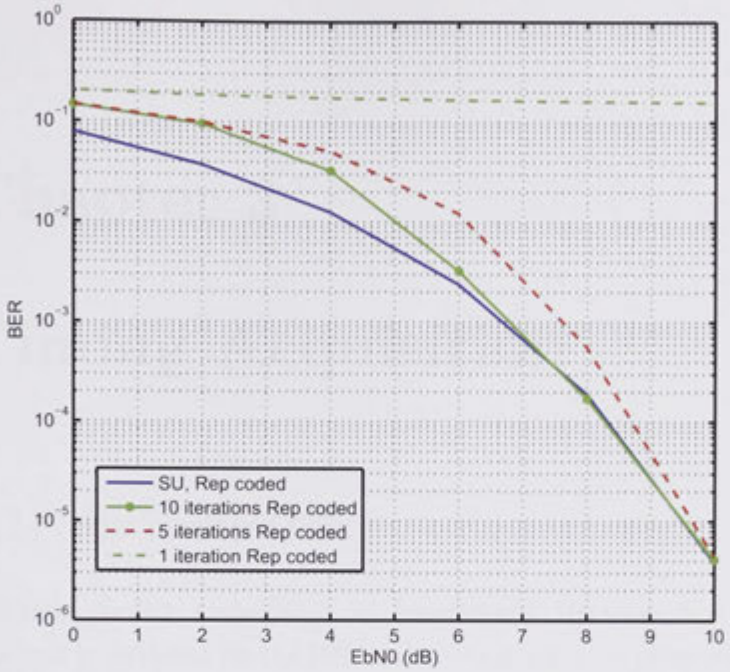

Figure 2.11: Performance results for rate 1/16 repetition coded IDMA system

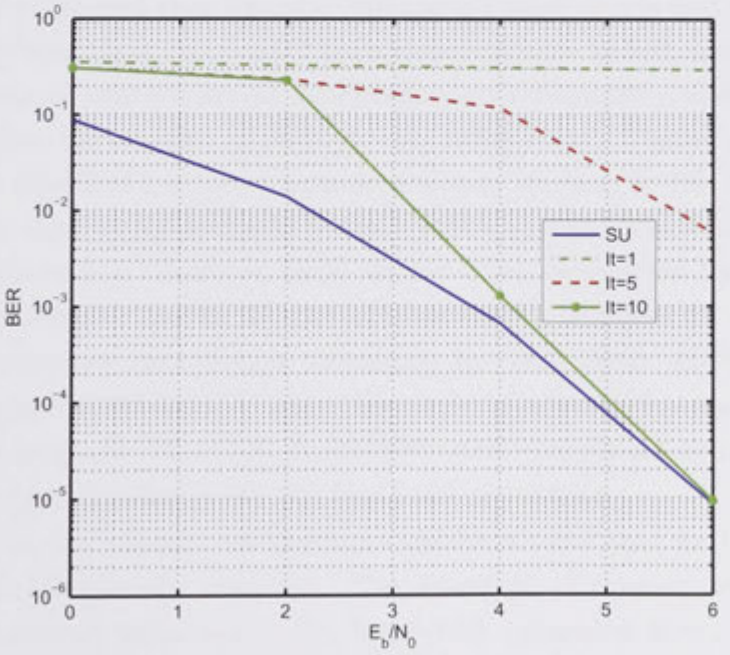

Figure 2.12: Performance results for IDMA using concatenated rate 1/8 repetition code and $(7,5)_8$ CC

Chapter 3

Timing Acquisition

3.1 Introduction

Efficient timing acquisition in Interleaved Division Multiple Access (IDMA) systems is essential for the IDMA detection schemes presented in literature [10–12] are typically chip synchronous. Timing is the first parameter that needs to be estimated in a receiver. The objective of any acquisition function is to determine the chip timing to within a half a chip interval, such that a tracking unit can refine the estimated chip timings. Minimising false alarms and missed detections are also important functions of the acquisition unit. In fully loaded systems with high levels of multiple access interference, poor acquisition performance can severely reduce the capacity of multiple user systems [46]. Timing acquisition techniques for DS-CDMA systems have been widely studied. In [40, 41] the authors define the capacity of multiple access CDMA systems while maintaining acceptable performance. However, these studies often assume low levels of multiple-access interference. In [46, 47] the authors develop a model for acquisition using soft interference cancellation techniques for DS-CDMA. IDMA can be seen as a variant of DS-CDMA where the order of interleaving and spreading functions are swapped. Therefore we are motivated to apply acquisition techniques similar to those detailed in [46, 47] for IDMA acquisition.

In this Chapter we develop acquisition techniques for IDMA that operate in high interference scenarios. The situations of interest are those in which the number of users equals the bandwidth expansion factor (inverse of the FEC code rate). Since IDMA has been shown to outperform CDMA under high MAI scenarios [10], we expect that acquisition techniques for IDMA using interference cancellation will outperform those for CDMA [47], in terms of probability of false

alarms and missed detections for the same E_b/N_0 and system load.

We describe here a data directed acquisition system where the intermediate decoding information is used to assist detecting new users. This method is commonly known as soft interference cancellation. The method is independent of the specific acquisition technique [47], however for analysis and simulation in this Chapter we use the simple correlator techniques [160].

3.2 System Model

We employ a repetition coded IDMA system [10, 12] where K users transmit QPSK symbols $d_k[n]$. In the model user k is allocated the random interleaver π_k. The model assumes that a new user attempting to connect to the system, transmits a known preamble of N chips (as in 3GPP [136]). Now we are interested in two scenarios of operation; (i) the on-time point where the new user is transmitting a preamble and the receiver's correlator is synchronised with the transmitted preamble, and (ii) the off-time points, where either there is no user attempting to connect, or the new user's preamble is not synchronised with the receiver correlator.

In the on-time the sum of all users transmitted signals at chip interval j according to the amended IDMA model of (2.3) is then,

$$y_{\text{on}}[j] = \sum_{k=1}^{K} h_k x_k[j] + h_{K+1} x_{K+1}[j], \tag{3.1}$$

where $x_k[j] = x_k^{\text{Re}}[j] + \text{i}x_k^{\text{Im}}[j]$,

$$x_{K+1}[j] = \begin{cases} s_{K+1}[j] + \text{i}s_{K+1}[j], & 1 \leq j \leq N, \\ 0, & \text{otherwise}, \end{cases} \tag{3.2}$$

is the preamble for user $K+1$ and is a complex unique spreading sequence where $s_{K+1}[j] \in \pm\frac{1}{\sqrt{N}}$, we assume that uniform power control (as is commonly the case in 3GPP systems [54, 136]) is employed for users connected to the system such that $h_k = 1, \forall k \in \{1, \ldots, K\}$ and $h_{K+1} = h_{K+1}^{\text{Re}} + \text{i}h_{K+1}^{\text{Im}}$ is the channel coefficient of the new user's channel.

During the off-time points we make the general assumption that the preamble x_{K+1} has a negligible autocorrelation function compared with the MAI plus noise at the receiver. Furthermore, it is expected that the time duration over which

there is no new user attempting to connect to the system is far greater than the duration of the asynchronous preamble being received. Therefore during the off-time the new user's preamble can be ignored and the sum of transmitted signals is then,

$$y_{\text{off}}[j] = \sum_{k=1}^{K} h_k x_k[j]. \tag{3.3}$$

The channel model described in (2.14) adds zero mean complex white Gaussian noise (AWGN) with variance $\sigma^2 = N_0/2$, where N_0 is the single sided noise power spectral density. The channel output during the on-time is therefore,

$$\begin{aligned} r_{\text{on}}[j] &= \sum_{k=1}^{K} x_k[j] + h_{K+1} x_{K+1}[j] + n[j] \\ &= \zeta_{K+1}[j] + h_{K+1} x_{K+1}[j], \end{aligned} \tag{3.4}$$

and during the off-time is,

$$\begin{aligned} r_{\text{off}}[j] &= \sum_{k=1}^{K} x_k[j] + n[j] \\ &= \zeta_{K+1}[j]. \end{aligned} \tag{3.5}$$

The first term in (3.4) describes K interfering users where the MAI plus noise is $\zeta_{K+1}[j]$ (defined in (2.4)) and the second term is the signal of the new user, whereas (3.5) is only the MAI plus noise. Without loss of generality synchronous chip timing is assumed, therefore square chip pulses are used. As random spreading codes are used the same result would be expected for a symbol asynchronous system. We assume that the effects of carrier frequency offset are negligible over the period of the preamble sequence, as this is generally the case for practical frequency offsets. The system model also assumes no multipath, however, assuming the system is power constrained and because of the use of random codes, the interference levels would be similar [47], therefore little difference would be expected in the performance results. The system assumes no time variation during acquisition, such as time drift or change in channel conditions, as the effects of these would also be negligible over the duration of the preamble sequence. The model also assumes that users already connected to the system (user's with index, $k = 1, \ldots, K$) have synchronised timing and carrier frequency, as they can be continuously tracked after the initial acquisition

process.

3.3 Acquisition with Iterative MUD under High MAI

In conditions where the number of users (K) equals the spreading gain (N) traditional code acquisition techniques based on correlating techniques fail [40]. This is because the MAI is too severe, resulting in low cross-correlation between the correlator and the desired signal. As a direct result acquisition performance suffers from noise and interference from other users. In the uplink of a mobile cellular system the base station receiver is assumed to use an IDMA multiuser receiver [10]. The conventional IDMA receiver computes soft information of all users being detected. These signals cause the MAI in the acquisition module, which is looking for users not yet known to the receiver.

Initially the base station is turned on and no terminals are connected, over time users connect and disconnect. The receiver estimates the transmitted signals from all connected users, using the known channel state information. If the receiver cancels estimated data of all connected users from the received baseband signal, what is left is system noise, residual interference, and signals from unknown users. The received data from connected users must meet frame error rate requirements, therefore their data estimates are accurate enough to be used for interference cancellation. If this was not the case then the user would be dropped as part of the Radio Link Control functionality [47].

We assume the received spread signal, $r[j]$, now consists of both signals that are being tracked by the receiver $\mathrm{E}\{\zeta_{K+1}[j]\}$, and during the on-time, the desired user's signal, $x_{K+1}[j]$. The decision directed approach then computes a residual term during the on-time,

$$\eta_{\mathrm{on},K+1}[j] = r_{\mathrm{on}}[j] - \mathrm{E}\{\zeta_{K+1}[j]\}, \tag{3.6}$$

or during the off-time the residual term is,

$$\eta_{\mathrm{off},K+1}[j] = r_{\mathrm{off}}[j] - \mathrm{E}\{\zeta_{K+1}[j]\}. \tag{3.7}$$

Note that the chip values of $\eta_{K+1}[j]$ during the on or off times, are taken over the length of the preamble, N.

The added complexity of computing either $\eta_{\mathrm{on},K+1}[j]$ or $\eta_{\mathrm{off},K+1}[j]$ is very low

due to the use of an IDMA IMUD. Figure 3.1 shows the implementation of the IDMA acquisition unit. Essentially the idea is that soft information from the IMUD, which is the estimate of the MAI is subtracted from the received signal. If the receivers estimation is perfect the remaining signal only contains noise and signal from new users. A correlator can then be used to acquire these signals. It is clear that the performance of the system relies heavily on the performance of the IMUD. Figure 3.1 also highlights the need for a delay between input signal and the cancellation process. This is because the IMUD requires a certain amount of time to determine its estimate of the received signal.

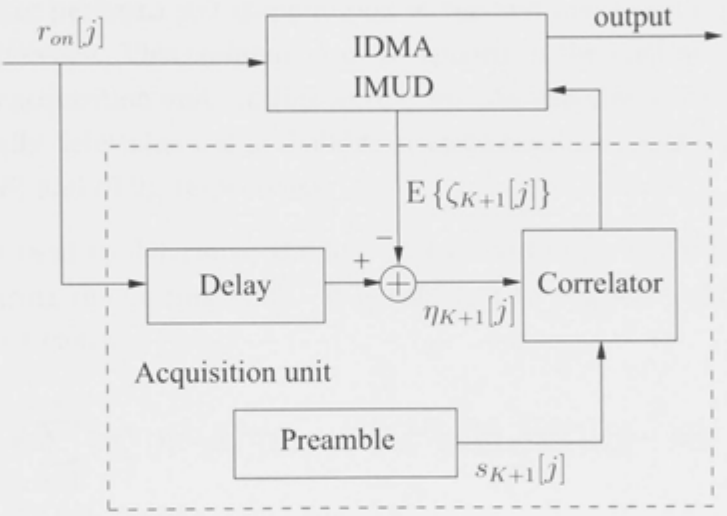

Figure 3.1: IDMA Receiver with Acquisition unit

In the correlator, the residual term given in either (3.6) or (3.7) is correlated with the desired user's signal, such that the timing position can be determined. This method enhances the conventional correlation approach by use of soft information. The resultant on-time signal can be written (Assuming that it is intended to determine the starting position of the preamble, x_{K+1}),

$$r_{\mathrm{on},p} = \sum_{j=1}^{N} \eta_{\mathrm{on},K+1}[j] s_{K+1}[j], \tag{3.8}$$

and during the off-time the correlation can be written as,

$$r_{\mathrm{off},p} = \sum_{j=1}^{N} \eta_{\mathrm{off},K+1}[j] s_{K+1}[j]. \tag{3.9}$$

3.4 Analysis

In this section the goal is to analyse the performance of the proposed system in terms of false alarm and missed detection probabilities. The false alarm probability (P_{fa}) is defined as the probability of the signal level being above the threshold where the timing point is incorrect. The missed detection probability (P_{md}) is defined as the probability of the signal level being below the threshold when the timing point is correct. This result is parameterised on the number of users, processing gain, noise variance and the cancellation factor of the system. In [10] the IDMA detector performs soft computation of the first and second order statistics of the interference. This technique can be applied in the realisation of the above mentioned acquisition unit. In this section we take this result one step further and analytically determine the probability density functions of the cross correlation terms (3.8) and (3.9), respectively.

To start with we need to determine the first and second order statistics of the residual term during the on-time (3.6). It is sufficient to consider only the distribution of the real metric,

$$\begin{aligned}
\eta^{Re}_{\text{on},K+1}[j] &= \sum_{k=1}^{K} \left(x^{Re}_k[j] - \tilde{x}^{Re}_k[j]\right) + \left(h^{Re}_{K+1} - h^{Im}_{K+1}\right) x^{Re}_{K+1}[j] + n[j], \\
\mathrm{E}\left\{\eta^{Re}_{\text{on},K+1}[j]\right\} &= \left(h^{Re}_{K+1} - h^{Im}_{K+1}\right) s_{K+1}[j], \\
\mathrm{Var}\left\{\eta^{Re}_{\text{on},K+1}[j]\right\} &= \sum_{k=1}^{K} \|s_k[j]\|^2 \,\mathrm{E}\left\{\left(x^{Re}_k[j] - \tilde{x}^{Re}_k[j]\right)^2\right\} + \sigma_n^2, \\
&= K\sigma_x^2 + \sigma_n^2, \\
&= \frac{K}{N}\sigma_d^2 + \sigma_n^2. \qquad (3.10)
\end{aligned}$$

where $\tilde{x}^{Re}_k$ is the soft information of x^{Re}_k, $\sigma_d^2 = \frac{1}{N}\sigma_x^2$, is the symbol variance function, since the coded chips (x_k) are encoded using a rate $1/N$ repetition code.

Thus, the distribution of the on-time residual term given in (3.6) can be approximated by a complex Gaussian distribution with mean, $\mu_\eta = \left(h^{Re}_{K+1} - h^{Im}_{K+1}\right) s_{K+1}[j] + \mathrm{i}\left(h^{Re}_{K+1} + h^{Im}_{K+1}\right) s_{K+1}[j]$ and variance, $\sigma_\eta^2 = \frac{K}{N}\sigma_d^2 + \sigma_n^2$ in each dimension.

We can apply a similar technique to determine the statistics of the off-time

residual term given in (3.7),

$$\begin{aligned}
\eta^{Re}_{\text{off},K+1}[j] &= \sum_{k=1}^{K} \left(x^{Re}_k[j] - \tilde{x}^{Re}_k[j]\right) + n[j], \\
\mathrm{E}\left\{\eta^{Re}_{\text{off},K+1}[j]\right\} &= 0, \\
\mathrm{Var}\left\{\eta^{Re}_{\text{off},K+1}[j]\right\} &= \frac{K}{N}\sigma_d^2 + \sigma_n^2.
\end{aligned} \tag{3.11}$$

3.4.1 Analysis of Off-time Density

We now develop a method to determine the density of the off-time signal, that is, where the correlator sequence is not time matched with the transmitted sequence or when there is no transmitted preamble. We know that the distribution of $\eta^{Re}_{\text{off},K+1}[j]$ is a complex Gaussian distributed random variable. Now we wish to determine the statistics of the cross correlation term (3.9). According to the central limit theorem, $r_{\text{off},p}$, can be seen as a complex Gaussian random variable. We first determine the distribution of the term $r^{\text{Re}}_{\text{off},p}$ by computing its mean and variance,

$$\begin{aligned}
\mathrm{E}\left\{r^{Re}_{\text{off},p}\right\} &= \mathrm{E}\left\{\mathrm{Re}\left\{\sum_{j=1}^{N} \eta_{\text{off},K+1}[j]x_{K+1}[j]\right\}\right\}, \\
&= 0, \\
\mathrm{Var}\left\{r^{Re}_{\text{off},p}\right\} &= \sum_{j=1}^{N} \mathrm{Var}\left\{\mathrm{Re}\left\{x_{K+1}[j]\eta_{\text{off},K+1}[j]\right\}\right\}, \\
&= \frac{K\sigma_d^2}{N} + \sigma_n^2.
\end{aligned} \tag{3.12}$$

Thus, the real valued distribution is given by,

$$f_{r^{\text{Re}}_{\text{off},p}}(r) = \frac{1}{\sqrt{2\pi\sigma^2_{r^{\text{Re}}_p}}} \exp\left(-\frac{r^2}{2\sigma^2_{r^{\text{Re}}_p}}\right), \tag{3.13}$$

where $\sigma^2_{r^{\text{Re}}_{\text{off},p}} = \mathrm{Var}\left\{r^{\text{Re}}_{\text{off},p}\right\}$, and the imaginary distribution $f_{r^{\text{Im}}_{\text{off},p}}(r)$ is given by a similar density function. Utilising a result in [161] the term $\|r_{\text{off},p}\|$ is given by a Rayleigh distribution, with parameter, $\sigma^2_{\text{off}} = \sigma^2_{r_p}$,

$$f_{\|r_{\text{off},p}\|}(r) = \frac{r}{\sigma^2_{\text{off}}} \exp\left(-\frac{r^2}{2\sigma^2_{\text{off}}}\right). \tag{3.14}$$

We have now developed the so-called "off-time" density as a function of the number of users, K, the spreading factor N, the noise variance σ_n^2, the variance of the soft output estimator σ_d^2 and a threshold value of r_p. This density will be later used to determine the false alarm probability (P_{fa}).

3.4.2 Analysis of On-time Density

We now derive the on-time density. The real valued Gaussian distribution of the peak correlation function during on-time is given in (3.16). The first and second order statistics of $r_{\text{on},p}^{Re}$ can be computed as,

$$\begin{aligned}
\mathrm{E}\left\{r_{\text{on},p}^{\text{Re}}\right\} &= \mathrm{E}\left\{\mathrm{Re}\left\{\sum_{j=1}^{N}\eta_{\text{on},K+1}[j]x_{K+1}[j]\right\}\right\}, \\
&= h_{K+1}^{Re} - h_{K+1}^{Im}, \\
\mathrm{Var}\left\{r_{\text{on},p}^{\text{Re}}\right\} &= \sum_{j=1}^{N}\mathrm{Var}\left\{\mathrm{Re}\left\{x_{K+1}[j]\eta_{\text{on},K+1}[j]\right\}\right\}, \\
&= \frac{K\sigma_d^2}{N} + \sigma_n^2. \qquad (3.15)
\end{aligned}$$

Therefore, the term $r_{\text{on},p}^{Re}$ has real-time density function given by,

$$f_{r_{\text{on},p}^{Re}}(r) = \frac{1}{\sqrt{2\pi\sigma^2_{r_{\text{on},p}^{\text{Re}}}}}\exp\left(-\frac{\left(r-(h_{K+1}^{Re}-h_{K+1}^{Im})\right)^2}{2\sigma^2_{r_{\text{on},p}^{\text{Re}}}}\right), \qquad (3.16)$$

where $\sigma^2_{r_{\text{on},p}^{\text{Re}}} = \mathrm{Var}\left\{r_{\text{on},p}^{\text{Re}}\right\}$.

This density represents the random variable in the real axis, a similar density function can be found for the imaginary axis as,

$$f_{r_{\text{on},p}^{Im}}(r) = \frac{1}{\sqrt{2\pi\sigma^2_{r_{\text{on},p}^{\text{Im}}}}}\exp\left(-\frac{\left(r-(h_{K+1}^{Re}+h_{K+1}^{Im})\right)^2}{2\sigma^2_{r_{\text{on},p}^{\text{Im}}}}\right), \qquad (3.17)$$

where $\sigma^2_{r_{\text{on},p}^{\text{Im}}} = \sigma^2_{r_{\text{on},p}^{\text{Re}}}$.

To convert this to a density which represents the absolute value of the signal we utilise a result the Rician distribution [161]. Therefore the "on-time" distribution is,

$$f_{\|r_{\text{on},p}\|}(r) = \frac{r}{\sigma^2_{\text{on}}}\exp\left(-\frac{r^2+s^2}{2\sigma^2_{\text{on}}}\right)\mathrm{I}_0\left(\frac{rs}{\sigma^2_{\text{on}}}\right), \qquad (3.18)$$

where $\sigma_{\text{on}} = \frac{K\sigma_d^2}{N} + \sigma_n^2$, $s^2 = 2\|h_{K+1}\|^2$ and $\mathrm{I}_0(\cdot)$ is the zero order modified Bessel function of the first kind.

3.4.3 False alarm / Missed Detection probabilities

Now we have derived the probability densities we wish to integrate these functions to determine the probabilities of the missed detection and false alarms. This means we need to integrate (3.18) from $0 \rightarrow$ a to determine the probability of missed detection, where a is the detection threshold used to acquire a new user. Similarly, we need to integrate (3.14) from a $\rightarrow \infty$ to the determine probability of false alarm. Starting first with (3.18),

$$\begin{aligned} \mathrm{P}_{md} &= \Pr(0 < R < a), \\ &= \int_0^a \frac{r}{\sigma_{\text{on}}^2} \exp\left(-\frac{r^2+s^2}{2\sigma_{\text{on}}^2}\right) \mathrm{I}_0\left(\frac{rs}{\sigma_{\text{on}}^2}\right) dr. \end{aligned} \tag{3.19}$$

The probability of missed detection is therefore the CDF of the Rician density given (3.18) which is given in [161] as,

$$\mathrm{P}_{md} = 1 - \mathrm{Q}_1\left(\frac{s}{\sigma_{\text{on}}}, \frac{a}{\sigma_{\text{on}}}\right), a \geq 0, \tag{3.20}$$

where $\mathrm{Q}_1(\cdot)$ is the generalised Marcum's Q function where $m = \frac{n}{2} = 1$ as the degrees of freedom is $n = 2$. We now derive the probability of false alarm by integrating the Rayleigh distribution from (3.14), therefore

$$\begin{aligned} \mathrm{P}_{fa} &= \Pr(R > a), \\ &= \exp\left(-\frac{a^2}{2\sigma_{\text{off}}^2}\right). \end{aligned} \tag{3.21}$$

3.4.4 Determining Residual Interference

The residual interference from the IMUD receiver will determine the performance of the acquisition unit. The purpose of this section is to determine a typical residual interference level (σ_d^2), in order to achieve the expected performance of the system. The typical frame error rate (FER) that maximises capacity in a cellular environment has been arguably shown to be approximately FER=0.1 [136]. We assume that the bit error rate is equal to or lower than 10^{-4}, based on a block size of 1000. We represent the soft values prior to a decision as Gaussian

distributed random variables, where $\Pr(d_k[n] < 0 | d_k[n] = +1) = \mathrm{P}_e = \mathrm{BER}$. We now wish to determine σ_d^2 in terms of P_e using the assumption above and that IDMA achieves single user performance. We know from [161] that,

$$\sigma_d = \frac{\sqrt{\varepsilon_b}}{\mathrm{Q}^{-1}(\mathrm{P}_e)}. \tag{3.22}$$

Therefore for a probability of error, $\mathrm{P}_e = 3.87 \times 10^{-6}$ the variance estimate is $\sigma_d^2 = 0.05$ for an $E_b/N_0 = 10$dB, and for a $\mathrm{P}_e = 7.27 \times 10^{-4}$ the variance estimate is $\sigma_d^2 = 0.1$ corresponding to an $E_b/N_0 = 7$dB. From simulation we validated the theoretical computation of σ_d in (3.22) as compared with the cancellation factor (σ_d) during simulation. This is expected under good channel conditions where the IDMA IMUD achieves near single user performance. We will utilise these figures to determine expected performance of the acquisition approach defined.

3.5 Analytical and Numerical performance results

In this section we show results from both our analytical development and from our simulation. The simulation consists of transmitting 2000 blocks where the codes/interleavers for the multiple access interference are randomly selected for each user. In all cases the spreading gain was chosen to be $N = 16$ and the IDMA receiver was run for 10 iterations. However, it has been shown that IDMA has equivalent or better performance as N increases due to the increased interleaver lengths (resulting in better turbo decoding performance). The system is chip and symbol synchronous and we normalise the energy of the channel for user $K+1$ such that $\|h_{K+1}\|^2 = 1$. Note that it is possible to simulate the results for a Rayleigh fading channel by marginalising the probabilities of missed detection and false alarm in (3.19) and (3.21), over the distribution of h_{K+1}. For the purpose of illustration we deem that it is sufficient to consider a normalised channel power, i.e. $\|h_{K+1}\|^2 = 1$.

Figure 3.2 shows the on and off-time distributions for three different scenarios at an $E_b/N_0 = 7$dB. The first plot is the single user(SU) scenario, here the on-time density is centered around $\sqrt{2}$ and is Rician distributed while the off-time distribution is centered around $\frac{1}{2\sqrt{2}}$ and is Rayleigh distributed. For the single user case there is a distinct separation between the two densities, for example, a threshold set around a = 0.85 would provide both a low false alarm probability

and a low missed detection probability. In practical systems the threshold is determined for a particular P_{fa}, this sets the amount of time the receiver will be occupied processing false alarms. The choice of a determine the trade-off between false alarms and missed detections.

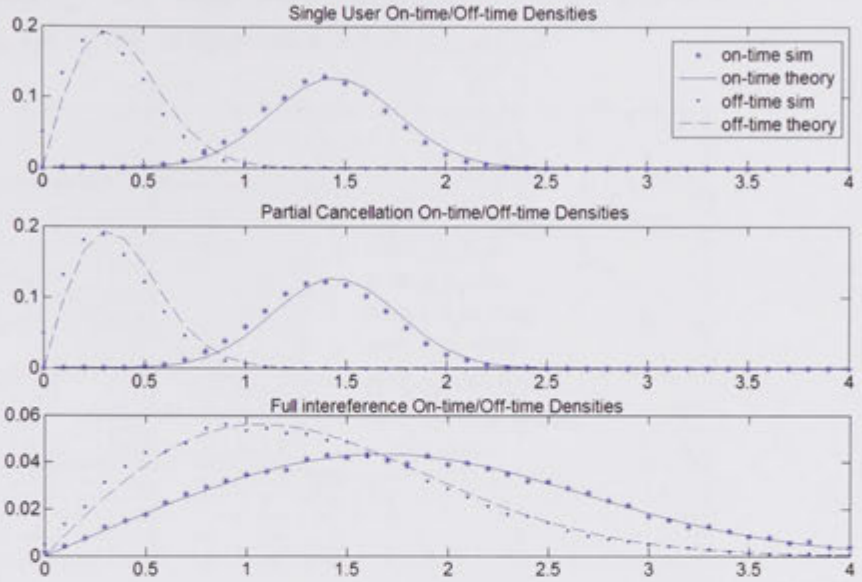

Figure 3.2: On-off densities for different scenarios

In the last subplot the densities for the full interference(FI) case with K = 16 users in the system is shown. The full interference case is where no soft information is used for interference cancellation ($\tilde{d}_{K+1}[n] = 0$). As such the acquisition unit suffers from severe MAI. It is clear that a logical threshold point is not achievable as the on and off-time densities are not separated, this will also be seen later in Figure 3.3. In the second subplot the densities for K = 16 are shown, however partial cancellation (PC) is used where $\sigma_d^2 = 0.1$. It can be seen that the resultant densities are significantly improved such that they are equally as distinct as the single user case due to the near single user performance of the IDMA IMUD [10]. This is where an IDMA IMUD outperforms CDMA, resulting in better IC (better cancellation factor σ_d^2) for heavily loaded multiple user systems. For the same reasons it is expected that it is possible to perform acquisition (with near single user performance) for overloaded systems using the IDMA IMUD.

In Figure 3.3 we show the performance of the full interference and two partial cancellation cases ($\sigma_d^2 = 0.1$ and $\sigma_d^2 = 0.05$). We compare the analytical result (solid line) to the simulation results (points). The plot is for an integration period

of 1 symbol, with $E_b/N_0 = 7$dB for $\sigma_d^2 = 0.1$ and $E_b/N_0 = 10$dB for $\sigma_d^2 = 0.05$. As can be seen the performance of the partial cancellation scheme is substantially better than that of the fully loaded system without cancellation. For example fixing $P_{fa} = 10^{-4}$ the partial cancellation results are $P_{md} = 0.03$ and $P_{md} = 0.5$ for $\sigma_d^2 = 0.05$ and $\sigma_d^2 = 0.1$ respectively. In comparison to the fully loaded system where $P_{md} = 1$, i.e. 100% of detections would be missed.

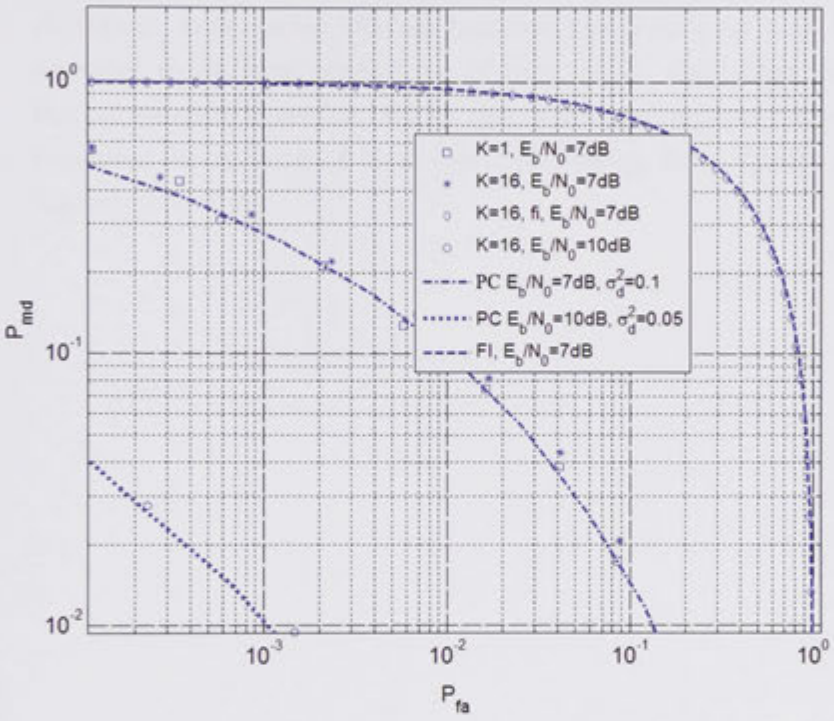

Figure 3.3: Performance of the Acquisition unit

3.6 Summary

In this Chapter we have investigated an acquisition technique based on soft interference cancellation applied to IDMA. This has been performed under severe multiple access interference.

We derived density functions to represent the so-called on-time and off-time random variables and compared these densities to simulation results. These densities are functions of the number of users, the processing gain, the cancellation factor and the noise variance. We integrated these densities to determine the probability of false alarm and probability of missed detection, as a function of

threshold value. We compared both analytical results and simulation results for P_{fa} vs. P_{md} for $K = 16$ users with partial cancellation from the IDMA receiver. The results show that acquisition using conventional correlation techniques for CDMA is not practical when the number of users equals the spreading gain, however, when utilising the IDMA IMUD good performance of a conventional correlator for acquisition is possible.

It is demonstrated in this Chapter that for high performance multiuser detection, information sharing between the correlator unit and the receiver is essential to perform acquisition of new users. Depending on the reliability of the information from the IMUD, this technique improves the system capacity by reducing the amount of time spent processing false alarms and the number of missed detections.

Chapter 4

Timing Tracking

4.1 Introduction

Heavily loaded IDMA systems, where the number of users (or layers) is much greater than the spreading gain are necessary in order to accommodate the need for higher data rates and increased capacity of future wireless broadband systems. The performance of acquisition algorithms can be severely degraded by the effects of severe multiple access interference. Efficient acquisition and tracking of the timing information for each user is essential for the IDMA detection to work. The synchronisation function is essential to track the chip timings, such that the interleavers for each user are synchronous with the user's data.

Conventional timing tracking/synchronisation techniques for DS-CDMA systems involve pilot aided timing recovery using code-locked loops which have been widely studied [50, 61]. Although iterative timing synchronisation techniques have been studied for single user turbo-coded systems, they have not been applied to CDMA or IDMA systems, where they result in significant performance improvements for severe drift scenarios. To the best of our knowledge timing tracking for IDMA systems has not been simulated or analysed before. The interference canceller in a heavily loaded IDMA system operates at a very low SNR due to the nature of the chip-by-chip processing required. It can been shown by experimentation that in fully loaded systems with high levels of multiple access interference, poor acquisition performance can severely reduce the capacity of multiple user systems [48]. The severity of the multiple access interference is increased by the fact that pilot channel has much lower power than the data channel in most practical systems (for example 3GPP [54]).

In this Chapter we develop a theoretical framework for soft data aided

turbo synchronisation techniques for multiuser IDMA systems that operate in high multiple access interference. We construct an iterative soft data aided synchronisation system for IDMA where the intermediate soft information is used to assist the task of synchronisation on each iteration. We use MMSE combining to fuse timing estimates from the pilot and data channels respectively in order to construct the optimal timing error discriminator (TED). We justify our analysis by providing simulation results for an IDMA receiver where there is a very large timing drift at the receiver. We compare the iterative approach with a conventional single-shot timing recovery circuit.

4.2 System Model

In order to design the tracking algorithm we provide an amended transmitter model to the one given in Chapter 2. In this Chapter we consider a chip asynchronous IDMA model where each user uses QPSK modulation. The quadrature carrier is a dedicated pilot channel used for synchronisation of the carrier frequency and timing respectively. Without loss of generality, we assume that the channel phase, channel amplitude, and carrier frequency are perfectly known in the model and we focus upon timing synchronisation. The amended transmitter model for a particular user (user k) is shown in Figure 4.1. For simplicity the FEC used is a repetition code with a scrambling mask (alternating ± 1)[12], although the technique is essentially independent of the FEC code used. A user specific interleaver is applied to the chip sequence resulting in the interleaved chip sequence ($x_k^{\mathrm{Re}}[j]$). A user specific random sequence of pilot chips ($p_k[j]$) is superimposed with the data chip sequence using the quadrature carrier. The combined signal is given by,

$$x_k[j] = \sqrt{E_d} x_k^{\mathrm{Re}}[j] + \mathrm{i}\sqrt{E_p} p_k[j], \tag{4.1}$$

where $\sqrt{E_p}$ denotes the power of the pilot chips and $\sqrt{E_d}$ the power of the data chips respectively. After this the signal ($x_k[j]$) is up-sampled by a rate of M samples per chip and pulse shaped using a square root raised cosine pulse shaping filter $g[m]$ with roll-off factor, α, as proposed in the 3GPP standards [53, 54]. The pulse shaped signal for user k, ($z_k[m] = a_k[m] + \mathrm{i}b_k[m]$), is transmitted through a frequency flat complex AWGN channel with channel coefficient h_k. In this Chapter the index m is used for signals sampled at the sample rate whereas index j is used for signals sampled at the chip rate. We assume that fast power

control is employed such that each users channel has equal power, nominally $\|h_k\| = 1$. Each users signal is subjected to a different timing drift $\{\tau_k(t)\}$. All the users signals are superimposed and then AWGN noise, $n(t)$, with single sided power spectral density $N_0/2$ (and variance σ_n^2) is added to the received signal,

$$r(t) = \sum_k h_k z_k(t - \tau_k(t)) + n(t), \tag{4.2}$$

where $z_k(t) = \sum_n x_k[j] g(t - jT_c)$, and the SRRC pulse shaping function is given by,

$$g\left(\frac{t}{T_c}\right) = \frac{\sin\left(\frac{\pi t(1-\alpha)}{T_c}\right) + 4\alpha t \cos\left(\frac{\pi t(1-\alpha)}{T_c}\right)/T_c}{\pi t\left(1 - \left(\frac{4\alpha t}{T_c}\right)^2\right)/T_c}. \tag{4.3}$$

The matched filtered pulse shape denoted as, $R_g(t/T_c) \triangleq g(t/T_c) * g(-t/T_c)$ is written as,

$$R_g\left(\frac{t}{T_c}\right) = \frac{\sin(\pi t/T_c)}{\pi t/T_c} \frac{\cos(\alpha\pi t/T_c)}{1 - (2\alpha t/T_c)^2}. \tag{4.4}$$

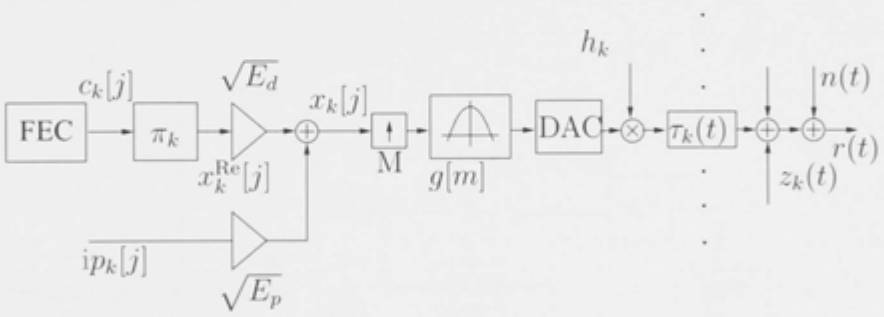

Figure 4.1: The IDMA transmitter for the kth user

In this Chapter we consider two synchronisation techniques: (1) conventional timing recovery where the timing of the chips of each user is estimated once; (2) iterative timing recovery where the timing for each user is refined after every iteration of the decoder. In the first approach the timing of each user is tracked once only, the timing information for each user is then passed to the chip asynchronous IC as seen in Figure 4.2. In the second approach the timing information is renewed after each iteration of decoding as can be seen in Figure 4.3. Both techniques essentially pass chip timing information to the IC in the same manner. Considering that each user is chip asynchronous it is important that the IC be chip asynchronous, which takes as input the chip timing vector $\{\hat{\tau}_k\}$. We dedicate the proceeding Section to the chip asynchronous IC, and then

the following Section to the timing synchronisation algorithms.

Throughout this Chapter the rounded brackets denote continuous time indexing of a signal and square brackets denote discrete time indexing respectively.

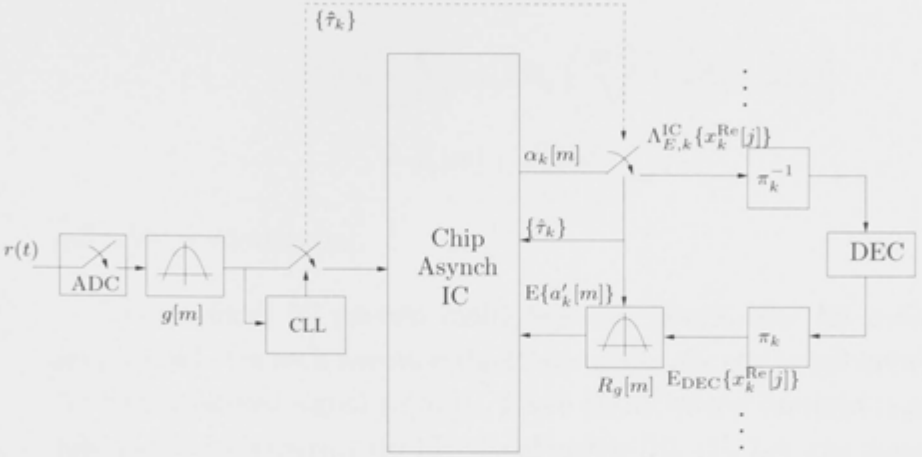

Figure 4.2: The IDMA receiver for the kth user with chip asynchronous IC and one-shot conventional timing recovery

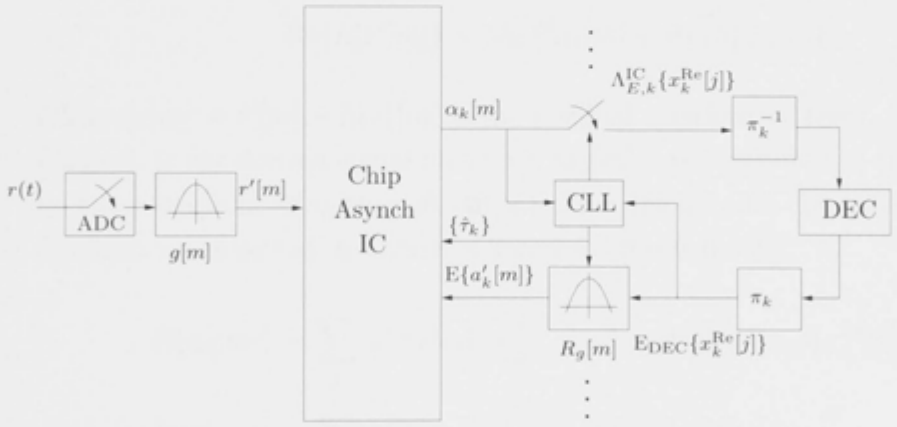

Figure 4.3: The IDMA receiver for the kth user with chip asynchronous IC iterative timing recovery

4.3 The Chip Asynchronous IC

The received signal given in (4.2) is oversampled at a rate of M samples per chip, and then match filtered with the Square Root Raised Cosine (SRRC) pulse shape

filter as illustrated in Figures 4.2 and 4.3 respectively. The oversampled received signal is,

$$r'[m] = \sum_k h_k z'_k[m] + w[m], \tag{4.5}$$

where,

$$z'_k[m] = \sum_j x_k[j] R_g \left(\frac{mT_c}{M} - jT_c - \tau_k[j] \right) \tag{4.6}$$

$$= a'_k[m] + \mathrm{i} b'_k[m], \tag{4.7}$$

and $w[m] = n[m] * g[m]$.

The modified IC cancels multiple-access interference for each user at the sample level. On each iteration the IC computes the statistical information about the match filtered signal ($z'_k[m]$). These statistics are sampled using the timing information to construct the likelihood metric [10, 12]. Let, the channel coefficient be represented as $h_k = h_k^{\mathrm{Re}} + \mathrm{i} h_k^{\mathrm{Im}}$, and we denote h_k^* as the conjugate of h_k. In order to compute the log-likely hood ratio (LLR) for the coded bit sequence $x_k^{\mathrm{Re}}[j]$, we are required to determine statistical information about the term,

$$\mathrm{Re}\{h_k^* r'[m]\} = \|h_k\|^2 a'_k[m] + \mathrm{Re}\{h_k^* \zeta_k[m]\}, \tag{4.8}$$

where $\zeta_k[m] = r'[m] - h_k z'_k[m]$ is the residual interference term. The mean and variance of the desired signal for user k ($a'_k[m]$) are computed at the sample level by pulse shape filtering the soft outputs from the decoder (DEC) on the previous iteration (as depicted in Figures 4.2 and 4.3 respectively),

$$\mathrm{E}\{a'_k[m]\} = \sum_j \sqrt{E_d} \mathrm{R}_g \left(\frac{mT_c}{M} - jT_c - \hat{\tau}_k[j] \right) \mathrm{E}_{\mathrm{DEC}}\{x_k^{\mathrm{Re}}[j]\}, \tag{4.9}$$

$$\mathrm{E}\{b'_k[m]\} = \sum_j \sqrt{E_p} \mathrm{R}_g \left(\frac{mT_c}{M} - jT_c - \hat{\tau}_k[j] \right) p_k[j], \tag{4.10}$$

$$\mathrm{Var}\{a'_k[m]\} = \sum_j E_d \mathrm{R}_g^2 \left(\frac{mT_c}{M} - jT_c - \hat{\tau}_k[j] \right) \mathrm{Var}_{\mathrm{DEC}}\{x_k^{\mathrm{Re}}[j]\}, \tag{4.11}$$

$$\mathrm{Var}\{b'_k[m]\} \simeq 0, \tag{4.12}$$

where $\mathrm{E}_{\mathrm{DEC}}\{x_k^{\mathrm{Re}}[j]\}$ is the estimated soft information of the data chips from the outer decoder (DEC) and $\mathrm{Var}_{\mathrm{DEC}}\{x_k^{\mathrm{Re}}[j]\} = 1 - (\mathrm{E}_{\mathrm{DEC}}\{x_k^{\mathrm{Re}}[j]\})^2$ is the variance of the soft information. These two values are generated from the previous iteration

of the outer decoder in Figures 4.2 and 4.3.

In order to improve the estimate of a particular user's data and pilot signals ($\mathrm{E}\{a'_k[m]\}$ and $\mathrm{E}\{b'_k[m]\}$) the IC reconstructs the interference from all other users by first computing the statistics (mean and variance) for $r'^{\mathrm{Re}}[m]$ and $r'^{\mathrm{Im}}[m]$ respectively. The Algorithm 1 is amended using (4.9)-(4.12) as follows,

$$\mathrm{E}\{r'^{\mathrm{Re}}[m]\} = \sum_k h_k^{\mathrm{Re}}\mathrm{E}\{a'_k[m]\} - h_k^{\mathrm{Im}}\mathrm{E}\{b'_k[m]\}, \tag{4.13}$$

$$\mathrm{E}\{r'^{\mathrm{Im}}[m]\} = \sum_k h_k^{\mathrm{Im}}\mathrm{E}\{a'_k[m]\} + h_k^{\mathrm{Re}}\mathrm{E}\{b'_k[m]\}, \tag{4.14}$$

$$\mathrm{Var}\{r'^{\mathrm{Re}}[m]\} = \sum_k \Big((h_k^{\mathrm{Re}})^2\mathrm{Var}\{a'_k[m]\} + (h_k^{\mathrm{Im}})^2\mathrm{Var}\{b'_k[m]\}\Big) + \sigma_n^2, \tag{4.15}$$

$$\mathrm{Var}\{r'^{\mathrm{Im}}[m]\} = \sum_k \Big((h_k^{\mathrm{Im}})^2\mathrm{Var}\{a'_k[m]\} + (h_k^{\mathrm{Re}})^2\mathrm{Var}\{b'_k[m]\}\Big) + \sigma_n^2, \tag{4.16}$$

The statistics of the multiuser interference are now computed using (4.13-4.16). The covariance between $r'^{\mathrm{Re}}[m]$ and $r'^{\mathrm{Im}}[m]$, denoted $\Psi[m]$ is rewritten as,

$$\Psi[m] = \sum_k h_k^{\mathrm{Re}}h_k^{\mathrm{Im}}(\mathrm{Var}\{a'_k[m]\} - \mathrm{Var}\{b'_k[m]\}), \tag{4.17}$$

$$\begin{aligned}\mathrm{E}\{\mathrm{Re}\{h_k^*\zeta_k[m]\}\} &= h_k^{\mathrm{Re}}\mathrm{E}\{r'^{\mathrm{Re}}[m]\} + h_k^{\mathrm{Im}}\mathrm{E}\{r'^{\mathrm{Im}}[m]\} \\ &\quad - \|h_k\|^2\mathrm{E}\{a'_k[m]\},\end{aligned} \tag{4.18}$$

$$\begin{aligned}\mathrm{Var}\{\mathrm{Re}\{h_k^*\zeta_k[m]\}\} &= (h_k^{\mathrm{Re}})^2\mathrm{Var}\{r'^{\mathrm{Re}}[m]\} + (h_k^{\mathrm{Im}})^2\mathrm{Var}\{r'^{\mathrm{Im}}[m]\} \\ &\quad + 2h_k^{\mathrm{Re}}h_k^{\mathrm{Im}}\Psi[m] - \|h_k\|^4\mathrm{Var}\{a'_k[m]\}.\end{aligned} \tag{4.19}$$

The statistics of the interference for the imaginary component of $h_k^*r'[m]$ for the kth user can be computed in a similar manner, resulting in the terms $\mathrm{E}\{\mathrm{Im}\{h_k^*\zeta_k[m]\}\}$ and $\mathrm{Var}\{\mathrm{Im}\{h_k^*\zeta_k[m]\}\}$ respectively. Finally, the interference canceled signal for the real and imaginary components of $z'_k[m]$ are computed using (4.17)-(4.19), giving,

$$\alpha_k[m] = \mathrm{Re}\{h_k^*r'[m]\} - \mathrm{E}\{\mathrm{Re}\{h_k^*\zeta_k[m]\}\}, \tag{4.20}$$

$$\beta_k[m] = \mathrm{Im}\{h_k^*r'[m]\} - \mathrm{E}\{\mathrm{Im}\{h_k^*\zeta_k[m]\}\}, \tag{4.21}$$

$$\mathrm{E}\{z'_k[m]\} = \alpha_k[m] + \mathrm{i}\beta_k[m]. \tag{4.22}$$

Using the law of large numbers $\alpha_k[m]$ can be approximated as Gaussian distributed random variables with mean $a'_k[m]$ and variance $\mathrm{Var}\{\mathrm{Re}\{h_k^*\zeta_k[m]\}\}$.

Respectively $\beta_k[m]$ can be approximated as a Gaussian random variable with mean $b'_k[m]$ and variance $\mathrm{Var}\{\mathrm{Im}\{h_k^*\zeta_k[m]\}\}$. The Code Locked Loop (CLL) in either Figure 4.2 or Figure 4.3 is used to resample $\alpha_k[m]$ and $\beta_k[m]$ at the correct timing points. Using the afore mentioned Gaussian approximation and resampling technique the extrinsic LLR values for the coded chips ($x_k^{\mathrm{Re}}[j]$) and pilot chips ($p_k[j]$) can be computed,

$$\Lambda_{E,k}^{\mathrm{IC}}(x_k^{\mathrm{Re}}[j]) = 2\|h_k\|^2 \frac{\alpha_k(j\mathrm{T_c} + \hat{\tau}_k[j])}{\mathrm{Var}\{\mathrm{Re}\{h_k^*\zeta_k(j\mathrm{T_c} + \hat{\tau}_k[j])\}\}}, \tag{4.23}$$

$$\Lambda_{E,k}^{\mathrm{IC}}(p_k[j]) = 2\|h_k\|^2 \frac{\beta_k(j\mathrm{T_c} + \hat{\tau}_k[j])}{\mathrm{Var}\{\mathrm{Im}\{h_k^*\zeta_k(j\mathrm{T_c} + \hat{\tau}_k[j])\}\}}, \tag{4.24}$$

where $\hat{\tau}_k[j]$ is the estimate of the timing drift for chip j. The expectations of $x_k^{\mathrm{Re}}[j]$ and $p_k[j]$ are computed as,

$$\mathrm{E_{IC}}\left\{x_k^{\mathrm{Re}}[j]\right\} = \tanh(\Lambda_{E,k}^{\mathrm{IC}}(x_k^{\mathrm{Re}}[j])/2), \tag{4.25}$$

$$\mathrm{E_{IC}}\left\{p_k[j]\right\} = \tanh(\Lambda_{E,k}^{\mathrm{IC}}(p_k[j])/2). \tag{4.26}$$

Equations (4.9)-(4.26) are computed on every iteration of the IC. The DEC unit in Figures 4.2 and 4.3, follows exactly from the soft repetition decoder given in [12] which computes the extrinsic log-likely hood ratios for the coded chips $x_k^{\mathrm{Re}}[j]$.

4.4 Timing Tracking

In this Section we describe the two aforementioned timing recovery schemes for the receivers shown in Figure 4.2 and Figure 4.3, where the channel output is described by (4.2). In the following two subsections we describe the two alternative timing recovery schemes. Firstly, we consider the conventional code locked loop (CLL) adapted from the conventional CLL algorithms in [51]. The CLL can be easily adapted to a CLL for IDMA since the pilot channel for each user given in (4.2) is simply a spread spectrum pseudo-noise sequence. This is similar to the CLL mechanism for DS-CDMA systems in [50]. The main technique for mitigating MAI and MPI in the traditional CLL is by utilising spreading gain. This is useful for timing estimation since practical timing drifts are very small compared with realistic symbol/block sizes for spread spectrum communications. As such it is often possible to utilise a relatively long spreading codes in the pilot channel, and thus mitigate the effects of severe MAI.

In the second subsection we describe how timing recovery can be incorporated

into the iterative interference cancellation process. We describe an iterative approach to synchronisation where the timing is estimated on each iteration. We implement iterative timing recovery by having separate MAI cancelation and timing estimation stages within one iteration. First the IC cancels MAI at a sample level using the decoders output soft information and timing estimates from the previous iteration. Then the signal is passed through a digital delayed locked loop which uses the pilot channel with the help of the soft information from the data channel to estimate the timing information. The new timing information is used to re-sample (involving interpolation)[162] the data and pilot channel for each user.

4.4.1 Conventional Timing Recovery

In this subsection we describe the conventional CLL which is shown in Figure 4.4. We first describe the timing error discriminator (TED) in Figure 4.4, and then proceed to describe the dynamic behaviour and performance analysis of the CLL using well known control theory [51, 55]. We employ a code-locked loop for each user where the pilot channel uses random PN sequences of length N_s. From the perspective of timing error detection it is sufficient to only consider the power transmitted by the pilot channel of the desired user (user k) and regard the data and pilot channels of other users as interference. We choose the well known Mueller and Mueller timing error detector (MM TED) [60], due to its simplicity and powerful performance. Under steady state tracking conditions it is easy to show that the MM TED (where symbols are Nyquist pulse shaped) is immune to self noise (or ISI), for this reason it is easy to analyse its performance. We adapt the basic MM TED scheme presented in [51], in order to construct a CLL.

For simplicity of analysis we construct the MM TED using only the received pilot sequence $b'_k[m]$ in (4.6), and we ignore the effects of the channel, i.e. $h_k = 1, \forall k$. Furthermore, we assume that the continuous time pulse shaped waveform $b'_k(t)$, can be perfectly reconstructed from the sampled signal $b'_k[m]$ using interpolation. Therefore we write the signal $b'_k(t)$ in Figure 4.4 as,

$$\begin{aligned} b'_k(t) = &\sum_j \sqrt{E_p} p_k[j] R_g\left(t - jT_c - \tau_k[j]\right) \\ &+ \sum_{k' \neq k} \sum_{j'} \sqrt{E_p} p_{k'}[j'] R_g\left(t - j'T_c - \tau_{k'}[j']\right) + w(t) \end{aligned} \tag{4.27}$$

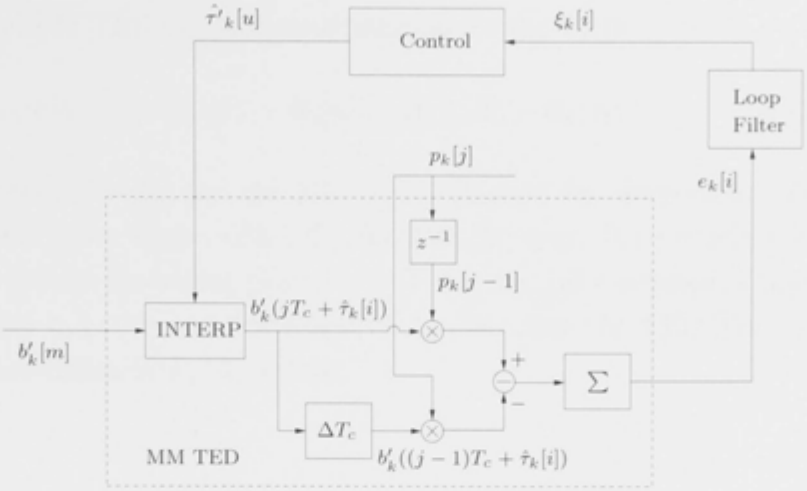

Figure 4.4: The single-shot timing recovery loop for an IDMA system.

where $E_p = 1/N_s$, and $w(t) \triangleq n(t) * g(t)$.

Now the MM TED for the CLL can be easily constructed as,

$$e_k[n] = \sum_{j=nN_s+1}^{(n+1)N_s+1} \Big(\sqrt{E_p} p_k[j-1] b'_k(jT_c + \hat{\tau}_k[j]) - \sqrt{E_p} p_k[j] b'_k\left((j-1)T_c + \hat{\tau}_k[j-1]\right) \Big), \tag{4.28}$$

where n is the pilot symbol index and for practical timing drifts the change in timing error is essentially static during one symbol, i.e $\hat{\tau}_k[j] \simeq \hat{\tau}_k[j-1]$. Note that the TED function is sampled at the symbol rate using the index n.

For the purposes of analysis we define the timing error term as the difference between timing offset and the estimated timing offset,

$$\Phi_k[n] = \tau_k[n] - \hat{\tau}_k[n]. \tag{4.29}$$

The MM TED discriminator function, or S-curve, can be computed as the expectation of the error function (4.28), conditioned on a static timing error, $\Phi_k[n]$, mathematically this is written as,

$$S(\Phi_k[n]) \triangleq \mathrm{E}\left\{ e_k[n] | \Phi_k[n] \right\}. \tag{4.30}$$

Substituting (4.27) into (4.28), and evaluating the expectation in (4.30) yields

the S-curve for the MM TED as, analytical solution for the TED

$$S_{MM}(\Phi_k[n]) = R_g(T_c - \Phi_k[n]) - R_g(-T_c - \Phi_k[n]) \tag{4.31}$$

Figure 4.5 shows the S-curves for the MM TED obtained by simulation. We use the raised cosine pulse shape with 22% rolloff in all cases. For the purposes of illustration we use no spreading gain ($N_s = 1$) for the pilot sequences since the S-curve function in (4.31) is independent of N_s. We show the TED function operating under two different E_s/N_0 values.

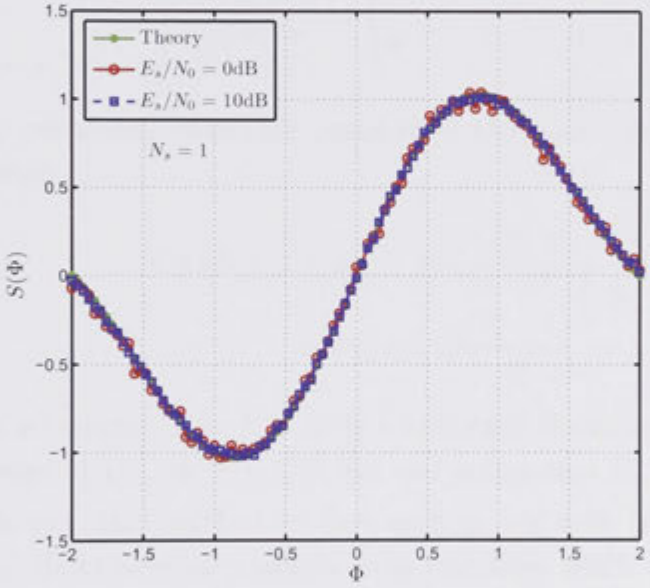

Figure 4.5: S-curves for the MM TED.

For practical timing drifts/offsets the TED operates within the linear region of the S-curve and thus the control loop of Figure 4.4 is linear. The TED error function in (4.28) can be approximated as,

$$e_k[n] = S(\Phi_k[n]) + N[n], \tag{4.32}$$

$$\simeq A\Phi_k[n] + N[n], \tag{4.33}$$

where $N[n]$ is the noise term defined as, $N[n] \triangleq e_k[n] - S(\Phi_k[n])$. For the MM TED the slope of the S-curve at the origin can be calculated by taking

the derivative of (4.31) as follows,

$$\begin{aligned} A &\triangleq \frac{d}{d\Phi} S(\Phi)\Big|_{\Phi \to 0}, \\ &= \frac{2\cos(\alpha\pi)}{T_c(1-4\alpha^2)}. \end{aligned} \tag{4.34}$$

It can be readily shown that the noise term ($N[n]$) in (4.32) is white Gaussian noise, i.e. $N[n] \sim \mathcal{N}(0, \mathrm{Var}\{N[n]\})$, with autocorrelation function,

$$R_N[\delta] = \mathrm{E}\{R_N[l]R_N[l+\delta]\}, \tag{4.35}$$

$$= \begin{cases} \mathrm{Var}\{N[n]\}, & \delta = 0 \\ 0, & \delta \neq 0 \end{cases}. \tag{4.36}$$

By expanding (4.27) the variance of the noise term $N[n]$ in (4.32) can be computed,

$$\mathrm{Var}\{N[n]\} = 2\sigma_n^2 + 2\frac{(K-1)}{N}\frac{1}{T_c}\int_{-\infty}^{\infty} R_g^2(\mathcal{T})d\mathcal{T} \tag{4.37}$$

$$\simeq 2\sigma_n^2 + 1.89\frac{(K-1)}{N} \tag{4.38}$$

where we assume $\mathcal{T} = \hat{\tau}_k - \tau_{k'}$ is a uniformly distributed random variable over the range $(0, T_c)$, i.e. $\mathcal{T} \sim \mathcal{U}(0, T_c)$, and noting that $E_s = 1$.

The standard method to cope with timing drift (as opposed to a constant timing offset) is to use a second-order loop filter which contains an integrator. A widely used scheme is indicated in Figure 4.6. By inspection it is seen that the governing equations are,

$$\hat{\tau}_k[n+1] = \hat{\tau}_k[n] + \xi_k[n] \tag{4.39}$$

$$\xi_k[n] = \xi_k[n-1] + \gamma(1+\rho)e_k[n] - \gamma e_k[n-1], \tag{4.40}$$

where ρ is a positive constant.

The influence of the second integrator on the static phase error may be assessed as follows. First, we rewrite (4.39) in terms of $\Phi_k[n]$,

$$\Phi_k[n+1] = \Phi_k[n] + f_d T_s - \xi_k[n]. \tag{4.41}$$

Next, assuming that a steady-state condition has been achieved, say $\Phi_k[n] = \Phi_{ss}$,

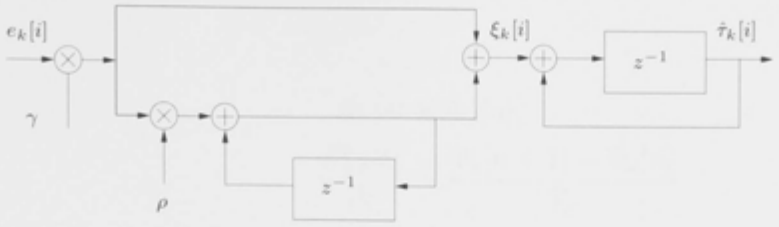

Figure 4.6: Second-order loop filter.

from (4.41) it follows that $\xi_k[n]$ must be constant:

$$\xi_{ss} = f_d T_s. \tag{4.42}$$

Then, from (4.40) it is seen that,

$$e_k[n] = \frac{1}{1+\rho} e_k[n-1], \tag{4.43}$$

whose steady-state solution is zero (for $\rho > 0$). Thus letting $N_k[n] = 0$ in (4.32) yields,

$$S(\Phi_{ss}) = 0, \tag{4.44}$$

and by using (4.31) it is concluded that, $\Phi_{ss} = 0$, and consequently static timing errors have been eliminated.

From the above derivation it appears that a second-order loop will eventually lock on the incoming carrier with no static error, whatever the value of ρ. In practise this is only true with very small values of f_d (on the order of the loop noise bandwidth). Furthermore, even in these conditions, the system response does depend on ρ and, therefore, it is of interest to look for ρ values that correspond to relatively short settling times. This problem is approached here under the assumption that the loop noise bandwidth is small compared with the symbol rate. Under these circumstances the variables $\Phi_k[n]$, $\xi_k[n]$ and $e_k[n]$ are slowly varying in time and the digital loop can be approximated by an analog system for which a well-established theory is available.

The analog system is arrived at postulating that its state variables $\Phi_k(t)$, $\xi_k(t)$ and $e_k(t)$ are related to $\Phi_k[n]$, $\xi_k[n]$ and $e_k[n]$ by relations of the type,

$$\Phi_k(t) \approx \Phi_k[n], \tag{4.45}$$

$$\frac{d\Phi_k(t)}{dt} \approx \frac{\Phi_k[n+1] - \Phi_k[n]}{T_s}, \tag{4.46}$$

for $nT_s + \tau_k[n] \leq t \leq (n+1)T_s + \tau_k[n]$. Making these approximations in (4.40)-(4.41) and letting,

$$e_k[n] \approx A\Phi_k[n], \tag{4.47}$$

after some manipulations it is found that,

$$\begin{aligned} \frac{d\xi_k(t)}{dt} &= \gamma d\frac{e_k(t)}{dt} + \frac{\gamma\rho}{T_s}e_k(t+T), \\ &= \gamma(1+\rho)\frac{e_k(t)}{dt} + \frac{\gamma\rho}{T_s}e(t), \end{aligned} \tag{4.48}$$

$$\frac{d\Phi_k(t)}{dt} = f_d - \frac{1}{T_s}\xi_k(t), \tag{4.49}$$

$$e(t) = A\Phi_k(t). \tag{4.50}$$

A solution for $\Phi_k(t)$ is now derived by Laplace transform methods, setting to zero the initial conditions. This yields the Laplace transform for $\Phi_k(t)$,

$$\Psi_k(s) = \frac{f_d}{s^2 + 2\varsigma\omega_n s + \omega_n^2}, \tag{4.51}$$

where the parameters ς and ω_n are defined as,

$$\varsigma \triangleq \frac{(1+\rho)\sqrt{\gamma A}}{2\sqrt{\rho}}, \tag{4.52}$$

$$\omega_n \triangleq \frac{\sqrt{\gamma A\rho}}{T_s}. \tag{4.53}$$

In the parlance of servomechanism theory, ς is the damping factor and ω_n the natural frequency of the loop. Next, the inverse Laplace transform of (4.51) is obtained from transform pairs. Figure 4.7 illustrates the effect of the damping factor on the response to a step in the frequency error. It is apparent that, as time increases, $\Phi_k(t)$ tends to zero anyway. Short transients are observed with

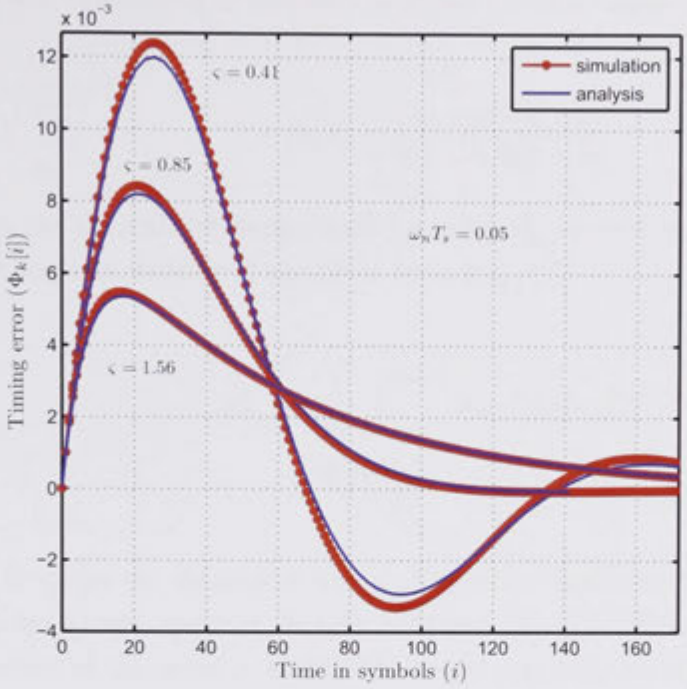

Figure 4.7: Transient timing estimation error due to a frequency error step.

damping factors in the range $0.6 \leq \varsigma \leq 1.0$. These are the ς values that are commonly adopted in practice.

Returning to the loop filter, we need to choose ρ so as to properly control the integrators action. This problem can be addressed considering the loop tracking performance. Briefly, let us start with the loop model as summarised by the equations

$$\Phi_k[n+1] = \Phi_k[n] - \xi_k[n] \tag{4.54}$$

$$\xi_k[n] = \xi_k[n-1] + \gamma(1+\rho)e_k[n] - \gamma e_k[n-1] \tag{4.55}$$

$$e_k[n] = A\Phi_k[n] + N_k[n] \tag{4.56}$$

In writing (4.54) we have dropped f_d since frequency errors are compensated in the steady-state. From these equations $\Phi_k[n]$ is found as the response to $N_k[n]$ of,

$$\mathrm{H_N}(z) = -\frac{\gamma[(1+\rho)z - 1]}{(z-1)^2 + \gamma \mathrm{A}[(1+\rho)z - 1]}. \tag{4.57}$$

The noise bandwidth of this filter is found with the methods in [163] and is given by,

$$\mathrm{B_L T_s} = \frac{2\rho + \gamma A(2+\rho)}{2[4 - \gamma A(2+\rho)]}. \tag{4.58}$$

Hence, the normalised timing error variance $\sigma^2_{\Phi_{\epsilon_k}}$ is now expressed in terms of the power spectral density of the noise term $\mathrm{S}_{N'_{T,k}}(f)$

$$\sigma^2_{\Phi_{\epsilon_k}} = \frac{1}{T_c^2}\int_{-1/2T_s}^{1/2T_s} \mathrm{S}_N(f)\|\mathrm{H_N}(f)\|^2 df \tag{4.59}$$

$$\simeq \frac{2\mathrm{S}_N(0)\mathrm{B_L}}{A^2 T_c^2} \tag{4.60}$$

Now in order to determine the timing error variance we need to determine the noise power spectral density function, $S_N(f)$. Using the autocorrelation properties of the noise in (4.36), the power spectral density function, $S_N(f)$ can be determined,

$$\begin{aligned} S_N(f) &= T_s N'_0 \\ &= N_s T_c N'_0 \end{aligned} \tag{4.61}$$

where the N'_0 is the variance of the noise plus interference term in (4.37),

$$N'_0 = 2\sigma_n^2 + 1.89\frac{(K-1)}{N}. \tag{4.62}$$

The timing error variance is now given by,

$$\sigma^2_{\Phi_k[n]} = \frac{2B_L N_s T_c N'_0}{4\pi^2 \eta}, \tag{4.63}$$

where,

$$\eta = \frac{1}{2\pi^2}\left[\frac{\cos(\alpha\pi)}{1-4\alpha^2}\right]^2 \tag{4.64}$$

In [51] the authors show that the modified Cramer-Rao Bound (MCRB) for a general timing estimator is given by,

$$\sigma^2_{MCRB} = \frac{B_L T_s N_0}{4\pi^2 \xi}, \tag{4.65}$$

where $\xi = \frac{1}{4}\left[\frac{1}{3} + \alpha^2\left(1 - \frac{8}{\pi^2}\right)\right]$, and $E_s = 1$ in this particular example. By comparing (4.63) and (4.65) it can be seen that the ratio of the MM based timing recovery loop is a factor of $\frac{\eta}{\xi}\frac{N_0'}{N_0}$ greater than the MCRB. This means that there is always a performance degradation with respect to the best achievable timing estimation algorithm. It can also be seen that the performance of the MM based timing estimator is interference limited, that is, for diminishing noise spectral density N_0 the value of N_0' is dominated by the interference term in (4.37).

4.4.2 The Code-Locked loop modified for Turbo synchronisation

In this Section we present a modified CLL shown in Figure 4.8 which is tailored for the iterative synchronisation mechanism in Figure 4.3. The CLL is adapted/modified from the algorithm described in the previous subsection (4.4.1), in order to be used iteratively. We employ a code-locked loop for each user where the data and pilot chips are effectively grouped into random codes of length N. Since the soft information for data symbols are computed at the FEC coding, it makes sense that $N = 1/R_c$ where R_c is the coding rate. This is different from the code-length of the previous subsection, i.e. $N_s \neq N$.

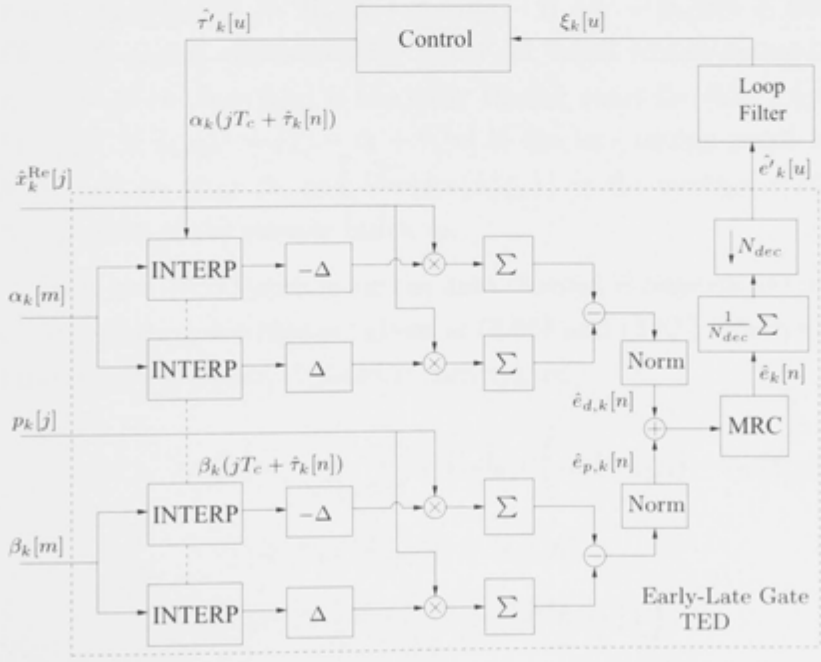

Figure 4.8: The Delayed-Locked Loop with pilot and data channel combining.

Contrary to the previous subsection, where the MM TED was used, we opt

to employ the early-late gate synchroniser for the turbo synchronisation. The discriminator function of the early-late gate based CLL in Figure 4.8 uses both the pilot channel and data channel in-order to compute the timing error function ($\hat{e}_k[n]$). We construct a TED metric by combining the timing estimates from the interference cancelled pilot and data signals as estimated in (4.20). In Figure 4.3 the interference cancelled signal for user k, $\mathrm{E}\{z'_k[m]\}$ as defined in (4.20), is passed to the CLL. We denote $\tilde{z}'_k[m] \triangleq \mathrm{E}\{z'_k[m]\}$.

Firstly we consider the TED function for the pilot channel. The early-late TED at the chip-level involves taking the difference between the pilot channel signal β_k sampled at early and late ($t_{e,k}[j]$ and $t_{l,k}[j]$ respectively) time instants from the estimated current chip time $jT_c + \hat{\tau}_k[n]$. Mathematically, the error function for the EL TED can be written as follows;

$$\begin{aligned}\hat{e}_{p,k}[n] &= \frac{1}{N\mathrm{E}_\mathrm{p}} \sum_j \sqrt{\mathrm{E}_\mathrm{p}} p_k[j] \Big(\beta_k\big(t_{e,k}[j]\big) - \beta_k\big(t_{l,k}[j]\big) \Big), \\ &= S_{EL}\left(\Phi_{\epsilon_k}[n]\right) + N_{p,k}[n], \qquad (4.66) \\ N_{p,k}[n] &\sim \mathcal{N}\left(0, \frac{2}{N\mathrm{E}_\mathrm{p}} \widetilde{\mathrm{Var}}\{\mathrm{Im}\{h_k^* \zeta_k\}\}\right), \qquad (4.67)\end{aligned}$$

where $S_{EL}\left(\Phi_k[n]\right) \triangleq \mathrm{R}_g(\Delta + \Phi_k[n]) - \mathrm{R}_g(\Delta - \Phi_k[n])$ is the S-curve for the EL TED and is approximately linear for small timing estimation error ($\Phi_k[n]$), $t_{e,k}[j] = jT_c + \Delta + \hat{\tau}_k[n]$ is the early timing point for chip j for user k advanced by time Δ, $t_{l,k}[j] = jT_c - \Delta + \hat{\tau}_k[n]$ is the late timing point for chip j for user k delayed by time Δ, and $\widetilde{\mathrm{Var}}\{\mathrm{Im}\{h_k^* \zeta_k\}\}$ is the average variance of $\mathrm{Im}\{h_k^* \zeta_k\}$ irrespective of the sample index m.

Now the TED function for the data channel is constructed in a similar manner to that of the pilot channel given in (4.66) and (4.67). Mathematically the TED function for the data channel is constructed,

$$\begin{aligned}\hat{e}_{d,k}[n] &= \frac{1}{N\widetilde{\mathrm{E}}_d} \sum_j \sqrt{\mathrm{E}_\mathrm{d}} \hat{d}_k[j] \Big(\alpha_k\big(t_{e,k}[j]\big) - \alpha_k\big(t_{l,k}[j]\big) \Big), \\ &\simeq S_{EL}\left(\Phi_{\epsilon_k}[n]\right) + N_{d,k}[n], \qquad (4.68) \\ N_{d,k}[n] &\sim \mathcal{N}\left(0, \frac{2}{N\widetilde{\mathrm{E}}_d} \widetilde{\mathrm{Var}}\{\mathrm{Re}\{h_k^* \zeta_k\}\}\right), \qquad (4.69)\end{aligned}$$

where, $\widetilde{\mathrm{E}}_d \triangleq \mathrm{E}_\mathrm{d} \sqrt{\mathrm{E}\{\|\tilde{d}_k\|^2\}}$ and $\hat{x}_k^{\mathrm{Re}}[j] \triangleq \mathrm{E}_{\mathrm{DEC}}(x_k^{\mathrm{Re}}[j])$ is the soft information out of the decoder block (Figure 4.3) from the previous iteration.

We now wish to combine the timing error estimators defined in (4.66) and (4.68) using linear weights w_1 and w_2, and then find the corresponding weights which minimise the mean square error (MSE) under the unbiased constraint. Mathematically this can be surmised,

$$\begin{aligned}\hat{e}_k[n] &= w_1\hat{e}_{p,k}[n] + w_2\hat{e}_{d,k}[n], \\ &= e_k[n] + N_{T,k}[n],\end{aligned} \tag{4.70}$$

where $N_{T,k}[n] = w_1 N_{p,k}[n] + w_2 N_{d,k}[n]$ is the statistical noise of the overall TED, and the unbiased constrained MSE is,

$$\begin{aligned}J = \arg\min_{w_1,w_2} &\left(w_1^2 \mathrm{Var}\left\{N_{p,k}[n]\right\} + w_2^2 \mathrm{Var}\left\{N_{d,k}[n]\right\}\right) \\ &+ \lambda(w_1 + w_2 - 1).\end{aligned} \tag{4.71}$$

where λ is the Lagrangian multiplier. Solving (4.71) we obtain the optimal weights as

$$w_1 = \frac{\mathrm{E_p}}{\mathrm{E_{T,k}}}, \tag{4.72}$$

$$w_2 = \frac{\widetilde{\mathrm{E}}_d}{\mathrm{E_{T,k}}}, \tag{4.73}$$

where $\mathrm{E_{T,k}} = \mathrm{E_p} + \widetilde{\mathrm{E}}_d$ can be viewed as the total energy of the pilot and data channels together.

As described in Section 4.4.1 the standard method to track timing drift in a CLL is to use a second order loop filter containing an integrator to update the timing estimate ($\hat{\tau}_k[n]$). An averaging filter and decimation stage was used in order to control the feedback period T (as illustrated in Figure 4.8), allowing for more flexible design of the loop parameters. A widely used loop filter is given in (4.39) and (4.40) where u is substituted for n and the decimated error function $\hat{e'}_k[u]$ is substituted $e_k[n]$, this is rewritten as,

$$\begin{aligned}\hat{\tau'}_k[u+1] &= \hat{\tau'}_k[u] + \xi_k[u], \\ \xi_k[u] &= \xi_k[u-1] + \gamma(1+\rho)\hat{e'}_k[u] - \gamma\hat{e'}_k[u-1].\end{aligned} \tag{4.74}$$

Here the timing error is computed at the decimated rate with period $T = N_{dec}NT_c$, and the index variable u is used to represent signals sampled at the decimated rate $\frac{1}{T}$. Interpolation is commonly used in-order to sample the

signal $\tilde{z}_k$, at the optimal chip timing points $(jT_c + \hat{\tau}_k[j])$. The early and late signals in Figure 4.8 are computed using simple bi-linear interpolation function.

We now provide performance evaluation the proposed iterative timing recovery scheme in a manner similar to the analysis in the previous subsection (4.4.1). We derive the error variance of the timing error term $(\Phi_{\epsilon_k}[u] = \tau_k[u] - \hat{\tau'}_k[u])$ using well known control theory [51, 163]. It is easy to show that the z-transform of the error term $(\Phi_{\epsilon_k}[u])$ can be expressed as,

$$\Phi_{\epsilon_k}(z) = \mathrm{H_N}(z) N'_{T,k}(z), \tag{4.75}$$

where $N'_{T,k}[u]$ is the averaged response of $N_{T,k}[n]$ from the averaging filter shown in Figure 4.8. In (4.75) the timing error signal may be viewed as the response to $N'_{T,k}[u]$ of a filter with transfer function $\mathrm{H_N}(z)$ in (4.57), where for the EL TED, the slope of the S-curve at the origin is, $A = -2\Delta R''_g(0)$. In order to find the frequency response of the transfer function we substitute $z = e^{j2\pi fT}$ into (4.57),

$$\mathrm{H_N}(f) = -\frac{\gamma[(1+\rho)e^{j2\pi fT} - 1]}{(e^{j2\pi fT} - 1)^2 + \gamma \mathrm{A}[(1+\rho)e^{j2\pi fT} - 1]}. \tag{4.76}$$

The normalised timing error variance $\sigma^2_{\Phi_{\epsilon_k}}$ is now expressed in terms of the power spectral density of the noise term $\mathrm{S}_{N'_{T,k}}(f)$

$$\begin{aligned} \sigma^2_{\Phi_{\epsilon_k}} &= \frac{1}{T^2} \int_{1/2T}^{1/2T} \mathrm{S}_{N'_{T,k}}(f) \|\mathrm{H_N}(f)\|^2 df \\ &\simeq \frac{2\mathrm{S}_{N'_{T,k}}(0)\mathrm{B_L}}{A^2T^2} \\ &= \frac{2\sigma^2_{N'_{T,k}}\mathrm{B_L}}{A^2T} \end{aligned} \tag{4.77}$$

where $\mathrm{B_L}$ is the bandwidth of the loop filter described in Section 4.4.1 defined in [51] and $\sigma^2_{N'_{T,k}}$ is the variance of $N'_{T,k}$. The product of the loop bandwidth and the symbol period is given in (4.58). The variance of $N'_{T,k}$ can be determined using (4.66), (4.68), (4.70) and (4.72), as,

$$\sigma^2_{N'_{T,k}} = \frac{1}{N_{dec} N \mathrm{E_{T,k}}} \big(2\widetilde{\mathrm{Var}}\{\mathrm{Re}\{h^*_k \zeta_k\}\}\big). \tag{4.78}$$

The term $\widetilde{\mathrm{Var}}\{\mathrm{Re}\{h^*_k \zeta_k\}\}$ can be viewed as a function of E_b/N_0 and the number of iterations. At high E_b/N_0 where the interference term can be canceled perfectly

$(\widetilde{\mathrm{Var}}\{a'_k\} = 0)$. The lower bound of the timing error variance in $\sigma^2_{\Phi_{\epsilon_k}}$ is given by,

$$\sigma^2_{\Phi_{\epsilon_k}} \geq \frac{N_0 \mathrm{B_L}}{N_{dec} N \mathrm{E_{T,k}} A^2 T}. \tag{4.79}$$

4.5 Numerical performance results

In this Section we compare the performance of the IDMA receiver using iterative timing recovery with the IDMA receiver using conventional timing recovery. We use the analysis presented in Sections 4.4.1 and 4.4.2 to verify the numerical results. We present simulations for two different scenarios we provide analysis for; (1) practical drift scenarios where users timing drifts are uniformly distributed in the range of 0 to 12 μs/s, and (2) severe drift scenarios where each user is subjected to a timing drift uniformly distributed in the range of 0 to 0.2 ms/s respectively.

4.5.1 Practical drift

In this subsection we present the simulation results for the timing recovery under practical drift scenarios. The drifts we simulate are within the range of 0 to 12 μs/s. For insignificant drifts it is impractical to employ the iterative timing recovery scheme given in Section 4.4.2. For example in a single block of data in a 3GPP which is 2560 chips long, a drift of 12 μ chips/chip, results in a total accumulated timing drift of 3×10^{-2} of a chip within a block, as a consequence the filter bandwidth is extremely small and there is virtually no SNR degradation due to such a small drift.

In the aforementioned scenario it is practical to employ long spreading codes for the pilot channel, and consider the data channel as primarily interference. We choose to employ random spreading codes of length $N_s = 256$ for the pilot channel. We construct the block length to be 2560 chips over 10ms which is similar to the 3GPP standard. We choose to employ random spreading codes of length, $N_s = 256$ for the pilot channel, however the data channel uses repetition codes of length $N = 16$, the number of users in the system is $K = 16$, the oversampling rate $M = 8$, the roll-off factor of the SRRC function is $\alpha = 0.22$ and the chip period is $T_c = 0.26\mu$s.

The main task of designing the tracking loop is to choose the loop filter parameters, such that the loop bandwidth is big enough to allow for the TED to detect timing error, but not too wide as to allow too much noise/interference

through. From (4.63) it can be seen that the timing error variance is proportional to the loop bandwidth, thus it is preferable to have a bandwidth as narrow as possible. Typically, the damping factor, ς, is set in the range $0.6 - 1.0$ to reduce the transient response of the tracking loop [51]. In the simulated system we used the parameters $\gamma = 4 \times 10^{-3}$, $\rho = 3.7 \times 10^{-3}$. The resultant control system response characteristics are a damping factor of $\varsigma = 0.72$ and angular frequency of $\omega_n T_s = 5.4 \times 10^{-3}$, and loop bandwidth of $B_L T_s = 2.9 \times 10^{-3}$, where $T_s = 256 T_c$.

The normalised timing error variance of the conventional timing synchronisation algorithm is presented in Figure 4.9. The comparison of the timing error variance for the fully loaded multiuser IDMA receiver, with the single-user (SU) receiver and the MCRB is shown. It can be seen that the SU performance is always worse than the MCRB by a constant factor of, $\frac{\eta}{\xi}$ as discussed in the last paragraph of Section 4.4.1. Furthermore we can observe the effect of MAI on the timing error variance of the MU receiver. At higher E_b/N_0 it can be seen that there is a error floor due to the fact that the noise plus interference term, N_0', is dominated by the MU interference.

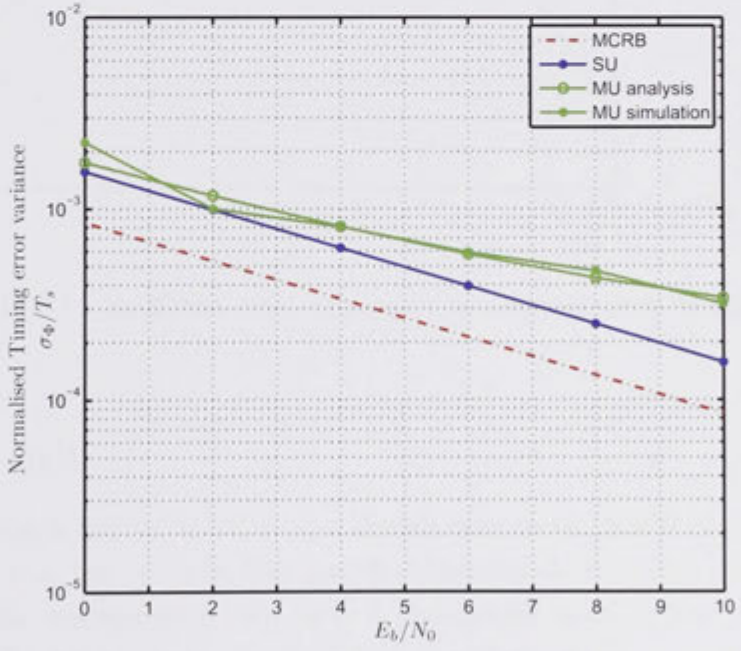

Figure 4.9: The comparison of timing error variances for IDMA receivers subject to practical drifts (0-12 μs/s).

Figure 4.10 shows the average BER performance of a fully loaded IDMA

system, ($K = 16$ and $N = 16$), where the users timing drifts are uniformly distributed in the range of 0-12 μs/s. It can be seen that there is virtually no difference in the performance between the single-user and the fully loaded system. However, we do notice that the performance of the fully loaded chip asynchronous IDMA system outperforms the fully loaded chip synchronous IDMA system in Figure 2.11. This is due to the interference reduction due to the pulse-shaping when the users timing points are not aligned.

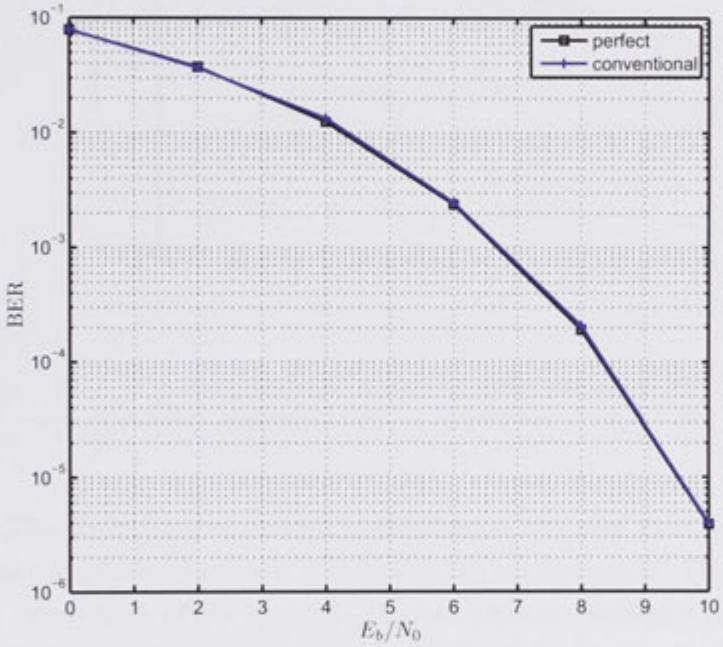

Figure 4.10: The BER for an IDMA receiver subject to practical drift (0-12μs/s)

4.5.2 Severe drift

We construct the block size to be 10ms in a similar way to the 3GPP standard the block length is $L = 160$ symbols, the spreading factor is $N = 16$, the number of users $K = 16$, the oversampling rate $M = 8$, the roll-off factor of the SRRC function is $\alpha = 0.22$, the chip period is $T_c = 0.26\mu S$ and the delay-advance time $\Delta = \frac{T_c}{2}$. In accordance with the 3GPP standard we have unequal power for the data and pilot channels. We set the energy per chip for the pilot channel to be 6 dB lower than the data channel $E_p = E_d/4$. This fully loaded system together with the significant drift place a critical condition on the timing synchronisation.

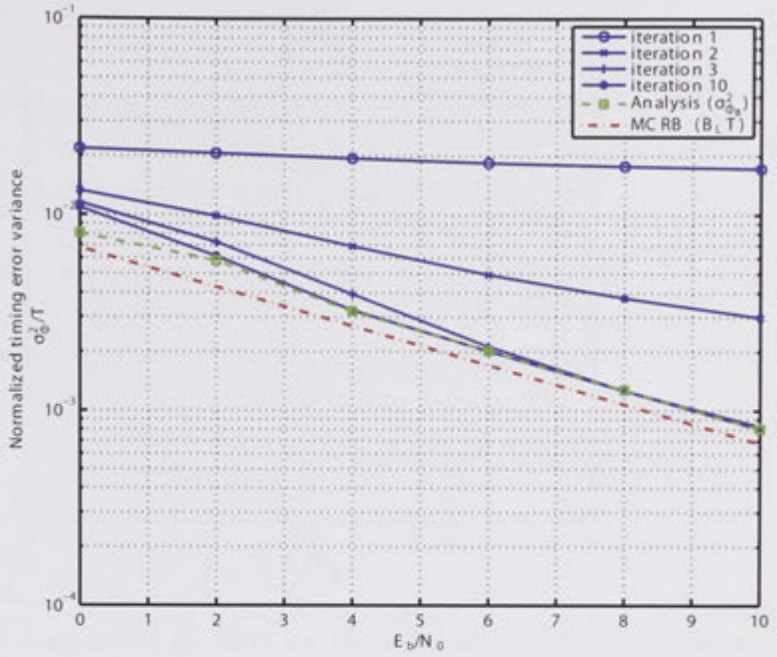

Figure 4.11: The comparison of timing error variance for IDMA receiver subject to severe drift (0-0.2ms/s).

The main task of designing the timing recovery circuit was to tune the loop filter parameters in-order to optimise the performance. There is a trade-off where the bandwidth of the loop (4.58) must be wide enough to track the timing drift, but not too wide so as to allow noise through the feedback. The parameters N_{dec},γ and ρ also effect the damping factor (ς) and frequency (ω_n). In the simulated system we used the parameters $N_{dec} = 2$, $\rho = 0.05$ and $\gamma = 0.4$. The resultant response characteristics of the loop are $\varsigma = 0.5$, $\omega_n T = 0.0447$ and bandwidth time product, $B_L T = 2.3 \times 10^{-2}$, where $T = 32T_c$.

It can be seen from Figure 4.11, there is a huge improvement in performance between the IDMA receiver using conventional timing recovery and the same receiver using iterative timing recovery after 10 iterations. It can be seen that the timing error variance is reduced by a factor of 15 times. This is mainly due to the much lower SNR of the pilot channel in the conventional approach. After a number of iterations the soft-information in the data channel becomes reliable, resulting in a much improved operating point of the timing recovery circuit. The timing error variance of the EL based timing recovery loop is affected by self interference (ISI) [51] and thus is greater than the MCRB.

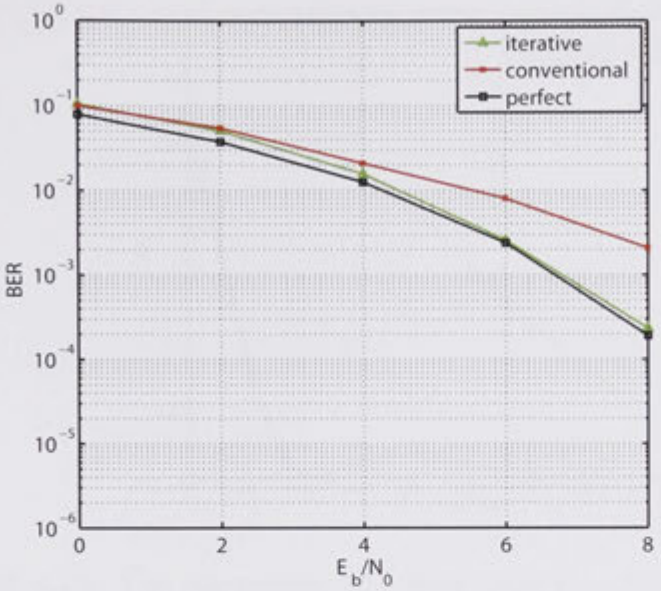

Figure 4.12: The comparison of BER for the conventional and iterative timing recovery schemes for the IDMA receiver subject to severe drift (0-0.2ms/s).

Figure 4.12 shows the numerical performance results for both conventional and iterative timing recovery circuits. It can be seen that for higher E_b/N_0, for example $E_b/N_0 > 5$ dB the iterative timing synchronisation results in a greater than 2 dB gain in performance. This can be explained by the fact that at higher E_b/N_0 the IC in the iterative receiver takes effect and the multiuser interference becomes negligible after many iterations, which leads to better timing recovery using both data and pilot channels, ultimately resulting in higher E_b/N_0 and reduced ISI of the sampled signal in (4.23). The conventional approach suffers from noise due to a loop filter with a wide bandwidth that allows more errors to enter the system. The interference cancellation approach removes the interference and thus the noise, enabling improved timing and thus bit error rate performance.

Figure 4.13 shows the mean squared timing error (MSE) with respect to the chip index where the system is run at an $E_b/N_0 = 8$dB. In the simulation the initial timing offset is set to 0.5 of a chip. The figure illustrates that there is a huge improvement in convergence between the conventional and iterative timing schemes. This is due to the effect of the high MAI on the tracking loop. The iterating timing circuit can lock on to the carrier within one transmission block, whereas the conventional scheme requires a lot longer to converge. This shows that for bursty, uncoordinated systems there may be a significant improvement

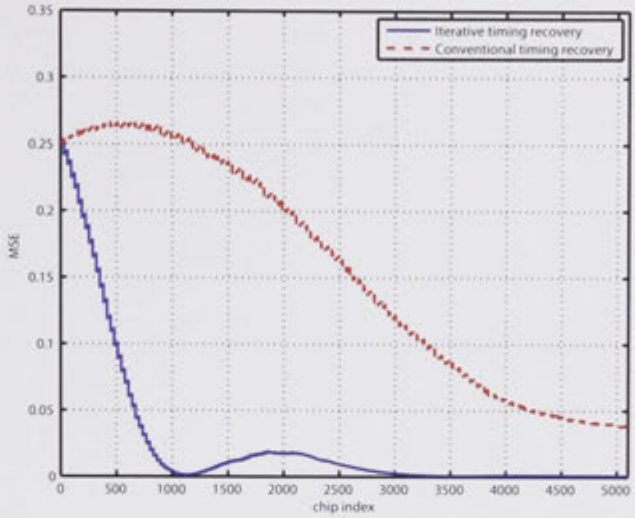

Figure 4.13: The comparison of timing error vs. chip index, for the first two blocks of transmission. This represents 20ms.

due to the iterative timing recovery.

4.6 Summary

In this Chapter we have developed a coherent receiver for IDMA systems by presenting conventional and iterative approaches for timing recovery. We show that conventional timing recovery achieves sufficient performance for a fully loaded system subject to low timing drift. Operating under these conditions we show that by using large spreading gains and a very low bandwidth loop filter the effects of MAI on the timing recovery loop can be mitigated. After this we compare the performance of the iterative timing recovery with conventional timing recovery for a fully loaded system under severe drift scenarios. The receiver using iterative timing recovery shows a huge performance improvement for higher E_b/N_0 where the reliability of the data channel increases. The performance in terms of BER is improved by a factor of greater than 2 dB. Where as the timing error variance is reduced by a factor of 15 times. We also derive the lower bound of the timing error variance which depends on the reliability of the soft information from the previous iteration.

Chapter 5

Optimal Detection of Block Asynchronous IDMA

5.1 Introduction

In the previous two Chapters we described methods for acquiring and tracking the chip timing points of a fully loaded asynchronous IDMA system. However, we did not consider any inter-block interference due to block asynchronism nor its effect on the receiver of an IDMA system. In this Chapter we assume that the acquisition technique described in Chapter 3 is first used to acquire each user's timing, and then the conventional timing tracking algorithm in Chapter 4 (Section 4.4.1) is used to track the chip timings continuously. After the timing information for each user has been estimated it is necessary to detect/decode the transmitted data. Previous chapters of this thesis have primarily focussed on the conventional iterative receiver for IDMA detailed in [10–12]. In this Chapter we design the maximum likelihood detector for a block asynchronous IDMA system.

In this Chapter we construct an optimal block asynchronous IDMA receiver. Traditional detection methods for IDMA [10–12] incur a performance cost due to block asynchronism. This is because of the time overlapping of blocks between users, which leads to inter-block interference (IBI). To avoid IBI the conventional methods of detection can be altered by using a guard interval. In [164] a matrix representation of the synchronous IDMA transmitter is derived. Based on this model the optimal detector is derived and for small systems the performance is compared to the iterative receiver proposed in [12].

In this Chapter we construct a system model for an asynchronous IDMA transmitter in matrix form. Using this model we derive an optimal detector and

for reasonably small systems the performance is compared to the conventional receiver proposed in [111]. We show that the Maximum Likelihood cost function can be interpreted as a structure trellis, and that finding the optimum estimate of data block, $\mathbf{d}$, is equivalent to finding the longest path in a trellis. This has significantly lower computational complexity than conventional exhaustive approaches for Maximum Likelihood detection.

5.2 System Model

In this Chapter we consider an asynchronous IDMA system with K users. We make the assumption that all users are subject to practical timing drifts as suggested in Section 4.5.1. As such the effect of drift over a block is negligible and the timing offset for user k can be modelled as a static delay τ_k. For simplicity and without loss of generality we can assume that users are ordered chronologically, i.e. $\tau_k \leq \tau_{k'}, \forall k, k'$ where $k' > k$ and $\tau_1 = 0$. Without loss of generality we assume a chip synchronous system where the user's chip delays τ_k are integers, however the model can be easily extended to be asynchronous by including the pulse shaping filter defined in Section 4.2. We assume a single path AWGN channel. In order to formulate a structured matrix we consider an IDMA system with a super-block structure consisting of M IDMA sub-blocks. There are L bits per IDMA sub-block, and a repetition code of length N is used as the FEC. We also assume rectangular pulse shaping is used. A general asynchronous IDMA sub-block structure is depicted in the Figure 5.1.

In order to define a matrix model of the received signal we first define a generator matrix $\mathbf{G}$, representing the transmitted IDMA signal. In [164] and [165] the generator matrix for a single synchronous IDMA block (sub blocks $i \in \{0, \ldots, M-1\}$) has been shown to be,

$$\mathbf{G_i} = [\mathbf{S}_1 \ldots \mathbf{S}_k \ldots \mathbf{S}_K], \tag{5.1}$$

where $\mathbf{S}_k$ denotes the generator matrix for user k,

$$\begin{aligned} \mathbf{S}_k &= [\pi_k(\mathbf{s}_{k,1})\pi_k(\mathbf{s}_{k,2}) \ldots \pi_k(\mathbf{s}_{k,L})], \\ &= [\mathbf{g}_{k,1}\mathbf{g}_{k,2} \ldots \mathbf{g}_{k,L}], \end{aligned} \tag{5.2}$$

where $\mathbf{s}_{k,i} = \left[s_{j-(i-1)N-\tau_k}\right]^T$, $j \in \{0, \ldots, LN-1\}$ and s_j represents the jth chip

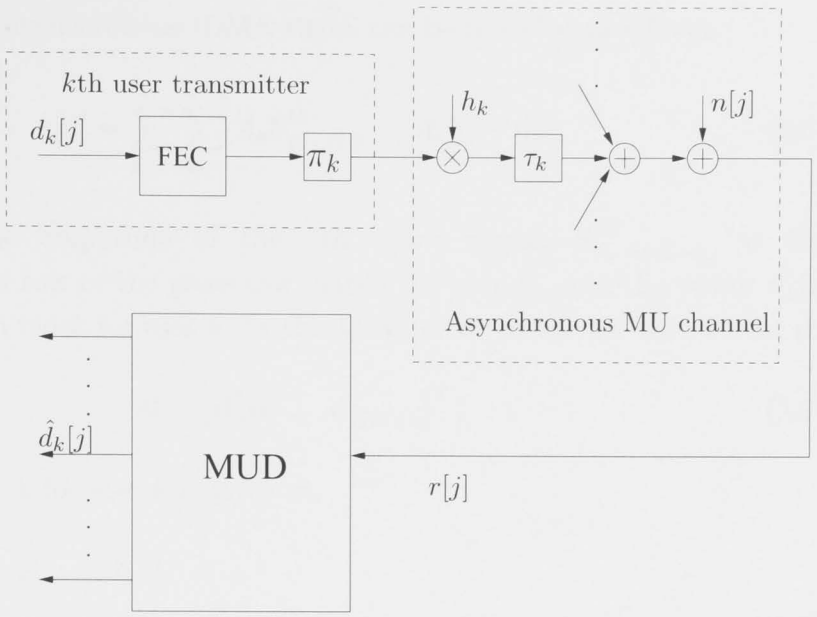

Figure 5.1: IDMA transmitter and receiver structures

of the repetition code, $s_j = 0$, $n \geq N$ or $n < 0$ and π_k is the interleaver for user k. For the asynchronous IDMA signal model the generator matrix (5.1) can be expanded,

$$\mathbf{G_i} = \begin{pmatrix} g_{1,1}^{(1)} & \cdots & g_{L,1}^{(1)} & & & & \\ g_{1,2}^{(1)} & & g_{L,2}^{(1)} & \ddots & & & \\ \vdots & & \vdots & & g_{1,1}^{(K)} & \cdots & g_{L,1}^{(K)} \\ g_{1,NL}^{(1)} & & g_{L,NL}^{(1)} & & g_{1,2}^{(K)} & & g_{L,2}^{(K)} \\ & & & \ddots & \vdots & & \vdots \\ & & & & g_{1,NL}^{(K)} & & g_{1,NL}^{(K)} \end{pmatrix},$$

$$= \begin{pmatrix} \mathbf{G}_i^{(0)} \\ \mathbf{G}_{\Delta i}^{(1)} \end{pmatrix}, \tag{5.3}$$

where $\mathbf{g}_{k,i} = [g_{i,1}^{(k)} \ldots g_{i,NL}^{(k)}]^T$, $\mathbf{G}_i^{(0)}$ represents the first NL rows of $\mathbf{G}_i$, and $\mathbf{G}_{\Delta i}^{(1)}$ represent the last τ_k rows of $\mathbf{G}_i$. Note that we also define a new matrix $\mathbf{G}_i^{(1)}$, as,

$$\mathbf{G}_i^{(1)} = \begin{pmatrix} \mathbf{G}_{\Delta i}^{(1)} \\ \mathbf{0}_{(LN-\tau_k)\times LK} \end{pmatrix}. \tag{5.4}$$

At the MUD the asynchronous IDMA signal can be modeled as follows,

$$r[n] = \sum_{k=1}^{K} \sum_{i=0}^{M-1} A_k \mathbf{S}^{(k)}_{(n-iLN-\tau_k)} \mathbf{d}_k[i] + \mathbf{n}[i], \tag{5.5}$$

where A_k is the amplitude of the kth user's signal, $\mathbf{S}^{(k)}_{(n-iLN-\tau_k)}$ is the $(n - iLN - \tau_k)$th row of the generator matrix for user k , and the vector $\mathbf{d}_k[i]$ represents the ith block for user k. In this Chapter we define the data vector $\mathbf{d}$,

$$\mathbf{d} = \left[\mathbf{d}_0^T \mathbf{d}_1^T \dots \mathbf{d}_{KM-1}^T\right]^T, \tag{5.6}$$

where the ith block for user k is given as,

$$\begin{aligned} \mathbf{d}_{k+iK-1} &= \mathbf{d}_k[i], \\ &= \left[d_{(k+iK-1)L}\, d_{(k+iK-1)L+1} \;\dots\; d_{(k+iK)L-1}\right]^T. \end{aligned} \tag{5.7}$$

Now (5.5) can be composed of sub-matrices G_i in a $(NLM + \tau_k) \times KLM$ matrix form.

$$\mathbf{r} = \mathbf{GAd} + \mathbf{n}, \tag{5.8}$$

where G is defined as,

$$\mathbf{G} = \begin{pmatrix} \mathbf{G}_0^{(0)} & \mathbf{0} & \dots & \mathbf{0} \\ \mathbf{G}_0^{(1)} & \mathbf{G}_1^{(0)} & \ddots & \vdots \\ \vdots & \ddots & \ddots & \mathbf{G}_{M-1}^{(0)} \\ \mathbf{0} & \dots & \mathbf{0} & \mathbf{G}_{M-1}^{(1)} \end{pmatrix}. \tag{5.9}$$

Assuming that equal power allocation for each user and $h_k = 1$ for $k \in \{1, \dots, K\}$ and consequently $\mathbf{A} = \mathbf{I}$. In the general chip asynchronous case the matrix elements of (5.2) can be oversampled and smoothed to a desired resolution such that equation (5.8) can be constructed.

5.3 Joint Maximum Likelihood Detector

In [166] the authors construct a ML detector for Asynchronous CDMA. In this Chapter we construct a Joint Maximum Likelihood detector for Asynchronous

IDMA in a similar manner using the defined matrix model (5.8). The goal of the ML detector is to choose the transmitted bit sequence $\mathbf{d}$ which maximises the joint likelihood function for the received block $\mathbf{r}$. This is shown to be equal to maximizing the conditional likelihood function given as,

$$\begin{aligned} L &= f(\mathbf{r}|\mathbf{d}), \\ &= \frac{1}{\sqrt{2\pi\sigma^2}} \exp\left\{ -\frac{1}{2\sigma^2}(\mathbf{r} - \mathbf{GAd})^T(\mathbf{r} - \mathbf{GAd}) \right\}. \end{aligned} \tag{5.10}$$

The maximisation of (5.10) is equivalent to selecting the $\mathbf{d}$ that maximises the cost function given as,

$$\Omega(\mathbf{d}) = 2h\mathbf{d}^T\mathbf{y} - h^2\mathbf{d}^T\mathbf{R}\mathbf{d}, \tag{5.11}$$

where $\mathbf{y} = \mathbf{G}^T\mathbf{r}$ is the correlation vector of generator $\mathbf{G}$ and received vector $\mathbf{r}$, and $\mathbf{R} = \mathbf{G}^T\mathbf{G}$ is the autocorrelation matrix of $\mathbf{G}$. The autocorrelation matrix $\mathbf{R}$ can be expressed as a function of $LK \times LK$ cross correlation matrices ($\mathbf{R}[0]$ and $\mathbf{R}[1]$),

$$\mathbf{R} = \begin{pmatrix} \mathbf{R}[0] & \mathbf{R}^T[1] & \mathbf{0} & \dots & \mathbf{0} & \mathbf{0} \\ \mathbf{R}[1] & \mathbf{R}[0] & \mathbf{R}^T[1] & \dots & \mathbf{0} & \mathbf{0} \\ \mathbf{0} & \mathbf{R}[1] & \mathbf{R}[0] & \mathbf{R}^T[1] & \mathbf{0} & \mathbf{0} \\ \dots & \dots & \dots & \dots & \dots & \dots \\ \mathbf{0} & \mathbf{0} & \mathbf{0} & \dots & \mathbf{R}[1] & \mathbf{R}[0] \end{pmatrix}. \tag{5.12}$$

The $LK \times LK$ cross-correlation matrices $\mathbf{R}[0]$ and $\mathbf{R}[1]$ are in turn defined in terms of cross-correlation matrices of individual user's generator matrices ($\mathbf{S}_k$),

$$\mathbf{R}[0] = \begin{pmatrix} \mathbf{I}_{L\times L} & \rho_{12} & \rho_{13} & \dots & \rho_{1K} \\ \rho_{12}^T & \mathbf{I}_{L\times L} & \rho_{23} & \dots & \rho_{2K} \\ \vdots & \rho_{23}^T & \mathbf{I}_{L\times L} & \dots & \dots \\ \vdots & \vdots & \vdots & \ddots & \rho_{(K-1)K} \\ \rho_{1K}^T & \vdots & \vdots & \vdots & \mathbf{I}_{L\times L} \end{pmatrix}, \tag{5.13}$$

$$\mathbf{R}[1] = \begin{pmatrix} \mathbf{0}_{L\times L} & \rho'_{21} & \rho'_{31} & \cdots & \rho'_{K1} \\ \mathbf{0}_{L\times L} & \mathbf{0}_{L\times L} & \rho'_{32} & \cdots & \rho'_{K2} \\ \vdots & \vdots & \mathbf{0}_{L\times L} & \cdots & \cdots \\ \vdots & \vdots & \vdots & \ddots & \rho'_{K(K-1)} \\ \mathbf{0}_{L\times L} & \vdots & \vdots & \vdots & \mathbf{0}_{L\times L} \end{pmatrix}. \tag{5.14}$$

The $L \times L$ matrices ρ_{jk} and ρ'_{jk} are defined as follows,

$$\begin{aligned} \rho_{jk} &= \mathbf{S}_j^T \mathbf{S}_k, \\ \rho'_{jk} &= \begin{bmatrix} \mathbf{0}_{L\times NL} & \mathbf{S}_k^T \end{bmatrix} \begin{bmatrix} \mathbf{S}_j \\ \mathbf{0}_{NL\times L} \end{bmatrix}. \end{aligned} \tag{5.15}$$

Now maximizing $\Omega(\mathbf{d})$ using an exhaustive approach would require complexity in the order of the exponential of KLM which is generally regarded as infeasible for any practical values of K, L and M. However, it is possible to exploit the structure of the matrix $\mathbf{R}$, in order to formulate a simplified solution. In order to decompose the quadratic for, $\mathbf{d}^T\mathbf{R}\mathbf{d}$, we will use the fact that the matrix $\mathbf{R}$ has bandwidth LK and its elements are periodic along the diagonals. Let us introduce the notation $\kappa(j) \in \{1, \ldots, K\}$ to represent the modulo-K remainder of j. A new correlation metric can be defined,

$$\varrho_{\kappa(j),\kappa(j-n)} = \begin{cases} \rho^T_{\kappa(j-n),\kappa(j)}, & \kappa(j-n) \leq \kappa(j) \\ \rho'_{\kappa(j-n),\kappa(j)}, & \kappa(j-n) > \kappa(j) \end{cases}. \tag{5.16}$$

We can summarise the properties of $\mathbf{R}$ as follows:

1. $\mathbf{R}_{[j,j]} = \mathbf{I}_{\mathbf{L}\times\mathbf{L}}$
2. $\mathbf{R}_{[k+iK,n+iK]} = \mathbf{R}_{[k,n]}$
3. $\mathbf{R}_{[j,l]} = \mathbf{0}$ unless $|j-l| < K$
4. $\mathbf{R}_{[i,j]} = \mathbf{R}^T_{[j,i]}$
5. $\mathbf{R}_{[j,j-n]} = \varrho_{\kappa(j),\kappa(j-n)}$

Note that we use the notation $\mathbf{R}_{[a,b]}$ to denote an $L \times L$ submatrix of $\mathbf{R}$. Using these properties and letting $\mathbf{d}_j = \mathbf{0}$ if $j < 0$ or $j \geq MK$. The quadratic term in $\Omega(\mathbf{d})$ can be decomposed as follows,

$$\begin{aligned}
\mathbf{d}^T\mathbf{R}\mathbf{d} &= \sum_{j=0}^{MK-1}\sum_{l=0}^{MK-1}\mathbf{d}_j^T\mathbf{R}_{[j,l]} \\
&= \sum_{j=0}^{MK-1}\mathbf{d}_j^T\mathbf{d}_j + \sum_{j=0}^{MK-1}\mathbf{d}_j^T\sum_{l=j-K+1}^{j-1}\mathbf{R}_{[j,l]}\mathbf{d}_l + \sum_{l=0}^{MK-1}\left(\sum_{j=l-K+1}^{l-1}\mathbf{d}_j^T\mathbf{R}_{[j,l]}\right)\mathbf{d}_l \\
&= \sum_{j=0}^{MK-1}\mathbf{d}_j^T\left(\mathbf{d}_j + 2\sum_{n=1}^{K-1}\mathbf{R}_{[j,j-n]}\mathbf{d}_{j-n}\right) \\
&= \sum_{j=0}^{MK-1}\mathbf{d}_j^T\left(\mathbf{d}_j + 2\sum_{n=1}^{K-1}\varrho_{\kappa(j),\kappa(j-n)}\mathbf{d}_{j-n}\right)
\end{aligned} \tag{5.17}$$

We can now express $\Omega(\mathbf{d})$ as a sum of MK terms such that (a) each term depends on K sub-blocks within $\mathbf{d}$ and (b) any consecutive terms share $K-1$ arguments. Specifically, we can write,

$$\Omega(\mathbf{d}) = \sum_{j=0}^{MK-1}\lambda_j(\mathbf{u}_j, \mathbf{d}_j). \tag{5.18}$$

where, $\mathbf{u}_j$ is the state of the shift register with $(K-1)$ data blocks,

$$\begin{aligned}
\mathbf{u}_{j+1}^T &= \left[\begin{array}{cccc}\mathbf{u}_{j+1}[1], & \mathbf{u}_{j+1}[2], & \ldots & \mathbf{u}_{j+1}[K-1]\end{array}\right] \\
&= \left[\begin{array}{cccc}\mathbf{u}_j[2], & \mathbf{u}_j[3], & \ldots & \mathbf{d}_j\end{array}\right],
\end{aligned} \tag{5.19}$$

and,

$$\lambda_j(\mathbf{u}_j, \mathbf{d}_j) = h\mathbf{d}_j^T\left(2\mathbf{y}_j - h\mathbf{d}_j - 2h\sum_{n=1}^{K-1}\varrho_{\kappa(j),\kappa(j-n)}\mathbf{u}[n]\right). \tag{5.20}$$

Noticing that the $h^2\mathbf{d}_j^T\mathbf{d}_j$ is a constant the transition metric λ_j can be simplified as,

$$\lambda_j(\mathbf{x}_j, \mathbf{d}_j) = \mathbf{d}_j^T\left(\mathbf{y}_j - h\sum_{n=1}^{K-1}\varrho_{\kappa(j),\kappa(j-n)}\mathbf{x}[n]\right). \tag{5.21}$$

It can be seen that in (5.18) the cost function depends on the state vector $\mathbf{u}_j$ and the current data block $\mathbf{d}_j$. As such the objective function can be interpreted graphically as layered directed graph [166]. We can represent each possible sequence $\mathbf{d}$ as a path from origin to destination as shown in Figure 5.2. Each

path cost is given by the function (5.20). The task of finding the vector $\mathbf{d}$ which maximises $\mathbf{\Omega}(\mathbf{d})$ is equivalent to finding the maximum weight path between the origin and destination. A dynamic programming algorithm [166] can be found to determine path resulting in the maximum distance between the origin and destination.

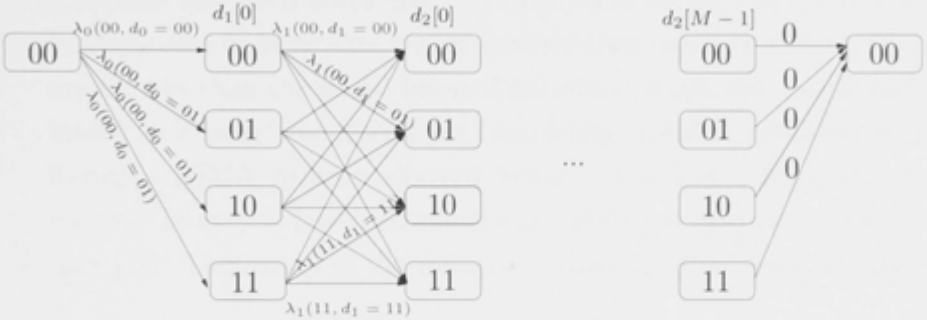

Figure 5.2: Trellis diagram for 2-user with block length $L = 2$, Asynchronous channel

An algorithm to find the maximum length path is based on the following simple observation: if the longest path from the origin to the destination goes through a certain node N, then the sub-path (within the longest path) that connects the origin with N must be the longest among those paths connecting the origin to N. So suppose we knew the longest path from the origin to each of the nodes at the ith stage. Denote the corresponding longest distances $\{J_i(S_0), \ldots, J_i(S_{2^L-1})\}$. Then it is evident that the longest distances at the $(i+1)$th stage satisfy:

$$J_{i+1}(\mathbf{u}_i) = \max\left\{\lambda_i\left(\mathbf{u}_j, S_i\right) + J_i(\mathbf{u}_j)\right\}, \forall i, j \in \left\{0, \ldots, 2^L - 1\right\}. \tag{5.22}$$

where J is initialised to 0 at the first stage of the algorithm. Once the destination node is reached we can read the longest path, which is the most likely sequence of the data $\mathbf{d}$ based on the received signal $\mathbf{r}$.

5.4 Conventional IDMA Receiver

In this Section we describe the iterative asynchronous IDMA receiver in order to compare with the ML approach described in the preceding Section. The iterative receiver uses the same transmitter model as illustrated in the Figure 5.1. It

is necessary to consider a single IDMA block per superblock in order to avoid IBI effects, thus $M = 1$. This structure is similar to the synchronous IDMA approaches given in [10–12]. A guard interval between blocks is necessary in order to prevent inter-block interference (IBI). The model derived in Section 5.3 shows that there is IBI between successive blocks due to asynchronism. The trellis structure and path costs given in (5.18) and (5.20) respectively are due to IBI. Without loss of generality we can assume that user's time delays $\{\tau_k\}, k = 1, .., K$ are shorter than the guard interval duration. When this constraint is maintained inter-block interference can be completely avoided resulting in the simplified iterative IDMA receiver derived below. The low complexity of the iterative receiver is only a few multiplications, additions and one division per chip per user [11]. The model of the iterative receiver is illustrated in Figure 5.3.

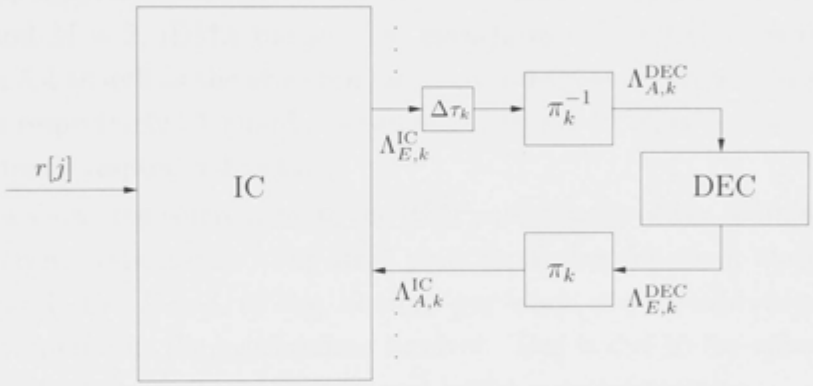

Figure 5.3: The Asynchronous Iterative IDMA Receiver

We assume chip synchronism where user k has delay τ_k. Let $\mathbf{x_k} = \{x_k[j-\tau_k]\}$, for $j \in \{1, \ldots, (NK + \tau_K)\}$ be the interleaved chips for user k, and π_k represent the chip permutation for user k. The ESE is essentially a MAP equaliser at the chip level which determines the Log-likelihood ratios (LLR) of the Maximum A Posteriori probabilities of chips $\mathbf{x_k}$ based on the received signal $\mathbf{r} = \{r[j]\}$, for $j \in \{1, \ldots, (NK + \tau_K)\}$. It is important to note that the block size needs to be increased to $NK + \tau_K$ to compensate for the IBI. We assume that the guard interval is known a priori at the receiver. We define the kth user's data block with guard interval as,

$$x_k(j) = \begin{cases} \pi_k(c_k[l]) & 0 \leq (j - \tau_k) \leq NK \\ 0, & \text{otherwise,} \end{cases} \tag{5.23}$$

where $\mathbf{c_k} = \{c_k[l]\}$ for $l \in \{1, \ldots, NK\}$ represents the repetition coded chips

before interleaving. Using this new model a similar derivation to the one in [12] can be made to construct a block asynchronous iterative IDMA receiver.

5.5 Numerical performance results

In this Section we compare the bit-error performance results of the optimal, asynchronous and synchronous IDMA receivers respectively. In all simulations we defined the spreading gain $N = 4$, the number of users $K = 4$ and the IDMA sub-block size $L = 3$. In performing these simulations the block sizes need to be very small due to the inability to run simulations for large block sizes with the ML receiver. The delay for user k was nominally selected such that $\tau_k = k - 1$ chips. The optimal receiver defined in Section 5.3 was simulated with super-block sizes of $M = 1$ and $M = 2$, IDMA blocks. The asynchronous iterative receiver defined in Section 5.4 as well as the synchronous receiver defined in [12] were run over 10 iterations respectively. A guard interval of length $\tau_k = 3$ chips was used to separate each user's respective blocks.

The Figure 5.4 shows the comparison of the BER performance of the optimal and iterative receivers respectively. The BER plots show that for small block sizes $M = 1$, $N = 4$, and $L = 3$, of size 12 chips per block, the asynchronous receiver slightly outperforms the synchronous receiver. This is due to the effect of the guard interval which results in an increased initial prior information.

From Figure 5.4 it can be seen that the optimal receiver outperforms the iterative receiver for E_b/N_0 values greater than 6dB. The use of very small block sizes detriments the performance of the iterative receiver approaches due to cross-correlation of user signals. For the ML approach when the super-block size was increased to $M = 2$ sub-blocks, a marked performance gain was observed. This can be related to the trellis structure of the receiver which accounts for the cross-correlation between users. As a result the ML receiver cancels inter-block interference between sub-blocks. This has the added effect of reducing wasted energy in the guard interval. In this case the optimal receiver achieves near single user performance at an E_b/N_0 of 9dB.

The biggest advantage of the iterative receiver techniques is the markedly reduced complexity. The complexity of the iterative receiver is in the order of $\mathrm{O}(LK)$ operations per block whereas the complexity of the optimal receiver is in the order of $\mathrm{O}(2^{L(K-1)})$ operations per block. By increasing the block size it is shown that the iterative receivers are capable of achieving near single user

performance [12]. This is due to improved diversity of the interleavers resulting in lower cross-correlation between user signals. Consequently a more realistic scenario would involve using larger block sizes for example $L = 256$ bits per block. In this case it is expected that there is little performance difference between the optimal and iterative receivers.

5.6 Summary

In this Chapter we have developed an optimal asynchronous IDMA receiver. We compared the performance of the system with the conventional iterative receiver. Our results show that the optimal receiver outperforms the iterative approaches for $E_b/N_0 > 6$dB. For the very small block sizes that we consider in this Chapter the performance of the iterative receiver is compromised due to ineffective interleaving causing cross-correlation between user signals. When the ML receiver is across multiple blocks for $M > 1$, the receiver is able to cancel IBI therefore significant improvement is achieved, albeit at the cost of exponential complexity. However, for larger block sizes it is expected that there is little performance difference between the optimal and iterative receivers.

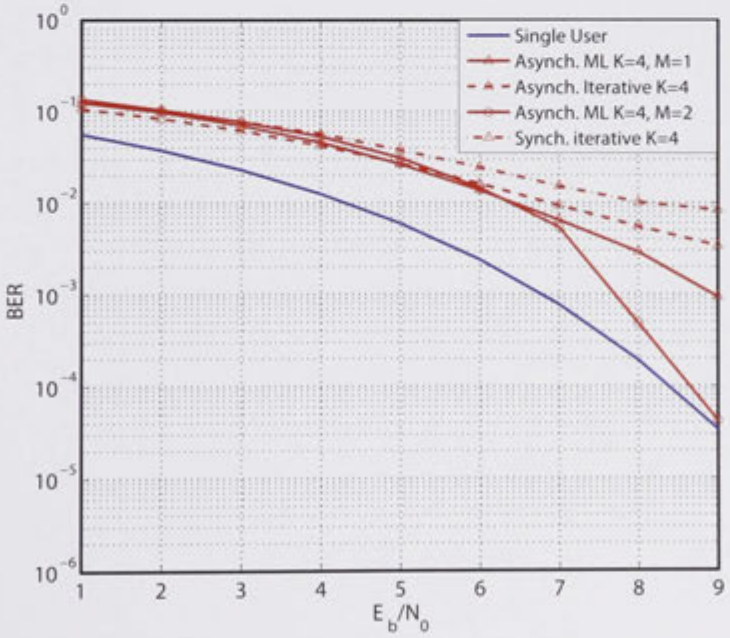

Figure 5.4: BER performance of the Optimal Asynch IDMA receiver vs. Iterative Asynch. IDMA receiver

Chapter 6

Convergence Analysis of Iterative Receivers

6.1 Introduction

In this Chapter we introduce techniques used to analyse and predict the convergence behavior of iterative decoders and receivers. EXIT charts [82, 83] are a popular and powerful tool for analysis of iterative techniques. This Chapter will give an introduction to EXIT analysis and further develop the tools for analysis of a range of receiver components and system configurations.

The design and optimisation of a multiuser system presents a number of challenges to the system engineers. The properties of the multiuser EXIT chart, as well as the power optimisation are two major issues addressed in this thesis. In this Chapter we present an introduction to the EXIT chart analysis tools, such that techniques for analysis and optimisation of IDMA systems can be easily comprehended in later Chapters. As discussed in the Section 1.2.5, EXIT analysis is generally considered to be the most general and best method for analysis of iterative receivers. Furthermore, EXIT functions for FEC codes and other receiver components are widely available in the literature. It has been shown that properties of the EXIT chart can be used to determine the ultimate performance of iterative receivers [86]. For the aforementioned reasons we choose to introduce the topic of EXIT chart analysis for general iterative receivers in this Chapter. We then provide EXIT analysis for equal power allocated IDMA systems, and show how it can be used to accurately predict the performance of such systems.

6.2 The Log Likelihood Ratio

The log likelihood ratio (LLR) is a convenient method for providing information about the sign and reliability of a random variable (RV). Specifically, the sign of a LLR indicates the most likely sign of the RV and the magnitude gives the probability that it is correct. Consider a RV λ which can represent *a priori* (A), *a posteriori* (D) or extrinsic ($E = D - A$) information. We define the log likelihood ratio (LLR) Λ of the RV λ as,

$$\Lambda \triangleq \ln\left(\frac{f(\lambda|x=+1)}{f(\lambda|x=-1)}\right), \tag{6.1}$$

where $x \in \{+1, -1\}$ can be either equiprobable information bits or coded bits. In iterative receivers it is convenient to operate in the log-domain as it enables easy separation of *a posteriori* information into *a priori* and extrinsic information. In general Λ is assumed to be a Gaussian LLR with a Gaussian consistent probability density function (PDF), that is,

$$\Lambda = \frac{\sigma_\Lambda^2}{2}x + n, \text{ where } n \sim (0, \sigma_\Lambda^2). \tag{6.2}$$

The soft information, $\tilde{x}$, can be defined as,

$$\tilde{x} \triangleq \tanh\left(\frac{\Lambda}{2}\right) = \frac{\exp(\Lambda) - 1}{\exp(\Lambda) + 1}, \tag{6.3}$$

and therefore $\tilde{x} \in [-1, +1]$. Like LLRs, soft bits represent the sign and reliability of a RV and are also a convenient metric for use in iterative receivers.

6.3 Mutual Information

In information theory, the Mutual Information (MI) between two RVs is a quantity that measures the mutual dependence of the two variables. Intuitively, MI measures the information that a random variable X contains about RV Y. That is, how much knowing one of these variables reduces the uncertainty about the other.

Mathematically, the MI between X and Y is written as,

$$I(X;Y) = \int\int f(x,y)\log\frac{f(x,y)}{f(x)f(y)}dxdy, \tag{6.4}$$

and since in general the communication system we use has a binary channel input, the MI becomes,

$$I(X;Y) = \frac{1}{2} \sum_{x=+1,-1} \int_{-\infty}^{+\infty} f(y|x) \log \frac{f(y|x)}{f(y)} dy, \tag{6.5}$$

where,

$$f(y) = \frac{1}{2}(f(y|x=+1) + f(y|x=-1)), \tag{6.6}$$

and, for the AWGN channel,

$$f(y|x=\pm 1) = \frac{1}{\sqrt{2\pi\sigma_y^2}} \exp\left(\frac{-(y-x)^2}{2\sigma_y^2}\right), \tag{6.7}$$

with a Gaussian assumption on the *a priori* input A as in (6.2),

$$A \simeq \mu_A x + n_A, \tag{6.8}$$

where $n_A \sim \mathcal{N}(0, \sigma_A^2)$ and $\mu_A = \sigma_A^2$. The MI between the transmitted data $x \in \{-1, +1\}$ and A becomes,

$$I_A(\sigma_A) = 1 - \int_{-\infty}^{+\infty} \frac{\exp\left(\frac{-(\lambda - \sigma_A^2/2)^2}{2\sigma_A^2}\right)}{\sqrt{2\pi\sigma_A^2}} d\lambda, \tag{6.9}$$

where λ are the samples of the *a priori* input.

The conventional method for calculating MI is to estimate the extrinsic information histograms, $f(\lambda|x=-1)$ and $f(\lambda|x=+1)$ from samples λ. The MI of the extrinsic output of a SISO block is calculated as,

$$I_E = \frac{1}{2} \sum_{x=-1,+1} \int_{-\infty}^{+\infty} f(\lambda|X=x) \log_2 \left(\frac{2f(\lambda|X=x)}{f(\lambda|x=-1) + f(\lambda|x=+1)}\right), \tag{6.10}$$

where in this case λ are the samples of E. When calculating MI in this fashion the λ must be grouped into N histogram bins. There is no method available to determine the optimal number of bins and the number used will affect the calculation of MI. In [152] the author finds that calculating the number of bins as,

$$N_{bins} = \lceil L^{\frac{1}{3}} \rceil, \tag{6.11}$$

where L is the number of samples, is a simple method which gives the most

consistent results.

6.4 J Functions

The term J function was coined by ten Brink in [83] and is the name given to the function describing MI as a function of variance. The J function proves to be extremely useful in convergence analysis with transfer charts where MI is used as a metric to describe the SINR reduction process which occurs in iterative receiver components.

6.4.1 The J Function

When the RV Λ is a Gaussian consistent distributed RV (according to (6.8)) and X is binary uniformly distributed RV, the MI $I(X;\Lambda)$ between X and Λ can be expressed as,

$$I_\Lambda = 1 - \int_{-\infty}^{+\infty} \log_2(1+\exp(-\lambda)) f(\lambda|x=+1) d\lambda. \tag{6.12}$$

Observing that the PDF $f(\lambda|x=+1)$ is a function of the variance of the LLR λ, and assuming that λ has a mixture Gaussian distribution as in (6.8), it is apparent that the MI is itself a function of the variance. The J function and its inverse are well known functions defining the relationship between MI $I_\Lambda = I(X;\Lambda)$ in (6.12) and variance σ_Λ^2 in (6.8). The J function is given by,

$$J(\sigma) \triangleq I_\Lambda(\sigma_\Lambda = \sigma), \tag{6.13}$$

$$\sigma_\Lambda = J^{-1}(I_\Lambda), \tag{6.14}$$

where Λ is generally A. Since the MI in (6.12) cannot be expressed in closed-form under the Gaussian assumption, close approximations have been developed in the literature. ten Brink *et al.* proposed an approximation in [83], however the approximation developed by Brännström *et al.* in [91] is generally considered to be superior and is given by,

$$J(\sigma) \approx \left(1 - 2^{-H_1 \sigma^{2H_2}}\right), \tag{6.15}$$

$$J^{-1}(I) \approx \left(-\frac{1}{H_1}\log_2\left(1 - I^{\frac{1}{H_3}}\right)\right)^{\frac{1}{2H_2}}, \tag{6.16}$$

where $H_1 = 0.3073$, $H_2 = 0.8935$ and $H_3 = 1.1064$ were obtained using numerical optimisation (Nelder-Mead simplex optimisation [167]) to minimise the total squared difference between (6.12) and (6.15).

The J function will be shown to be extremely useful in transfer chart derivation, however it also provides an easy means for estimating BER. The soft *a posteriori* output of the decoder can be written as $D = A+E$ for the outer decoder of an IDMA system. Under the assumption that both the *a priori* input A and the extrinsic output E are Gaussian distributed, then the *a posteriori* output is also Gaussian. Since hard decision are made on the *a posteriori* output, the BER can be estimated as,

$$P_b \approx Q\left(\frac{\sigma_D}{2}\right), \tag{6.17}$$

where σ_D^2 is the variance of D, and assuming independence,

$$\sigma_D^2 = \sigma_A^2 + \sigma_E^2. \tag{6.18}$$

Using (6.15) the variances of A and E are,

$$\sigma_A^2 = J^{-1}\left(I_A\right)^2, \tag{6.19}$$

$$\sigma_E^2 = J^{-1}\left(I_E\right)^2. \tag{6.20}$$

Using (6.17), (6.18), (6.19) and (6.20) the BER can be estimated as,

$$P_b \approx Q\left(\frac{\sqrt{J^{-1}\left(I_A\right)^2 + J^{-1}\left(I_E\right)^2}}{2}\right). \tag{6.21}$$

6.4.2 The J_s Function

Fidelity was first introduced in [168] and [169] as,

$$M_\Lambda = \mathrm{E}\left\{x\tilde{x}\right\}, \tag{6.22}$$

$$= \mathrm{E}\left\{\tanh^2\left(\frac{\lambda}{2}\right)\right\}, \tag{6.23}$$

$$= \mathrm{E}\left\{\tilde{x}^2\right\}, \tag{6.24}$$

where $\Lambda = A$ or E and $\tilde{x} = \tanh(\Lambda/2)$ for input and output fidelity respectively. Fidelity has been shown to be an accurate measure for tracking convergence behavior. In [170] the authors introduce a method for relating symbol variance

to MI using the defined fidelity metric (6.22). The expression for the fidelity function can be written,

$$M_\Lambda = 1 - \int_{-\infty}^{+\infty} \frac{2}{1+\exp(\lambda)} f(\lambda|x=+1)d\lambda. \tag{6.25}$$

The J_s function and its inverse are valuable tools in convergence analysis using fidelity as a metric. The J_s function is defined [152, 170] as,

$$J_s(\sigma) \triangleq M_\Lambda(\sigma_\lambda = \sigma). \tag{6.26}$$

And the inverse function is defined,

$$\sigma_\Lambda = J_s^{-1}(M_\Lambda), \tag{6.27}$$

where it is assumed that Λ is Gaussian according to (6.2). The J_s function has no closed-form solution but is closely approximated[170] by,

$$J_s(\sigma) \approx \left(1 - 2^{-H_1\sigma^{2H_2}}\right)^{H_3}, \tag{6.28}$$

$$J_s^{-1}(M) \approx \left(-\frac{1}{H_1}\log_2\left(1 - M^{\frac{1}{H_3}}\right)\right)^{\frac{1}{2H_2}}, \tag{6.29}$$

where $H_1 = 0.4282$, $H_2 = 0.8130$ and $H_3 = 1.1699$ were obtained using the Nelder-Mead simplex method [167] to minimise the squared difference between the approximation (6.28) and the actual function (6.26). Figure 6.1 shows the actual J_s and J functions along with their approximations, which are shown to be very close. The actual functions, (6.12) and (6.25) were obtained using numerical integration.

6.4.3 Relationship between Mutual Information and Symbol Error Variance

In [170] a function was proposed to relate MI as symbol error variance. This function is very useful in determining the extrinsic transfer functions for the IC, and also for translating between transfer charts. Considering the symbol error variance $\sigma_x^2 = \mathrm{E}\left\{(x-\tilde{x})^2\right\}$, this can be simplified,

$$\sigma_x^2 = 1 - \mathrm{E}\left\{\tilde{x}^2\right\}, \tag{6.30}$$

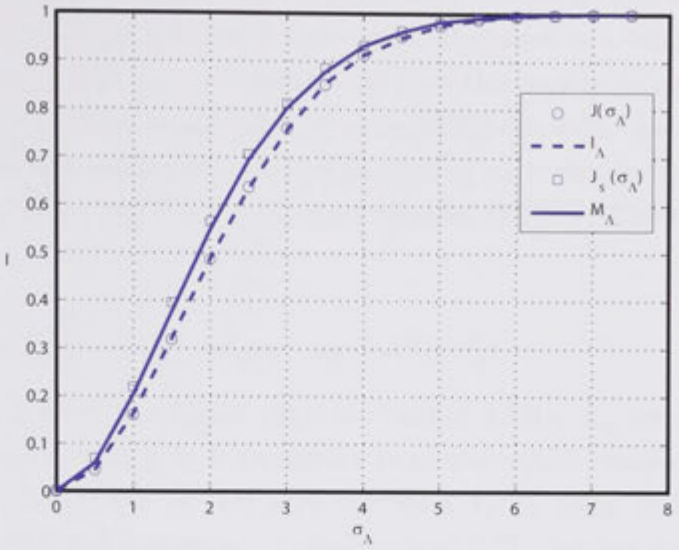

Figure 6.1: Comparison between analytical and simulated J and J_s functions respectively.

and,

$$M_\Lambda = 1 - \sigma_x^2. \tag{6.31}$$

The function which relates MI to fidelity was proposed [170],

$$I = T(M) = J(J_s^{-1}(M)) \approx 0.74M + 0.26M^2, \tag{6.32}$$

$$M = T^{-1}(I) \approx \frac{-0.74}{0.52} + \sqrt{\left(\frac{0.74}{0.52}\right)^2 + \frac{I}{0.26}}, \tag{6.33}$$

Moreover the symbol variance can be related to MI using,

$$\sigma_x^2 = 1 - T^{-1}(I). \tag{6.34}$$

6.5 EXIT Function for the Decoder

In general, EXIT functions must be generated using Monte Carlo simulations of the encoder/decoder. There have been published results [89] where closed formed EXIT functions have been derived for simple codes. However, these have been confined to the binary erasure channel. In coded IDMA systems the FEC and IC are concatenated in a serial fashion. EXIT functions for serially concatenated codes are generated according to the system diagram in Figure 6.2. Data blocks

$x \in \{+1, -1\}$ are randomly generated and encoded using the FEC encoder. The EXIT function for the Decoder in a serial concatenated system is a function of only the *a priori* channel. The *a priori* channel input to the decoder is modelled as follows. The *a priori* channel is modelled by multiplying the coded data bits c by σ_A^2 and adding noise of variance σ_A^2, where the value of σ_A is chosen using the inverse J function, $\sigma_A = J^{-1}(I_A^{DEC})$, for the desired value of I_A^{DEC}. The channel input is now,

$$A = \frac{\sigma_A^2}{2} c + n_A \quad \text{where} \quad n_A \sim \mathcal{N}(0, \sigma_A^2). \tag{6.35}$$

The decoder is then activated and the extrinsic output LLRs, E, are passed along with the systematic data x to a histogram generator which estimates the PDFs $f(E|x = +1)$ and $f(E|x = -1)$ and calculates I_E^{DEC} using (6.10). A detailed description of the steps required to generate an EXIT function are given in Section 4.4 of [152].

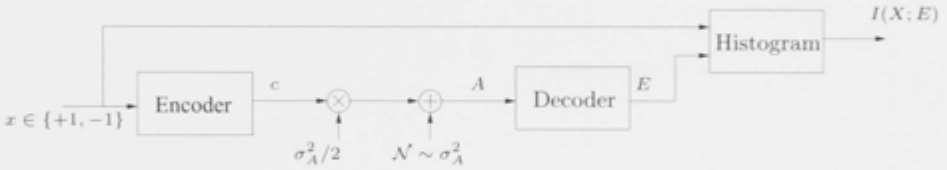

Figure 6.2: EXIT chart generation for the Decoder.

6.6 EXIT Function for the IC

In this Section we determine the EXIT function for the IC which can be determined either by Monte Carlo simulation, or as a closed form approximation using the J function. For illustrative purposes and for the sake of simplicity we only consider the equal power allocated transmission in this Chapter. The EXIT transfer function can be computed using a similar method to the one described in Section 6.5. The EXIT function can be determined using a Monte Carlo simulation as shown in the Figure 6.3. Each user's data sequence is generated randomly, the data sequence for user k is denoted as, $x_k \in \{+1, -1\}$. All of the user's data sequences are added in the multiuser channel and additive white Gaussian noise is then added. Mathematically, the received signal, r, is written as,

$$r = \sum_{k=1}^{K} x_k + n, \quad \text{where} \quad n \sim \mathcal{N}(0, \sigma_n^2) \tag{6.36}$$

The *a priori* input for user k denoted as A_k is a Gaussian consistent random variable generated using the user's data symbols x_k,

$$A_k = (\sigma_A^2/2)x_k + n_{A_k} \quad \text{where} \quad n_{A_k} \sim \mathcal{N}(0, \sigma_A^2). \tag{6.37}$$

The IC is then activated using r and the set of *a priori* extrinsic LLR inputs $\{A_k\}$, $\forall k$. The extrinsic LLR output vector of the IC, E, is passed along with the systematic data x_k to a histogram generator which estimates the PDFs $f(E|x_k = +1)$ and $f(E|x_k = -1)$ and calculates I_E^{IC} using (6.10).

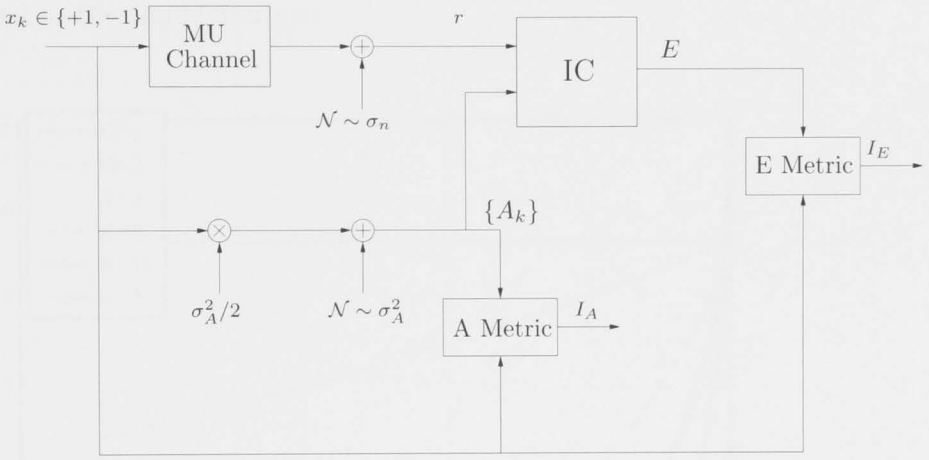

Figure 6.3: The EXIT function for the IC.

The variance of noise plus MAI for the coded chips input to the IC can be easily shown to be,

$$\sigma_\zeta^2 = (K-1)\sigma_x^2 + \sigma_n^2 \tag{6.38}$$

where σ_x^2, is the coded bit variance given in (6.30) and $\sigma_n^2 = \frac{N_0}{2R_c E_b}$. It follows that the variance of the output of the IC ($\sigma_E^2 \triangleq \text{Var}\left\{\Lambda_x^{IC}\right\}$), can be written,

$$\sigma_E^2 = \frac{4}{(K-1)\sigma_x^2 + \sigma_n^2}. \tag{6.39}$$

The fact that there is a closed-form solution for an IC variance transfer chart means that it is possible to easily derive the transfer chart without the use of Monte Carlo simulation. The EXIT chart for the IC can be computed using (6.39), (6.13) and (6.34), that is,

$$I_E^{IC} = J\left(\sqrt{\frac{4}{(1 - T^{-1}(I_A^{IC}))K + \frac{N_0}{2RE_b}}}\right), \tag{6.40}$$

where $T(\cdot)$ is from (6.32) - (6.33). The function (6.40) will be used throughout this Thesis as a closed-form EXIT function for the IC.

EXIT functions for the IC are shown in Figure 6.4 for various system loads, with spreading factor $S = 16$, at $E_b/N_0 = 10$dB. Note that in the SU case, $K = 1$, the MI of the extrinsic output is independent of the *a priori* input. The constant I_E^{IC} in the SU case is equal to $J(2/\sigma_n)$ as there is no MAI. Figure 6.4 shows that increasing the number of users increases the steepness of the transfer characteristics. Note that at the point where full *a priori* knowledge is available, $I_A^{IC} = 1$, which corresponds to the removal of all MAI, the MI of the extrinsic output is equal to the single user case.

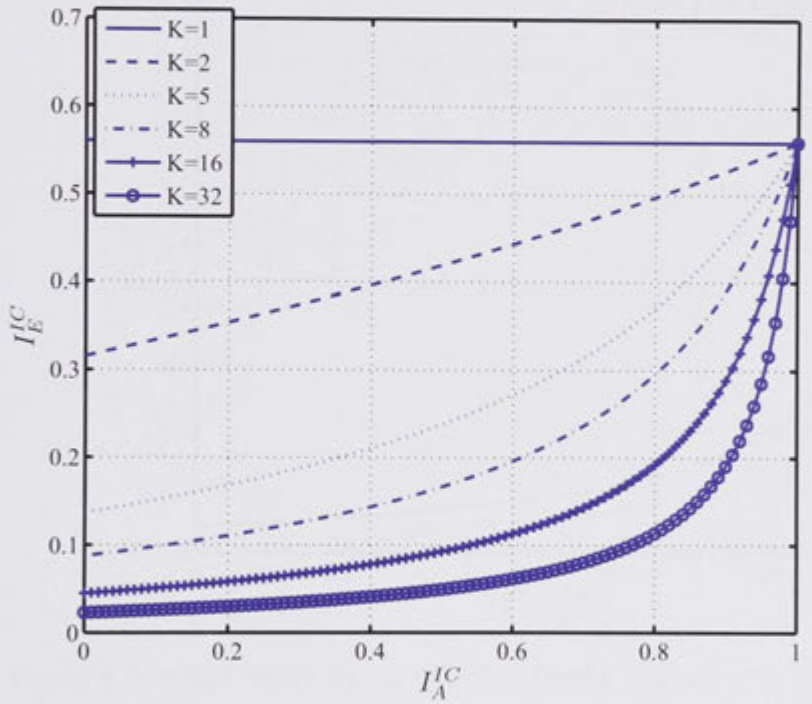

Figure 6.4: EXIT function of the IC under various system loads.

6.7 EXIT Chart

An EXIT chart is a plot including the transfer functions of all the receiver components. The functions are arranged such that the output of one component shares an axis with the corresponding input of the component to which it is connected. The simple case as shown in Figure 6.5 shows the EXIT chart for an

uncoded IDMA system where the Decoder is a soft repetition decoder (repetition code length, $S = 16$). In this scenario there are $K = 16$ users and each of them is allocated a repetition code of length $S = 16$, the receiver is operating at an $E_b/N_0 = 10$dB. Figure 6.6 shows the EXIT chart for a PCC coded IDMA system with $K = 16$ at an $E_b/N_0 = 2.7$dB. In this scheme the FEC code is a rate 1/2 PCC constructed with two $[23, 35]_8$ RSC codes concatenated with a repetition code of length $S = 16$. Note that the more powerful code has a much lower convergence threshold.

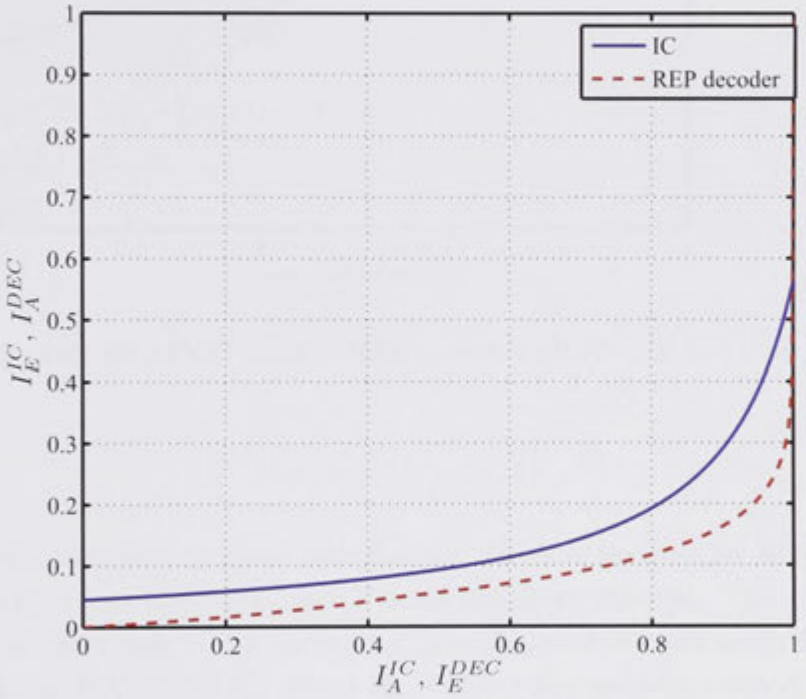

Figure 6.5: EXIT chart for an uncoded IDMA system with $K = 16$ and $S = 16$, $E_b/N_0 = 10$dB

6.7.1 Capacity

Since EXIT functions show the MI transfer properties of receiver components it is expected that EXIT charts can be used in capacity optimisation of IDMA systems. The relationship between EXIT curves, capacity and code rate in a binary erasure channel was proved in [86] and [87]. The area under an EXIT curve is given by $\mathcal{A} = \int_0^1 I_E(I_A)dI_A$. Consider a serially concatenated code with

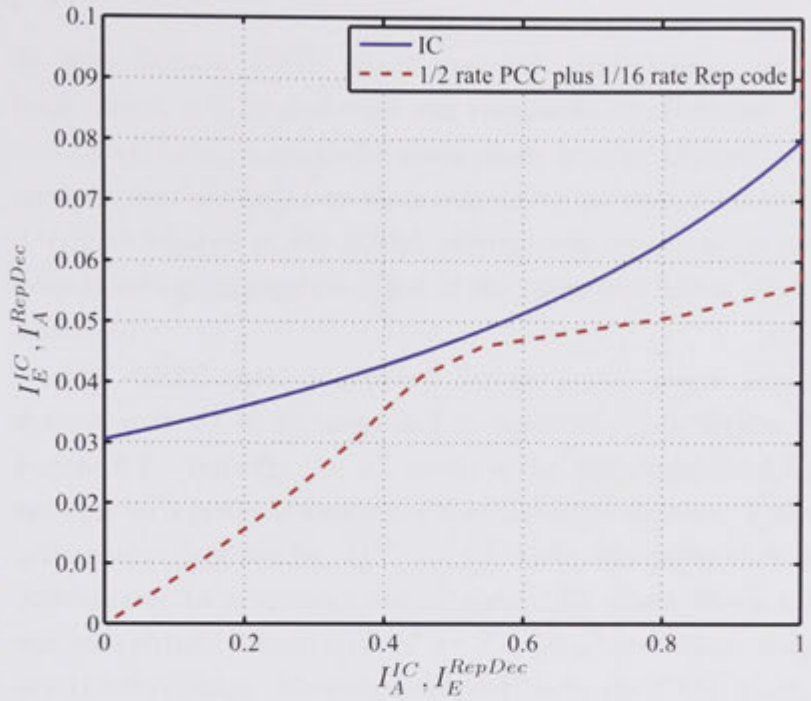

Figure 6.6: EXIT chart for a PCC coded IDMA system with $K = 16$ and $S = 16$, $E_b/N_0 = 2.7$dB

outer code rate R_{out} and inner code of rate $R_{in} = 1$, which is the case for IDMA systems in general, where the inner "code" is the multiuser channel. The area under the inverted outer code EXIT curve, is $\mathcal{A}_{out} = R_{out}$ and the area under the inner curve is $\mathcal{A}_{in} = I(X;Y)/n/R_{in}$ where $R_{in} = k/n$. For successful decoding the EXIT curves must not intersect and $\mathcal{A}_{in} - \mathcal{A}_{out} > 0$, so

$$R_{out} R_{in} < I(X;Y)/n \leq C. \tag{6.41}$$

Note that (6.41) shows that capacity can only be achieved if $R_{in} = 1$. Since the rate of the inner code, the IDMA channel, is equal to one, the area under the inner EXIT curve is $\mathcal{A}_{in} = C$ where C is the capacity of the channel. Therefore,

$$R_{out} \leq C. \tag{6.42}$$

This is a form of Shannon's capacity theorem [171], the outer code rate must be less than the capacity of the inner channel.

6.8 EXIT Chart Analysis vs. Simulation

In this Section EXIT chart snapshot trajectories, or simulated decoding trajectories, will be discussed and compared. Furthermore, EXIT chart analysis results will be compared with simulations in order to justify the use of EXIT chart analysis and demonstrate their suitability as tools for iterative receiver design. The performance of the IDMA receiver was predicted using EXIT charts for a fully loaded configuration (that is the spreading factor, N equals the number of users, K).

The EXIT chart trajectory for an equal power repetition coded IDMA system with $K = 16$ users and a repetition code length $S = 16$ is shown in Figure 6.7. Initially the IC receives the fully interference affected signal and receives no *a priori* information from the outer decoder. Thus the initial extrinsic information is given by, $I_E^{DEC} = I_A^{IC} = 0$. Hereafter each activation of the IC corresponds to a vertical line in the EXIT chart which corresponds with the output extrinsic information of the IC, using the output of the FEC decoder as *a priori* information. After each vertical line in the EXIT chart, the FEC decoder is activated resulting in a horizontal line which corresponds with the transformation of output extrinsic information of the IC (used as *a priori* to the FEC decoder) into output extrinsic information of the FEC decoder. Thus, each iteration of the IDMA receiver results in a step in the EXIT chart which bounces between the EXIT functions of the IC and FEC decoder. After each iteration of the IC the *a priori* input information to the FEC decoder is improved. Where the two EXIT functions intersect results in the final operating extrinsic information of the Decoders. Using this we can see that when there is an open tunnel in the EXIT chart the system converges to the operating extrinsic information point, ($I_E^{DEC} \simeq 1$), resulting in virtually error free decoding from the FEC decoder. The EXIT chart trajectory for an equal power IDMA system using a 1/2 rate turbo code composed of two $(23, 35)_8$ RSC codes concatenated with a repetition code length $S = 16$, with $K = 16$ users operating at an $E_b/N_0 = 2.7$dB is shown in Figure 6.8. In both examples we can see that the receiver converges due to the open tunnel in the EXIT chart.

6.8.1 BER Performance

The simulation results versus the EXIT chart predictions will now be presented. The simulations were carried out over a range of SNR. The performance of an

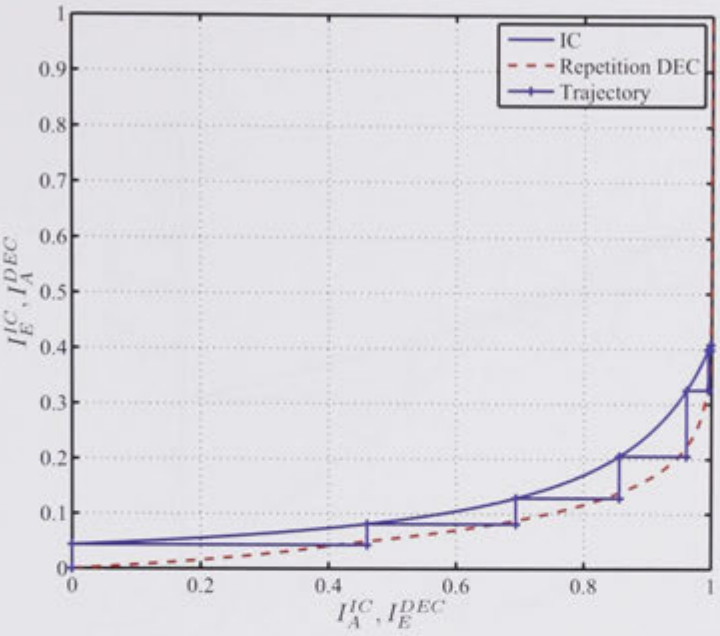

Figure 6.7: EXIT chart trajectory for an uncoded IDMA system with $K = 16$ and $S = 16$, $E_b/N_0 = 8$dB

equal power uncoded IDMA system with $K = 16$ users and spreading factor $S = 16$ is shown in Figure 6.9. The EXIT chart prediction (dashed line) closely matches the simulation (solid line) down to a BER of approximately 10^{-5}.

In Figure 6.10 the simulated and analytical BER are compared for a PCC coded IDMA system, where the FEC code is a 1/2 rate PCC concatenated with a 1/16 repetition code (same code described in Section 6.8). We can see from the Figure 6.10 that the system has a convergence threshold around 2.7dB, as this corresponds to the open tunnel in the EXIT chart. By inspection of Figure 6.8 we can see that there is a point close to ($I_A^{IC} \simeq 0.52, I_E^{IC} \simeq 0.048$) where there is tight gap in the EXIT chart. As the E_b/N_0 is reduced to be marginally less than 2.7dB the EXIT function for the IC will intersect with the inverted EXIT function of the decoder (DEC) at around ($I_E^{DEC} \simeq 0.52$) and the extrinsic information cannot be improved more than this resulting in a high BER (around $BER = 0.2$ according to Figure 6.10). When the E_b/N_0 approaches 2.7dB there begins to be an open tunnel between the EXIT functions for the IC and DEC which facilitates the convergence of the IDMA system and a sharp fall in BER, as can be seen by the step like form of the BER in Figure 6.10.

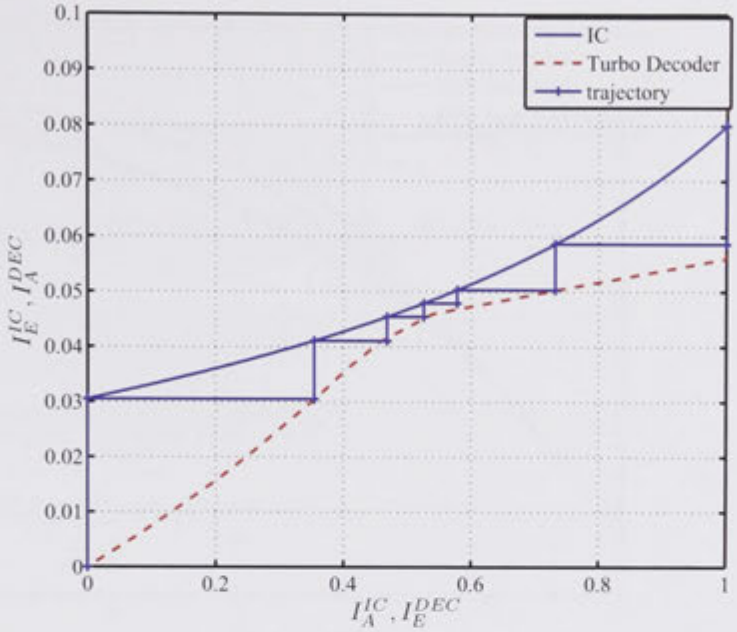

Figure 6.8: EXIT chart trajectory for a PCC coded IDMA system with $K = 16$ and $S = 16$, $E_b/N_0 = 2.7$dB

6.9 Summary

This Chapter investigated EXIT chart analysis for coded IDMA systems. The effect of the number of users, spreading factor and code rate were observed on the EXIT charts. A closed-form EXIT function for an IC was derived and the accuracy of the EXIT chart analysis of the IC was shown through simulations. In this Chapter and the preceding Chapters, tools for analysis of iterative receivers and decoders are described and developed. The focus has been on the multiuser coded IDMA system. These techniques for power optimisation of the receiver will be used in the next Chapter.

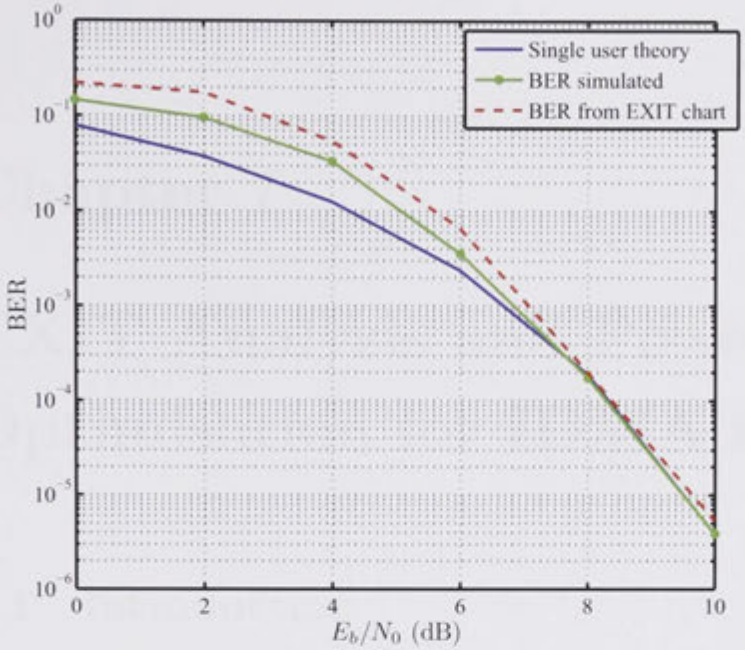

Figure 6.9: Simulated vs. analytical plot of BER for uncoded IDMA system with $K = 16$ and $S = 16$.

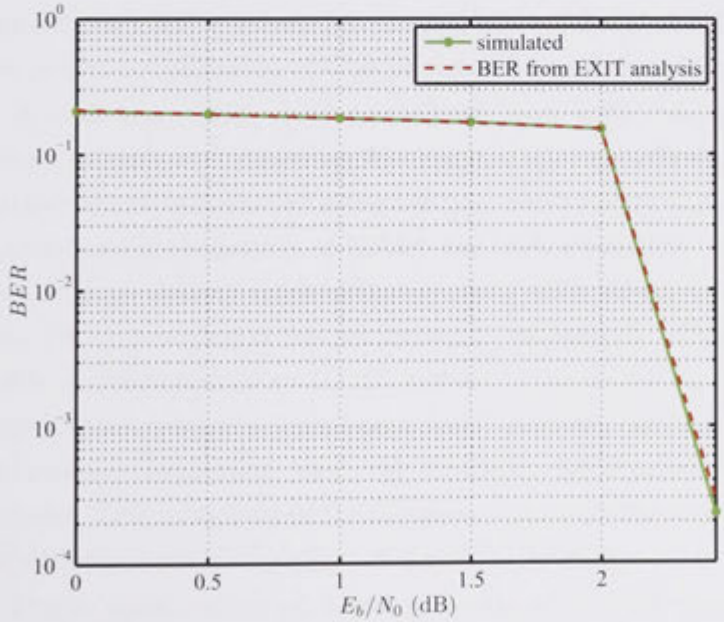

Figure 6.10: Simulated vs. analytical plot of fully loaded PCC turbo coded IDMA system with $K = 16$ and $S = 16$.

Chapter 7

EXIT Analysis and Power Optimisation for IDMA receivers

7.1 Introduction

In the previous Chapter we described the basic EXIT chart analysis technique for iterative receivers in general. We illustrated the EXIT chart for an equal power allocated IDMA system, and showed how it can be used to analyse and predict the performance of the aforementioned system. In this Chapter we extend and improve the EXIT analysis for unequal power allocated IDMA systems, and show how power optimisation can be performed using the new analytical tools.

Recent work [100, 101] has shown that with rate or power control and group stripping and decoding, the optimal spectral efficiency of a multiple-access channel can be approached using low level modulation (e.g. BPSK or QPSK). The analysis and optimisation of IDMA has been studied in [102], where the authors use the large system approximation along with signal to interference plus noise ratio (SINR) evolution for performance evaluation. They also consider power profile optimisation of an IDMA system to maximise its spectral efficiency. The large-system approximation-based SINR analysis method provides less accurate performance evaluation than the Extrinsic information transfer (EXIT) chart analysis. This is because of the Gaussian approximation made in order to compute the variance transfer function of the FEC decoder.

Power optimisation of a coded multiuser CDMA system using EXIT chart analysis was initially proposed in Shepherd *et al.* [104, 105]. In [105] the EXIT function for an unequal power allocated CDMA system was constructed by using the average variance transfer (VT) functions for the decoders (introduced in

Schlegel *et al.* [76, 103]). The VT charts are converted to EXIT charts using techniques in [170]. An approximation of the EXIT function for the interference canceler (IC) is made by using the VT chart for the IC given in [76]. The average effective EXIT function for all user groups presented in [104, 105] results in an imprecise and unintuitive analytical model. A more intuitive analysis tool for an IMUD would predict different convergence performance for user's in different power groups.

In this Chapter we illustrate multi-dimensional EXIT charts for unequal power IDMA receivers. For a system with K user groups the analysis consists of K multi-dimensional EXIT charts, where each user group has a separate EXIT chart and consequently differing convergence behavior. We define a low complexity mutual information tracking algorithm to predict the ultimate convergence of the system. We use the analysis technique presented to construct a nonlinear constrained optimisation problem. A differential evolution technique [172] is used to determine the optimum power profile, which minimises the total transmit power. The developed technique shows performance improvements over the analysis and optimisation methods in [104, 105], while still complying with the EXIT chart properties and assumptions given in [82, 83].

7.2 System Model

We consider an Interleave Division Multiple Access (IDMA) system. However, the work in this Chapter can be generalised for other iterative multiuser detection schemes such as Direct-Sequence Code Division Multiple Access (DS-CDMA)[129]. The system model for an iterative multiuser receiver is shown in Figure 7.1. There are a total of K_T transmitters generating independent data symbols, $b_k \in \{-1, 1\}$, which are encoded by a forward error correcting (FEC) code. The encoded symbols c_k are interleaved and mapped into BPSK symbols x_k. For simplicity all users are assumed to be synchronous. The received signal is,

$$r(j) = \sum_{i=1}^{K_T} \sqrt{P_i} x_i(j) + n(j), \tag{7.1}$$

where $\{x_i(j)\}$ are the interleaved coded chip sequence for user i, $x_i(j) = \pm 1$, P_i is the power allocated to the i-th user, and $n(j)$ is AWGN noise with variance σ_n^2, i.e. $n(j) \sim \mathcal{N}(0, \sigma_n^2)$. The effects of the channel and fast power control result

in a static power group P_i, which is a general assumption in most power control strategies. The optimisation technique described in this Chapter can be easily extended to an asynchronous system with a multipath channel.

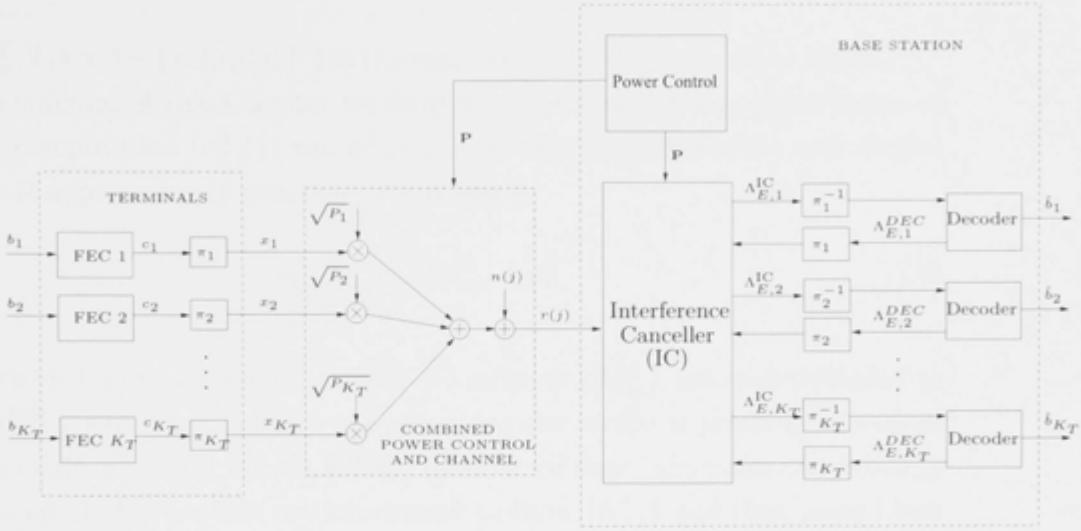

Figure 7.1: The architecture of an IDMA system for K users

The IMUD receiver, shown in Figure 7.1, consists of an interference canceller (IC) and K_T *a posteriori* probability (APP) decoders (DEC), operating iteratively. The IC performs chip-by-chip detection based upon the channel input and the *a priori* information provided by the decoders. Concentrating on the i-th user, (7.1) can be rewritten as, $r(j) = \sqrt{P_i}x_i(j) + \zeta_i(j)$, with, $\zeta_i(j) = \sum_{i' \neq i}^{K_T} \sqrt{P_{i'}}x_{i'}(j) + n(j)$, being the sum of the multiple access interference (MAI) and the additive noise with respect to this user. Each $x_i(j)$ is a binary random variable with mean $E\{x_i(j)\}$ and variance $\sigma_{x,i}^2(j)$ (initialised to 0 and 1 respectively) which are related to the *a priori* information of $x_i(j)$. When K_T is large, with the central limit theorem, the MAI term $\zeta_i(j)$, in (7.1) can be approximated as a Gaussian random variable, with mean and variance given respectively by,

$$\begin{aligned} E\{\zeta_i(j)\} &= \sum_{i' \neq i} \sqrt{P_{i'}} E\{x_{i'}(j)\}, \\ \text{and } \sigma_{\zeta,i}^2(j) &= \sum_{i' \neq i} P_{i'} \sigma_{x,i'}^2(j) + \sigma_n^2. \end{aligned} \tag{7.2}$$

The IC then computes the extrinsic log-likelihood ratios (LLRs) of $\{x_k(j)\}$

based upon (7.1) and (7.2) as,

$$\Lambda_{E,i}^{\mathrm{IC}}(j) = \frac{2\sqrt{P_i}\left(r(j) - \sum_{i' \neq i} \sqrt{P_{i'}} E\{x_{i'}(j)\}\right)}{\sigma_{\zeta,i}^2(j)}, \tag{7.3}$$

where $\sigma_{x,i'}^2(j) = 1 - \left(E\left\{x_{i'}(j)\right\}^2\right)$ is the variance of the estimate of the chip $x_{i'}(j)$. In the remainder of this Chapter we drop the (j) index in the approximation of variance computation ($\sigma_{\zeta,i}^2(j)$ and $\sigma_{x,i'}^2(j)$) assuming the interference and symbol variance is approximately constant over a block,

$$\sigma_{\zeta,i}^2 \simeq \sum_{i' \neq i} P_{i'} \sigma_{x,i'}^2 + \sigma_n^2. \tag{7.4}$$

As shown in Figure 7.1 for user i, the IC outputs $\{\Lambda_{E,i}^{\mathrm{IC}}\}$ are de-interleaved to form $\{\Lambda_{A,i}^{\mathrm{DEC}}\}$ which are fed into the outer decoder as the *a priori* information. The outer soft input soft output (SISO) decoder for user i generates the extrinsic LLR outputs $\{\Lambda_{E,i}^{\mathrm{DEC}}\}$ which are interleaved to form $\{\Lambda_{A,i}^{\mathrm{IC}}\}$ and then passed into the IC as *a priori* information for user i. The mean and variance of $x_i(j)$ can be computed using $\{\Lambda_{A,i}^{\mathrm{IC}}\}$ as follows,

$$\begin{aligned} E\{x_i(j)\} &= \tanh\left(\frac{\Lambda_{A,i}^{\mathrm{IC}}(j)}{2}\right), \\ \text{and } \sigma_{x,i}^2 &= 1 - E\{x_i(j)\}^2, \end{aligned} \tag{7.5}$$

which in turn are used by the IC to refine its output in (7.2) and (7.3) for the next iteration. In the final iteration, the SISO decoder produces hard decisions $\{\hat{b}_i(j)\}$ for the information bits $b_i(j)$ based on the *a posteriori* LLRs $\{\Lambda_{E,i}^{\mathrm{DEC}}(j)\}$. Also shown in Figure 7.1 is the power control block, which passes the optimised power profile $\mathbf{P} = \{P_1, \ldots, P_{K_T}\}$ to the transmitter. We do not specify the mechanism for the power control, although we do assume that it is sufficiently fast as to compensate for the effects of fading. With the provision of fast power control the i-th user's transmit power and the effects of the channel can be combined, such that at the IC input for the user has a static power level P_i.

7.3 Multi-Dimensional EXIT Analysis

Consider an IDMA system with K groups of different power levels. We define $\mathbf{K} = [K_1, \ldots, K_K]$ and $\mathbf{P} = [P_1, \ldots, P_K]$, where K_k and P_k are the number of users in the group k and their transmitted power, respectively, for $k = 1, \ldots, K$. The total number of users in the system is

$$K_T = \sum_{k=1}^{K} K_i. \tag{7.6}$$

We assume all users within a power group are essentially identical and we therefore consider each group a (virtual) single user. For convergence analysis, the traditional EXIT charts need to be adjusted to reflect the behavior of the system which has unequal power allocation.

We utilise the J function, which describes the mutual information as a function of variance, the equation (6.12) can be rewritten as,

$$I_\Lambda(\sigma_A) = J(\sigma_\Lambda), \tag{7.7}$$

$$= 1 - \int_{-\infty}^{+\infty} \log_2\left(1 + e^{-\xi}\right) \frac{1}{\sqrt{2\pi\sigma_\Lambda^2}} e^{\frac{-(\xi - \frac{\sigma_\Lambda^2}{2})^2}{2\sigma_\Lambda^2}} d\xi, \tag{7.8}$$

and ξ are the samples of Λ. Where Λ represents the extrinsic LLR, which is a Gaussian random variable with a Gaussian consistent probability density function, i.e $\Lambda \sim \mathcal{N}(\frac{\sigma_\Lambda^2 b}{2}, \sigma_\Lambda^2)$. The LLR outputs of the IC for the k-th user, $\{\Lambda_{E,k}^{\mathrm{IC}}\}$, can be approximated by a Gaussian random variable with mean and variance,

$$E\{\Lambda_{E,k}^{\mathrm{IC}}(j)\} = \frac{2P_k}{\sigma_{\zeta,k}^2},$$
$$\text{and } \sigma_{E,k}^2 = \frac{4P_k}{\sigma_{\zeta,k}^2}, \tag{7.9}$$

respectively. Observing that $\Lambda_{E,k}^{\mathrm{IC}}(j)$ is a Gaussian consistent random variable, it follows that the EXIT function for the IC can be approximated using the $J(\cdot)$ function,

$$\mathrm{I}_{E,k}^{\mathrm{IC}} = J\left(\sigma_{E,k}\right),$$

$$= J\left(\sqrt{\frac{4P_k}{\sigma^2_{\zeta,k}}}\right),$$
$$= J\left(\sqrt{\frac{4P_k}{\sum_{k'\neq k} K_{k'}P_{k'}\sigma^2_{x,k'} + (K_k-1)P_k\sigma^2_{x,k} + \sigma^2_n}}\right), \tag{7.10}$$

observing that $\sigma^2_{\zeta,k} = \sum_{k'\neq k} K_{k'}P_{k'}\sigma^2_{x,k'} + (K_k-1)P_k\sigma^2_{x,k} + \sigma^2_n$. Using the results of [170] the input extrinsic information ($\mathrm{I}^{\mathrm{IC}}_{A,k}$) for a user in power group k can be related to the symbol variance ($\sigma^2_{x,k}$)

$$\sigma^2_{x,k} = 1 - \mathrm{T}^{-1}\left(\mathrm{I}^{\mathrm{IC}}_{A,k}\right), \tag{7.11}$$

where $\mathrm{T}^{-1}(I) \triangleq \frac{-0.74}{0.52} + \sqrt{\left(\frac{0.74}{0.52}\right)^2 + \frac{I}{0.26}}$ is the fidelity function defined in (6.33). The $J(\cdot)$ function can be approximated in closed form using (6.15). The EXIT function for the IC can be approximated in closed form by combining (7.10) and (7.11), obtaining,

$$\mathrm{I}^{\mathrm{IC}}_{E,k} = J\left(\sqrt{\frac{4P_k}{\sum_{k'\neq k} K_{k'}P_{k'}(1-\mathrm{T}^{-1}\left(\mathrm{I}^{\mathrm{IC}}_{A,k'}\right)) + (K_k-1)P_k(1-\mathrm{T}^{-1}\left(\mathrm{I}^{\mathrm{IC}}_{A,k}\right)) + \sigma^2_n}}\right), \tag{7.12}$$

and then using (6.15) to approximate the J function in (7.12).

In [104, 105] the average Interference Canceller (IC) EXIT function is presented as,

$$\hat{I}^{IC}_{E,eff} = f_{mud}\left(\hat{I}^{IC}_{A,eff}, \hat{E}_b/N_0\right),$$
$$= J\left(\sqrt{\frac{4}{\left(1-T^{-1}\left(\hat{I}^{IC}_{A,eff}\right)\right)\frac{K_{eff}-1}{N_s} + \frac{N_0}{2RP_{ref}}}}\right), \tag{7.13}$$

where P_{ref} is an arbitrary reference power level (nominally $P_{ref} = 1$), N_s is the spreading factor (in the case of IDMA, $N_s = 1$), K_{eff} is the effective number of users given by,

$$K_{eff} = \frac{1}{P_{ref}}\sum_k K_k P_k,$$
$$= K_T P_{av}, \tag{7.14}$$

where P_k is the power level for user group k, $P_{av} = \frac{1}{K_T}\sum_k K_k P_k$ is the average power and K_T is the total number of users. We observe that the EXIT function for the IC given in (7.13) is independent of the user index k, and thus is independent of the user power level and only dependent on the average power level (P_{av}). This model is counter intuitive in the sense that the information transfer function of the IC for user's within a power group should be determined by the power level. Intuitively, stronger power user's should be able to resolve multiuser interference faster than weaker user's when both are operating at the same input extrinsic information. The IC EXIT function that we derive has an implicit dependence on the power levels of the user groups as well as the *a priori* extrinsic information from all other user groups.

The EXIT function of the IC for user group k (denoted as $\mathrm{I}_{E,k}^{\mathrm{IC}}$) is a function of the input *a priori* information from K user groups. We define the K dimensional EXIT function, $\mathrm{I}_{E,k}^{\mathrm{IC}}$, as,

$$\mathrm{I}_{E,k}^{\mathrm{IC}} = F_{\mathrm{k}}^{IC}\left(\mathbf{I}_{\mathbf{A}}^{\mathbf{IC}}, \mathbf{P}, \sigma_n^2\right), \tag{7.15}$$

where $\mathbf{I}_{\mathbf{A}}^{\mathbf{IC}} \triangleq [\mathrm{I}_{A,1}^{\mathrm{IC}}, \ldots, \mathrm{I}_{A,K}^{\mathrm{IC}}]$.

The EXIT function for the soft input soft output decoder of each user must be obtained through Monte Carlo simulation. The transfer function for the k-th user is defined as,

$$\mathrm{I}_{E,k}^{DEC} = f_{DEC}\left(\mathrm{I}_{A,k}^{DEC}\right). \tag{7.16}$$

The EXIT function for the k-th SISO decoder has one input parameter being the *a priori* information from the IC of the k-th user group($\mathrm{I}_{A,k}^{DEC} = \mathrm{I}_{E,k}^{\mathrm{IC}}$). This differs from the analysis presented in [104, 105] where the EXIT function for the FEC decoder for user group k is presented as,

$$I_{E,k}^{TD} = f_{DEC}\left(J\left(\sqrt{\frac{P_k}{P_{ref}}}J^{-1}(I_{A,eff}^{TD})\right)\right), \tag{7.17}$$

and the average of the EXIT functions for all decoders is presented as,

$$\hat{I}_E^{TD} = \frac{1}{K_{eff}}\sum_k K_k P_k I_{E,k}^{TD}. \tag{7.18}$$

Note that the function in (7.17) is dependent on both P_k (Power level of group k) and $I_{A,eff}^{TD}$ (average input extrinsic information for all users). From our

viewpoint it is more intuitive to interpret all user's decoder functions to have an EXIT function independent of the multiuser channel (in a similar fashion to the EXIT functions defined in [82, 83]). An analogy can be drawn to traditional single user EXIT analysis for turbo-equalisation, where the equaliser (inner decoder) EXIT is a function of the E_b/N_0 of the channel and the input extrinsic information. On the other hand the outer decoder EXIT function is a function of only its input extrinsic information.

The inverse of the decoder EXIT function ($f_{DEC}(\cdot)$) is needed to generate the EXIT chart as in [83]. Thus we define the inverted EXIT function of the decoder, $\mathrm{I}_{A,k}^{DEC}$, as

$$\mathrm{I}_{A,k}^{DEC} = f_{DEC}^{-1}\left(\mathrm{I}_{E,k}^{DEC}\right). \tag{7.19}$$

To construct a K dimensional EXIT chart for each user group it is useful to construct a projection of $\mathrm{I}_{A,k}^{DEC}$ onto K dimensions producing the function, $F_{\mathrm{k}}^{DEC}\left(\mathbf{I}_{\mathbf{E}}^{\mathbf{DEC}}\right)$, defined as,

$$\begin{aligned} F_{\mathrm{k}}^{DEC}\left(\mathbf{I}_{\mathbf{E}}^{\mathbf{DEC}}\right) &\triangleq \mathrm{I}_{A,k}^{DEC} \\ &= f_{DEC}^{-1}\left(\mathrm{I}_{E,k}^{DEC}\right). \end{aligned} \tag{7.20}$$

The K-dimensional EXIT chart trajectory for K user groups is described in Algorithm 2. Initially the input extrinsic information, $\mathrm{I}_{A,k}^{\mathrm{IC}}$ for the k-th user is set to zero. In the next step the input extrinsic information is converted to the symbol variance for the k-th user ($\{\sigma_{x,k}^2\}$) by use of (7.11). Then the K-dimensional EXIT function for the IC is computed according to, (7.12),by substituting $\{\sigma_{x,k}^2\}$ from the previous step. The output extrinsic information from the IC of the k-th user is then passed to the FEC decoder of the k-th user as input extrinsic information, $\mathrm{I}_{A,k}^{DEC}$. The output extrinsic information from the FEC decoder is computed using the function $f_{DEC}(\cdot)$ and the output is then used as *a priori* input, $\mathrm{I}_{A,k}^{\mathrm{IC}}$ for the next iteration. The process is iterated until there is no gain in mutual information over an iteration.

The Algorithm 2 can be interpreted as the mutual information trajectory traced between the two K dimensional EXIT functions namely, $F_{\mathrm{k}}^{IC}\left(\mathbf{I}_{\mathbf{A}}^{\mathbf{IC}}, \mathbf{P}, \sigma_n^2\right)$ and $F_{\mathrm{k}}^{DEC}\left(\mathbf{I}_{\mathbf{E}}^{\mathbf{DEC}}\right)$, respectively. Since both EXIT functions are monotonic increasing, the convergence point on the EXIT chart must lies upon the intersection between the two EXIT functions. This can be graphically interpreted

Algorithm 2 Analytical EXIT chart trajectory

$\mathrm{I}_{E,k}^{DEC}(0) \Leftarrow 0 \vee k$
while i==0 or $(\mathrm{I}_{E,k}^{DEC}(i) \neq \mathrm{I}_{E,k}^{DEC}(i-1))$ **do**
  for k:=1 to K **do**
    $\mathrm{I}_{A,k}^{\mathrm{IC}}(i) \Leftarrow \mathrm{I}_{E,k}^{DEC}(i)$
    $\sigma_{x,k}^2(i) \Leftarrow 1 - \mathrm{T}^{-1}\left(\mathrm{I}_{A,k}^{\mathrm{IC}}(i-1)\right)$
  end for
  for k:=1 to K **do**
    $\mathrm{I}_{E,k}^{\mathrm{IC}}(i) \Leftarrow J\left(\sqrt{\frac{4P_k}{\sum_{l\neq k} K_l P_l \sigma_{x,l}^2(i) + (K_k-1)P_k\sigma_{x,k}^2(i) + \sigma_n^2}}\right)$
    $\mathrm{I}_{A,k}^{DEC}(i) \Leftarrow \mathrm{I}_{E,k}^{\mathrm{IC}}(i)$
    $\mathrm{I}_{E,k}^{DEC}(i) \Leftarrow f_{DEC}\left(\mathrm{I}_{A,k}^{DEC}\right)(i)$
  end for
end while

as the intersection between two K dimensional subspaces,

$$F_{\mathrm{k}}^{IC}\left(\mathcal{I}_{\mathbf{E,k}}^{\mathbf{DEC}}, \mathbf{P}, \sigma_n^2\right) = F_{\mathrm{k}}^{DEC}\left(\mathcal{I}_{\mathbf{E,k}}^{\mathbf{DEC}}\right), \tag{7.21}$$

where $\mathcal{I}_{\mathbf{E,k}}^{\mathbf{DEC}}$ is a K dimensional subspace. The ultimate convergence point for K Decoders, defined as $\mathbf{I}_{\mathbf{E}}^{\mathbf{DEC}^*} \triangleq \left[\mathrm{I}_{E,1}^{DEC*}, \ldots, \mathrm{I}_{E,K}^{DEC*}\right]$, lies upon the intersections of the K, K dimensional subspaces $\mathcal{I}_{\mathbf{E,k}}^{\mathbf{DEC}}$. The graphical visualisation of higher dimensional EXIT charts is infeasible, however the complexity of the mutual information tracing algorithm is only linearly dependent on the number of dimensions and the number of iterations required from the IMUD. Hence, there is no significant increase in complexity in the multidimensional EXIT analysis compared with 2D EXIT analysis, even though it may be difficult to visualise graphically.

The convergence behavior of the receiver is predicted in Algorithm 2, and can be used to estimate the bit error rate (BER) performance for the kth user (denoted as $P_{b,k}$). The BER can be approximated using the Gaussian approximation for output LLR of the decoder [83] as,

$$P_{b,k} \approx Q\left(\frac{\sqrt{J^{-1}\left(\mathrm{I}_{E,k}^{\mathrm{IC}*}\right)^2 + J^{-1}\left(\mathrm{I}_{E,k}^{DEC*}\right)^2}}{2}\right). \tag{7.22}$$

The average BER for all user's can be estimated as

$$P_b \simeq \frac{1}{K_T} \sum K_k P_{b,k}. \tag{7.23}$$

7.4 Power Optimisation

Spread spectrum systems like IDMA are interference limited, consequently minimizing the total transmitted power has numerous benefits for the system in terms of increasing;

- connectivity range
- battery life for the terminals
- number of users per cell

We therefore want to minimise the sum power of all users, which we address in this Section. Allocation of users into power groups is commonly used to simplify the optimisation problem, meanwhile still promising near capacity performance [100].

7.4.1 The Optimisation problem:

Consider a code-spread IDMA system with K_T users which are grouped into K user groups (or classes). Given the number of users in each group are specified in $\mathbf{K} = [K_1, \ldots, K_K]$, we propose a power optimisation problem that aims to minimise the total transmit power while guaranteeing a quality of service to users in all power groups. We ensure that all users have a guaranteed quality of service, defined as a tolerable bit error rate (BER) of ϵ (i.e. $P_{b,k} < \epsilon, \forall k$). The problem can be succinctly defined as the joint power allocation and user loading which minimises total transmit power while guaranteeing convergence of the iterative multiuser detector. As a result there must be an open tube in the K dimensional EXIT chart such that enough MAI is removed, resulting in $P_{b,k} \leq \epsilon$ for all users.

The cost function can be written as,

$$F(\mathbf{K}, \mathbf{P}) = \sum_{k}^{L} K_k P_k = \mathbf{K}\mathbf{P}^T, \tag{7.24}$$

the convergence requirement can be evaluated using Algorithm 2 takings parameters $\mathbf{K}$,$\mathbf{P}$ and σ_n^2 and then computing the associated BER for all user's (7.22), at the final decoding iteration.

To avoid solving the above joint optimisation problem which is difficult to solve, we may resort to the two following simpler sub-optimal approaches: (1) fix the received power levels $\mathbf{P}$, and then consider the optimisation of the number of users per group in $\mathbf{K}$; (2) fix the user group profile $\mathbf{K}$ and optimise the power levels $\mathbf{P}$. Note that in an IMUD systems the user groups contain an integer number of users. To avoid the discrete optimisation problem, here we consider the second approach, in which the optimisation variables $\{P_k\}$ are continuous. The cost function and the constraints can be rewritten mathematically as,

$$\begin{aligned} &\min_{\mathbf{P}} F(\mathbf{K}, \mathbf{P}), \\ &\text{subject to:} \quad \begin{cases} P_k > 0, \\ P_{b,k} \leq \epsilon, \end{cases} \end{aligned} \tag{7.25}$$

where $P_{b,k}$ denotes the worst BER among the K class users.

7.4.2 The Optimisation procedure:

Differential evolution [172] is a powerful population based genetic algorithm which can be applied to solve nonlinear optimisation problems. The essential idea behind differential evolution is to simulate evolution of a set of test vectors from the domain of the objective function. An evolutionary process is simulated over the population of test vectors. Random and infrequent mutations are applied to the test vector population in each generation, resulting in a set of trial vectors. Subsequently the trial vectors in the population which have smaller cost than the test vectors, survive until the next generation of evolution. After a given number of generations, the vector with the smallest cost value among the population is the optimised parameter vector.

To solve (7.25) for a given $\mathbf{K}$, we first choose a system σ_n^2 and find a vector $\mathbf{P}$ using DE that satisfies the BER constraint ϵ. If at least one $\mathbf{P}$ exists, the values of $\mathbf{P}$ are reduced and the procedure is repeated until no further refinement of $\mathbf{P}$ is possible. The value of $\mathbf{P}$ which minimises the cost function $F(\mathbf{K}, \mathbf{P})$ and satisfies the BER constraint is the desired minimum power profile $\mathbf{P}$. During the differential evolution, in order to obtain the BERs $\{P_{b,k}\}$ for a given $\mathbf{K}$ and $\mathbf{P}$,

we resort to the mutual information tracking algorithm given in Algorithm 2 to obtain the ultimate extrinsic information from both the IC ($\mathrm{I}_{E,k}^{\mathrm{IC}*}$) and the decoder ($\mathrm{I}_{E,k}^{DEC*}$), followed by substitution into (7.22).

7.5 Analytical and Simulation Results

In this Section we present examples of power optimisation and EXIT chart analysis using the techniques described previously. We first present the power optimisation and multi-dimensional EXIT chart analysis presented in Section 7.3, for a two user group system ($K = 2$). This first subsection is used to illustrate the benefits of the EXIT chart analysis in an easy to interpret example. Note that power optimisation for two user groups does not achieve good performance results due to the limited degrees of freedom in the optimisation algorithm. In the second subsection we present power optimisation based on the multi-dimensional analysis, for a system with three user groups. We use this system configuration in order to compare the results with literature. The EXIT functions defined in Section 7.3 assume a very long block size (interleaver length), such that the MAI can be approximated as a white Gaussian random variable. We define $\hat{E}_b/N_0$ to be the average E_b/N_0 for all users and use it as a metric to compare power allocation strategies.

7.5.1 3D EXIT analysis for $K = 2$

We performed power optimisation on the IDMA system with $K = 2$ user groups ($K_1 = 8$ and $K_2 = 8$) where the outer code for all user's was a combination of a 1/3 rate ($R_{tc} = 1/3$) PCC turbo code consisting of two 16 state $(23, 35)_8$ RSC codes and a 1/8 rate ($R_s = 1/8$) repetition code. This is a coding scheme for IDMA similar to the one presented in [13]. The optimal power allocation results in the power profile $\mathbf{P} = [1.046, 1.708]$ where, $\hat{E}_b/N_0 = 2.39$ dB.

Figure 7.2 illustrates the EXIT charts for both user groups. As we can see the EXIT trajectory bounces between the EXIT function for the IC $\left(F_{\mathrm{k}}^{IC}\left(\mathbf{I}_{\mathbf{A}}^{\mathbf{IC}}, \mathbf{P}, \sigma_n^2\right)\right)$ at $\hat{E}_b/N_0 = 2.39$ dB and the Decoder $\left(F_{\mathrm{k}}^{DEC}\left(\mathbf{I}_{\mathbf{E}}^{\mathbf{DEC}}\right)\right)$ for $k = 1$ in Figure 7.2a and $k = 2$ in Figure 7.2b respectively. As expected the higher power user group $k = 2$, converges much faster (in around 8 iterations in this example) whereas the lower power user $k = 1$ converges much slower. From the Figure 7.2a we can see the convergence point of the multiuser receiver for user group 1 lies upon the intersection between the two surfaces $F_1^{IC}\left(\mathbf{I}_{\mathbf{A}}^{\mathbf{IC}}, \mathbf{P}, \sigma_n^2\right)$

and $F_1^{DEC}\left(\mathbf{I_E^{DEC}}\right)$. Similarly the convergence point for user group 2 occurs at the intersection of $F_2^{IC}\left(\mathbf{I_A^{IC}}, \mathbf{P}, \sigma_n^2\right)$ and $F_2^{DEC}\left(\mathbf{I_E^{DEC}}\right)$ according to Figure 7.2b. Figure 7.3 shows the intersection subspaces (as defined in (7.21)) for user group 1 ($\mathcal{I}_{\mathbf{E},1}^{\mathbf{DEC}}$) and user group 2 ($\mathcal{I}_{\mathbf{E},2}^{\mathbf{DEC}}$) respectively. Inspection of Figure 7.3 verifies that at $\hat{E}_b/N_0 = 2.39$ dB the receivers for user group 1 are operating very close to the pinch-off point[83], due to the very narrow tunnel at two points, $[I_{E,1}^{DEC} \simeq 0.21, I_{E,2}^{DEC} \simeq 0.49]$ and $[I_{E,1}^{DEC} \simeq 0.47, I_{E,2}^{DEC} \simeq 1]$. However, the two intersection subspaces, $\mathcal{I}_{\mathbf{E},1}^{\mathbf{DEC}}$ and $\mathcal{I}_{\mathbf{E},2}^{\mathbf{DEC}}$ do not intersect until $[I_{E,1}^{DEC} \simeq 1, I_{E,2}^{DEC} \simeq 1]$. Thus we predict that the system converges at $\hat{E}_b/N_0 = 2.39$ dB this can be observed in the BER plot (Figure 7.4). We compared the power allocated (PA) system based upon multi-dimensional EXIT analysis with PA system based on the average EXIT chart analysis (presented in [104, 105]). According to the Figure 7.4 the averaged EXIT analysis is more pessimistic than the multi-dimensional analysis which predicts convergence at $\hat{E}_b/N_0 = 2.39$ dB. Figure 7.4 illustrates that utilising multi-dimensional analysis improves the power optimisation by more than 0.2 dB in this particular scenario. The simulation results in Figure 7.4 outperforms the EXIT-chart analysis because of the imperfections in the fidelity function approximation ($\mathrm{T}^{-1}(I)$) which is used to compute the symbol variance $\sigma_{x,k}^2$. It can be seen within the Figure 3 in [170], that the approximate fidelity function always underestimates the true fidelity function. As a result the computed variance using this approximation will always be overestimated, resulting in slightly pessimistic BER estimates from the analysis.

7.5.2 4D EXIT analysis for $K = 3$

In this subsection we provide a more realistic illustration of the power optimisation algorithm which was developed in Section 7.4. The power optimisation was performed for $K = 3$ user groups, with uniform load distribution over each group. As described in [103] the capacity of power allocated CDMA systems is optimised when the load is uniformly distributed among user groups ([103], *Lemma* 1). We simulate the receiver for the outer code which is the combination of a 1/3 rate ($R_{tc} = 1/3$) PCC turbo code consisting of two 16 state $(23, 35)_8$ RSC codes and a 1/8 rate ($R_s = 1/8$) repetition code.

The 4D EXIT chart analysis for $K = 3$ user groups corresponding to $F_{\mathrm{k}}^{DEC}\left(\mathbf{I_E^{DEC}}\right)$ and $F_{\mathrm{k}}^{IC}\left(\mathbf{I_A^{IC}}, \mathbf{P}, \sigma_n^2\right)$ for $k = 1 \ldots 3$, is difficult to represent in graphical form. However, the complexity of the analysis algorithm 2 is only

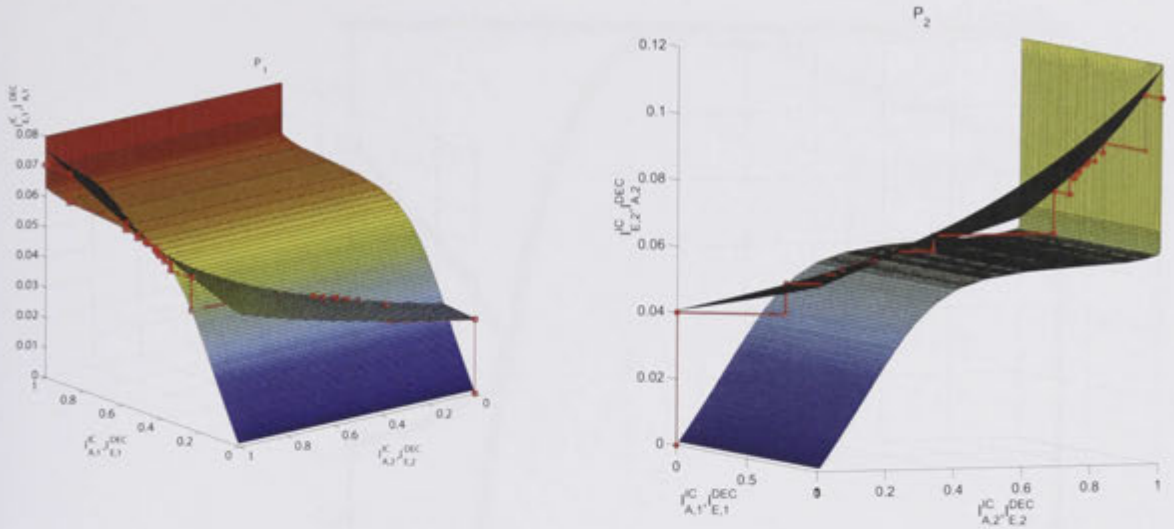

(a) The EXIT chart for user group 1 with power level P_1.(b) The EXIT chart for user group 2 with power level P_2.

Figure 7.2: The joint EXIT chart where $\hat{E}_b/N_0 \simeq 2.4$ dB for 1/3 rate PCC concatenated with a 1/8 rate repetition code.

dependent linearly on the number of dimensions and the total number of iterations required. As a result higher dimensional analysis is both feasible and efficient despite being difficult to visualise graphically. The intersection subsurfaces for the three user groups defined in (7.21), can be illustrated graphically. We optimised a system with uniform load distribution among groups, $\mathbf{K} = [4, 4, 4]$ and found the optimal power profile, $\mathbf{P} = [0.88, 1.059, 1.33]$, resulting in a $\hat{E}_b/N_0 = 1.38$ dB. Figure 7.5a illustrates the intersection subspaces for the three user groups namely, $\mathcal{I}^{\mathbf{DEC}}_{\mathbf{E},1}$ for user group 1, $\mathcal{I}^{\mathbf{DEC}}_{\mathbf{E},2}$ for user group 2, and $\mathcal{I}^{\mathbf{DEC}}_{\mathbf{E},3}$ for user group 3. Close inspection of the three dimensional plot will show that there is in fact an open volume between the three subspaces. Consequently, convergence of the system is predicted. In the Figure 7.5a we observe that the system is operating near its pinch-off point due to the very narrow tunnel width and height at the point $\left(I^{DEC}_{E,1}, I^{DEC}_{E,2}, I^{DEC}_{E,3}\right) \simeq (1, 0.5, 0.35)$. We observe that the volume between the three subspaces is very small at the optimum power allocation. This agrees with the minimum area EXIT properties for 2D EXIT chart analysis derived in [86]. We conjecture that the channel capacity is approached when the volume of the open tube in the 4D EXIT chart corresponding to $F^{DEC}_{\mathrm{k}}\left(\mathbf{I}^{\mathbf{DEC}}_{\mathbf{E}}\right)$ and $F^{IC}_{\mathrm{k}}\left(\mathbf{I}^{\mathbf{IC}}_{\mathbf{A}}, \mathbf{P}, \sigma^2_n\right)$ for $k = 1 \ldots 3$, goes to zero. Figure 7.5b illustrates the trajectory of the extrinsic information after each iteration, we omit subsurface $\mathcal{I}^{\mathbf{DEC}}_{\mathbf{E},3}$ for clarity.

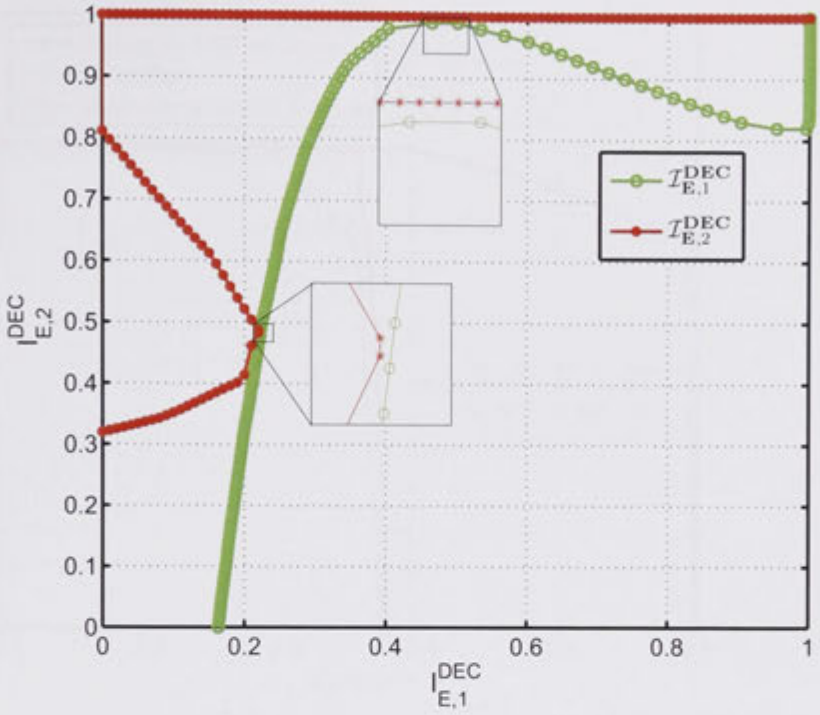

Figure 7.3: The intersection subspaces for user group 1($\mathcal{I}^{\mathbf{DEC}}_{\mathbf{E},1}$) and user group 2 ($\mathcal{I}^{\mathbf{DEC}}_{\mathbf{E},2}$) respectively. We note the two regions of the plot indicating near pinch-off operation of the IC.

7.5.3 Higher dimensional EXIT analysis

In Figure 7.6 the sum rate capacity plots for the power optimised IDMA systems are presented for the channel code described above. The sum rates are varied by changing the total number of users, K_T, (assuming uniform load distribution in the user groups), while fixing the decoder rates. The power optimisation algorithm is run for each different user loading, resulting in an optimal $\hat{E}_b/N_0$ for varying sum rates. EXIT charts of 6 dimensions are used in-order to find the optimal optimal $\hat{E}_b/N_0$ values. The table showing the power optimisation profiles are given in the Table 7.1. We compare the channel capacity using PA based on multi-dimensional analysis with the PA based on the average EXIT analysis. Our results show that for higher capacity systems the gain using the proposed approaches are improved over the average EXIT analysis in [104, 105], where we achieve a gain of more than 0.5dB for sum rate equal to 2 bits/chip.

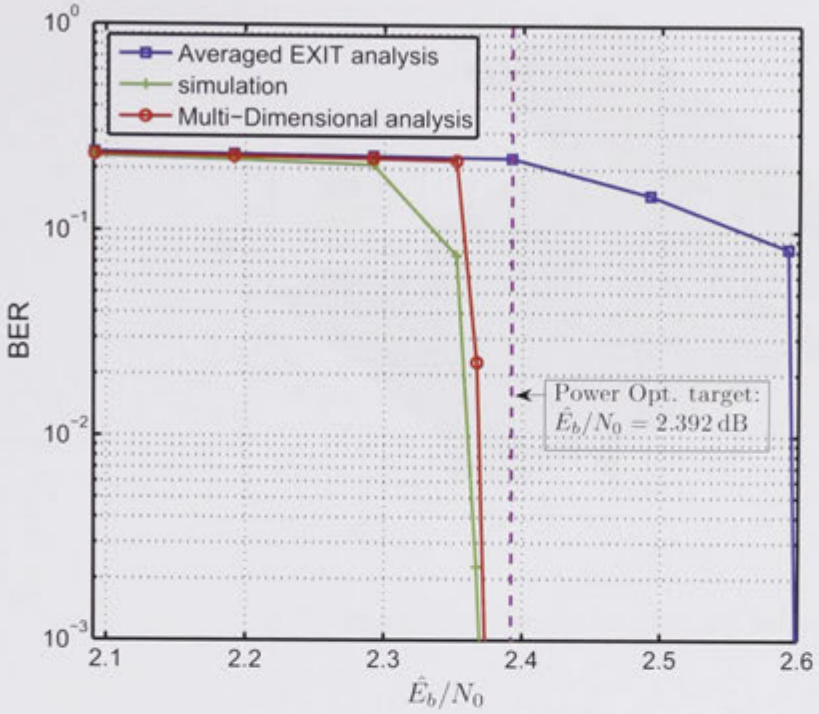

Figure 7.4: A comparison of the average BER plots for simulation and analysis.

Sum Rate (bits/sec/Hertz)	Users per group (**K**)	Power profile (**P**)	$\hat{E}_b/N_0$
0.5	[2,2,2]	[0.87, 0.88, 0.99]	0.6174
1.0	[2,2,2,2,2,2]	[0.98, 1.10, 0.87, 1.25, 0.85, 1.39]	1.3183
1.5	[3,3,3,3,3,3]	[1.64, 0.85, 1.37, 1.15, 1.96, 0.98]	2.1688
2.0	[4,4,4,4,4,4]	[1.07, 2.84, 1.72, 1.35, 2.20, 0.88]	3.247

Table 7.1: Power levels and average E_b/N_0 obtained by optimisation

7.6 Summary

We have developed a new technique for the analysis of a multiuser iterative detector with unequal power allocation using multi-dimensional EXIT analysis. We provide analysis which can accurately predict convergence behavior of such a system, and show that our proposed analysis gives further insight into the convergence behavior of a multiuser receiver with multiple power levels. The multi-dimensional analysis technique has complexity which is linearly dependent on the number of dimensions (number of user groups). Therefore it is conceivable

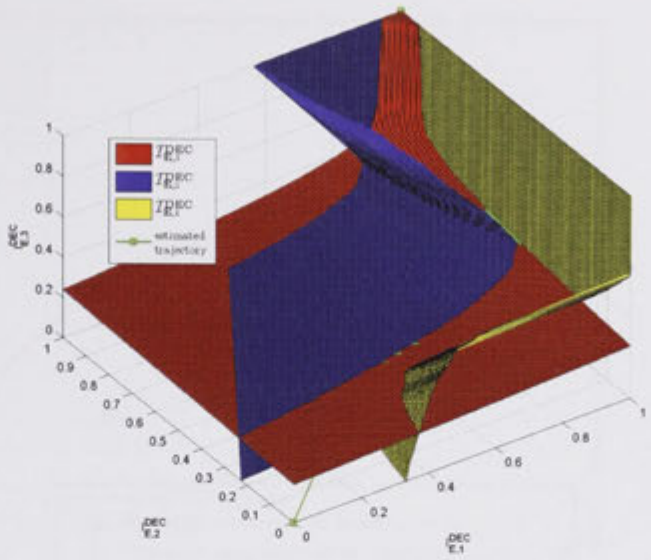

(a) The intersection subspaces for three user groups.

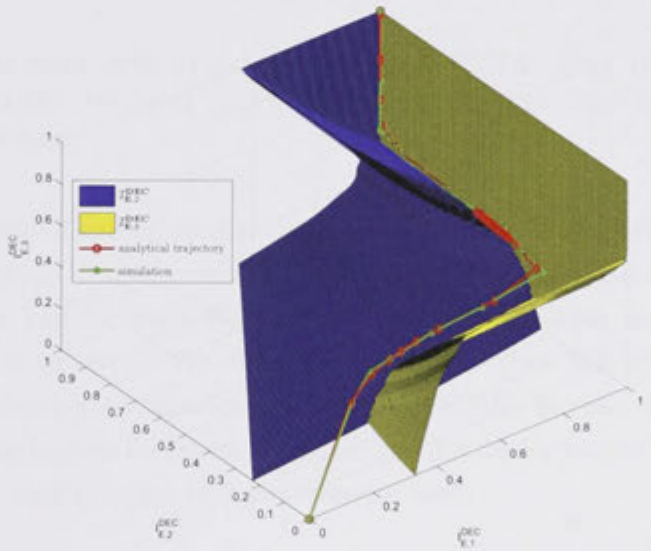

(b) The extrinsic information $((I_{E,1}^{DEC}, I_{E,2}^{DEC}, I_{E,3}^{DEC}))$ trajectory for three user groups.

Figure 7.5: The intersection subspaces for $K = 3$ for a 1/3 rate PCC concatenated with 1/8 rate repetition code where, $K_k = [4, 4, 4]$, $P_k = [0.88, 1.059, 1.33]$ and $\hat{E}_b/N_0 = 1.38$ dB

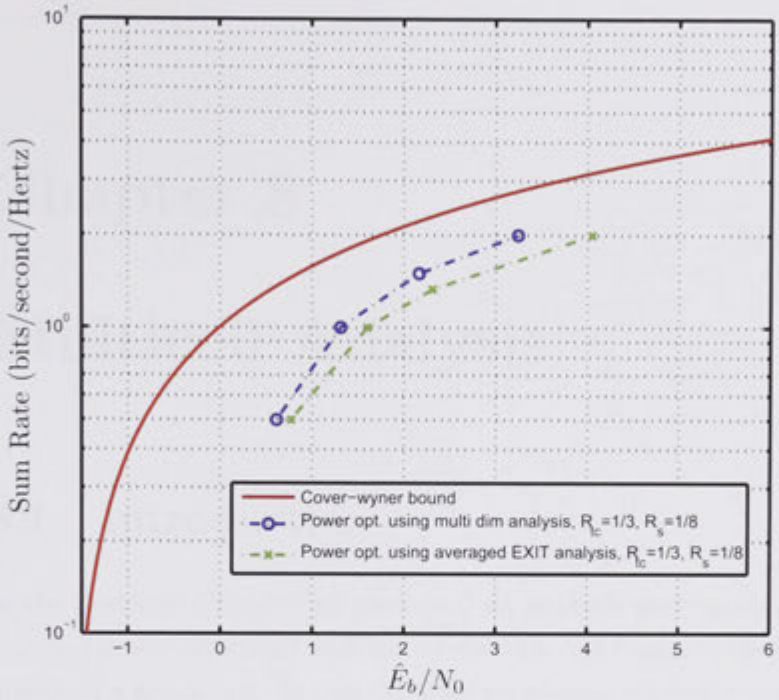

Figure 7.6: Achievable sum rate of power optimised IDMA using proposed technique compared to the averaged EXIT analysis, and single user capacity bound(Cover-Wyner bound).

that the technique presented can be used to analyse a system with a large number of user groups. The multi-dimensional EXIT chart has been presented as an engineering tool which can be used for improved power allocation and code selection of a multiuser receiver. We show by simulation that the presented technique improves the sum rate capacity of a multiuser IDMA receiver over the averaged EXIT chart analysis in literature by more than 0.5 dB for heavily loaded systems where the sum rate is equal to 2 bits/second/hertz.

Chapter 8

Multicell Analysis

8.1 Introduction

In the previous Chapter we presented an analysis and optimisation technique for unequal power allocated multiuser receivers. We focussed upon the analysis of the uplink of a single cell. In this Chapter we present a novel power allocation/zoning technique for multi-cell multiuser receivers. We also provide analysis for the multi-cell system, and show the benefits of power allocation along with cell zoning.

Most of the literature that investigates multiuser receiver design omits the effects of out-of-cell (intercell) interference. Newson *et. al* in [106], showed that in a typical urban environment roughly 33% of the receiver interference comes from users in other cells (intercell interference), the other 67% coming from users within the cell (intracell interference). Alexander [107] shows how intracell interference on the uplink can be can be mitigated using MU receivers at the BS, and that intercell interference can be partially mitigated using soft hand over (SHO)[108]. As a result huge signal to interference (SIR) gains with respect to conventional single user (SU) receivers can be observed. Dawy *et. al* in [109] propose relays at the edge of the cell to improve coverage and capacity while lowering the UL interference for cellular systems. In [110] the capacity and cell coverage by using successive interference cancelation along with service classes is used to show capacity and coverage gains over single user receivers. However, we believe that the average signal to interference ratio limitation due to intercell interference for the system in [110] must still conform to that given in [107], if the power levels are normalised.

In this Chapter we expand on [107] and show how the use of unequal power allocated MU receivers along with power zones can be incorporated into cellular

systems, and then illustrate the benefits of such a scheme. The MU receivers at the BS of interest experience two positive effects of such a scheme: firstly, the BS receiver can be designed optimally using power allocation [98, 99]; and secondly, the intracell interference can be reduced resulting in a very significant increase in spectral efficiency, of up to 50%. The results show that as the cell loading gets larger the gain in SIR due to power allocation increases with respect to the equal power MU receivers described in [107]. We were able to determine the maximum achievable cell loading, which is limited by intercell interference, and show that it can be substantially increased by using power zoning.

8.2 Cellular System with Power zones and Power allocation

We consider an unequal power allocated CDMA system with K user groups, where there are a total of K_T users per radius $R_{z,K}$ and a spreading code length of N chips per symbol. The users are assumed to be uniformly distributed in space, i.e.

$$\rho = \frac{K_T}{\pi R_{z,K}^2} \text{users/(km)}^2 \tag{8.1}$$

8.2.1 Power Control

The power control assumes K user groups where the kth user group is allocated power level P_k (Watts). The unequal power allocation algorithm shall be the power optimisation technique presented in the Chapter 7 Section 7.4 tailored for DS/CDMA. Although in principle any optimal power allocation scheme can be used in conjunction with the analysis provided. It is important to note that closed loop power control is implemented such that all users in group k receive P_k watts of power. In practise each user group is allocated a particular C/I (carrier to interference ratio) in order to meet a quality of service (QoS) requirement.

We propose that a cell is arranged into zones for each different power group. The higher power groups are closer to the home base station and lower power groups farther away. The reasoning for this is that in the uplink this reduces the power for users on the edge of the cell which are also the users which generate

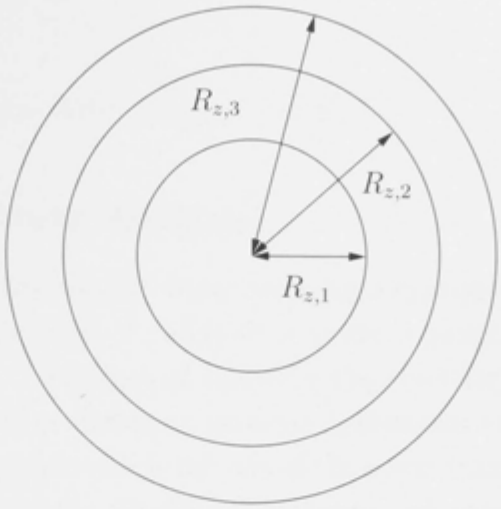

Figure 8.1: The zones for 3 power group cell.

the majority of the inter-cell interference. As a result,

$$P_1 \geq P_2 \geq \ldots \geq P_K. \tag{8.2}$$

The Figure 8.1 shows the proposed cell layout. Using (8.1) and defining the number of users in group k as K_k, the zone boundary for user group $k > 0$ can be described as,

$$\begin{aligned} R_{z,0} &= 0, \\ R_{z,k} &= R_{z,K}\sqrt{\frac{\sum_{k'=1}^{k} K_k}{K_T}}, 1 \leq k \leq K_T. \end{aligned} \tag{8.3}$$

8.2.2 Propagation

The power received at the base station of interest from a user equipment (UE) in zone k due to free space loss is given by,

$$p_{BS}(r) = P_k = \frac{p_{MS}^k}{\beta r^{\gamma}}, R_{z,k-1} < r \leq R_{z,k} \tag{8.4}$$

where, p_{MS}^k is the transmit power of mobile station in zone k, in urban areas the path loss exponent $\gamma \simeq 4$, and β is a constant. The closed loop power control and power zoning will ensure that $p_{BS}(r) = P_k$ and consequently,

$$p_{MS}^{k}(r) = P_k \beta r^{\gamma}, R_{z,k-1} < r \leq R_{z,k}. \tag{8.5}$$

8.2.3 Interference Power Analysis

For simplicity we model the inter-cell interferers assuming a multiple macro tiered cellular system with $6n$ circular cells of radius $R_{z,K}$ in tier n uniformly centered on a circle of radius $2nR_{z,K}$. This model simplifies the traditional hexagonal structure for analysis as well as providing an accurate approximation for the first few tiers [107]. The intercell interference is the sum of the power transmitted from UEs in neighboring cells. Given the circular cell structure, we assume there are at most $N_T = 3$ tiers of neighboring cells, as interference from the cells beyond this are negligible. The total inter-cell interference can be written,

$$I_{MU,PA} = \sum_{n=1}^{N_T} 6n I_{MU,PA}^{n}, \tag{8.6}$$

where $I_{MU,PA}^{n}$ is the received interference from a cell in tier n.

The geometry for a UE in tier n is shown in Figure 8.2, where r_{II} is distance between the UE and its serving base station (BS_n), r_{ID} is the distance between the UE and the BS of interest(BS_0), and θ is the angle between a line from BS_0 to BS_n and a line from BS_n to UE.

The distance between an interferer and the base station of interest can be obtained as,

$$r_{ID}(n, R, r_{II}, \theta) = \sqrt{4n^2R^2 - 4nRr_{II}\cos\theta + r_{II}^2}. \tag{8.7}$$

The power that base station (BS_0) receives from UE at distance r_{ID} which is distance r_{II} from its own BS will have power,

$$p_I^k(r_{II}, r_{ID}) = \frac{P_k \beta r_{II}^{\gamma}}{\beta r_{ID}^{\gamma}} = P_k \left(\frac{r_{II}}{r_{ID}}\right)^{\gamma}, \tag{8.8}$$

where $R_{z,k-1} < r_{II} \leq R_{z,k}$.

For DS/CDMA with spreading gain N, the effective interference power at the output of a single user (SU) receiver is reduced by a factor of N, p_I/N. For IDMA

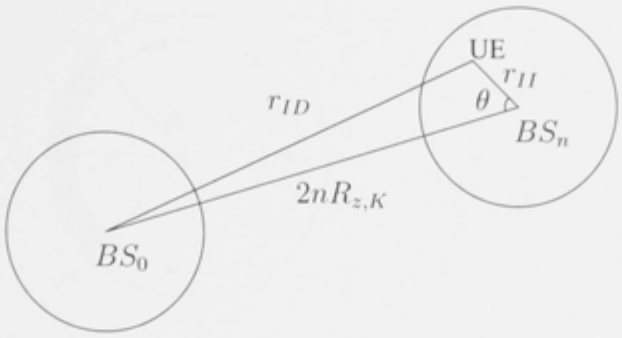

Figure 8.2: The geometry of UE in tier n interfering with BS_0.

receivers on the other hand it is simply p_I since the interference is canceled before the decoding/despreading process. We will assume DS-CDMA is used in order to compare the results with [107].

The accumulative interference from all UEs serviced by base station at tier n (BS_n) is then given by,

$$I^n_{MU,PA} = \frac{K_T}{N\pi R^2_{z,K}} \sum_{k=1}^{K} \int_{r_{II}=R_{z,k-1}}^{R_{z,k}} \int_0^{2\pi} \frac{P_k r_{II}^{\gamma+1}}{r_{ID}(n, R_{z,K}, r_{II}, \theta)} d\theta dr_{II}. \tag{8.9}$$

The total interference for tiers 1 to N_T is then,

$$I_{MU,PA} = \frac{6K_T}{\pi N R^2_{z,K}} \sum_{n=1}^{N_T} n \sum_{k=1}^{K} \int_{r_{II}=R_{z,k-1}}^{R_{z,k}} \int_0^{2\pi} \frac{P_k r_{II}^{\gamma+1}}{r_{ID}(n, R_{z,K}, r_{II}, \theta)} d\theta dr_{II}. \tag{8.10}$$

In soft handover (SHO) the users at the edge of a cell are served by two base stations. Therefore multiuser receivers can be designed to detect users from neighboring cells within a SHO region. The SHO region is assumed to be within power zone K, and can be described geometrically as a portion of a sector of a circle with $\phi < \theta < \phi$ and $R_{z,K} - \delta < r < R_{z,K}$ (as shown in Figure 8.3). The center line connects the centers of the interferers BS (BS_n) and the home BS (BS_0). The total interference after SHO can be computed,

$$I_{\text{MU,PA,SHO}} = I_{\text{MU,PA}} - \frac{6K_T P_K}{\pi N R^2_{z,K}} \int_{r_{II}=R_{z,K}-\delta}^{R_{z,K}} \int_{-\phi}^{\phi} \frac{r_{II}^{\gamma+1}}{r_{ID}(n, R_{z,K}, r_{II}, \theta)} d\theta dr_{II}. \tag{8.11}$$

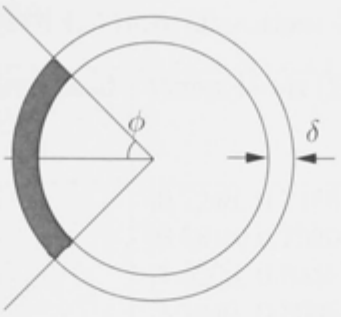

Figure 8.3: An illustration of the soft handover region.

8.3 Analytical and Simulation Results

In our simulation we assume that the MU receivers are operating at the desired C/I power ratio, and as such are capable of canceling all in-cell interference perfectly. We run power optimisation over systems with loading varying from $K/N = 0.45$ to $K/N = 3$. A rate 1/3 PCC code consisting of two 32 state $(70, 56)_8$ convolutional codes is used for our simulations. The power allocation used in Chapter 7 Section 7.4 tailored for DS/CDMA, is used where we initialise the $SNR = 2.0$dB, resulting in a fixed noise spectral density $N_0 = 1.89$. In all cases we simulate the power allocation with uniform loading such that $K_k = \frac{K_T}{K}$, as this was shown in [103] to coincide with optimal power allocation for CDMA with ideal codes. In all simulations the spreading length is fixed as $N = 20$, and the cell radius is fixed as $R_{z,K} = 1$km. The power allocations for different cell loading were collated in the Table 8.1. Note that the PA algorithm (in Chapter 7 Section 4 7.4) automatically increases the SNR such that the MU receiver converges according to EXIT chart analysis. The resultant average SNR required for optimal power allocations for the different loadings are also collated in Table 8.1.

The intercell interference analysis derived in Section 8.2.3 was computed using numerical integration techniques, for a number of different scenarios. We calculate the average signal to interference ratio $(\bar{P}_k/I)$ as a metric for comparison over the different loadings and power allocations given in Table 8.1. The Figure 8.4 shows a comparison of the SIR of the system under different scenarios, namely, equal power allocated multiuser receiver (MU) as given in [107], multiuser power allocated (MU,PA) as given in (8.10), multiuser receivers using SHO (MU,SHO), where $\phi = \frac{\pi}{6}$ and $\delta = 0.2R_{z,K}$ as given in [107], and multiuser power allocated with SHO with the same SHO region dimensions. As the cell loading increases the

Table 8.1: Power allocations for different loadings

System Load (K/N)	Power levels ($\mathbf{P}$)	Average SNR(dB) (SNR^*)
0.45	[0.7248, 0.7165, 0.7090]	-1.22
0.75	[0.8816, 0.7520, 0.7070]	-0.84
1.05	[1.0500, 0.8438, 0.7058]	-0.37
1.3	[1.1440, 0.8905, 0.7050]	-0.16
1.5	[1.3748, 0.9990, 0.7361]	0.38
1.8	[1.6673, 1.1272, 0.7714]	0.98
2	[2.3917, 1.581 , 1]	2.42
3	[7.5714, 3.6409, 2.5747]	6.85

SIR improvement of MU,PA and MU,PA,SHO receivers increase with respect to the conventional MU receivers. At a cell loading of $K/N = 2$ there is about a 2dB increase in SIR for MU,PA and MU curves, and a similar result for MU,PA,SHO and MU,SHO respectively. Although it must be stated that SHO also has the complexity trade-off since it increases the computational load on multiple base stations.

The cellular system proposed is interference limited, therefore the interference provides a limit on the maximum operating point (SNR) of the MU receiver. Therefore we are interested in determining the signal to interference (SIR) level onto the multiuser system due to the inter-cell interference. We can see that the effective SNR limit can be read from Figure 8.4, $SIR = \bar{P}_k/I$, which must be greater than the required average SNR for the receiver to operate, $SIR > SNR^*$. From the Table 8.1 the needed average SNR (SNR^*) required for the receiver under different loading is stipulated. Using this in conjunction with the SIR computation from Figure 8.4, we can observe that as the cell-loading gets higher the SIR due to inter-cell interference coincide with the SNR requirements for the receiver, thus, providing a limit on the loading of a cell. For example we can see a loading of $K/N = 2$ is not achievable unless multiuser receivers with power allocation are deployed since the required SNR^* of 2.42 dB is greater than the effective average SIR for the MU curve (see Figure 8.4). Using a similar argument we can state that at cell loading $K/N = 3$, the required $SNR^* = 6.85$ dB of the receiver is un-achievable. This suggests that the maximum cell capacity under this particular coding and power allocation scheme is between $K/N = 2$ and $K/N = 3$, but probably closer to $K/N = 2.6$ using the MU,PA,SHO scheme. We also observe that using power allocation along with SHO we can increase the

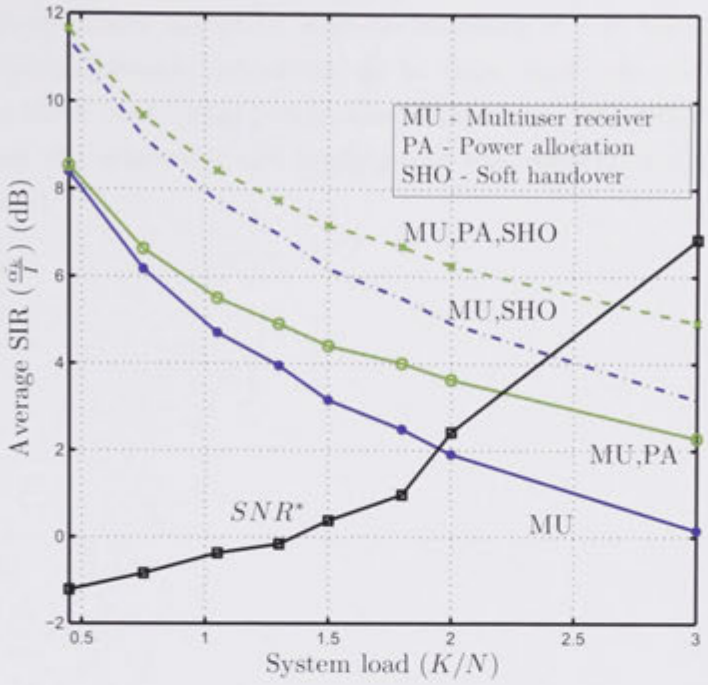

Figure 8.4: A comparison of Average SIR for BS_0 using different MU schemes.

achievable cell loading over the conventional techniques previously described. For example at a loading of $K/N = 2.7$ the MU,PA,SHO scheme can achieve this for an $SIR = 5.5$dB. The equivalent K/N for a PA,SHO scheme is 1.8, which is therefore a 50% spectral efficiency improvement. Compared to regular multiuser detection (MU) the system could only achieve a system load of 0.9, equating to an improvement of 200% or 3 times. These improvements are very significant and demonstrate how smart allocation of users into power groups can make a very significant difference to overall system performance.

8.4 Summary

We propose a multiuser multi-power cellular design, using power zones in order to reduce intercell interference. The proposed scheme has a two fold advantage, firstly it improves performance of the iterative multiuser receivers by power leveling and secondly there is an increase SIR power due to zoning technique. We observe close to 2dB gain in SIR ratio for heavily loaded systems $K/N = 2$. Alternatively the benefits over Multi-user detection with soft handover for an SIR

of 5.5 dB is an increase from $K/N = 1.8$ to $K/N = 2.7$, or 50%. Compared to regular multiuser detection with no inclusion of soft handover the benefits are even more dramatic, providing up to three times the spectral efficiency. Our results show that using power allocation along with SHO we can significantly increase the achievable cell loading over the conventional techniques previously described.

Chapter 9

Summary and Conclusions

9.1 Summary

This thesis has primarily focused on the design and optimisation of practical IDMA systems. The algorithms developed in this thesis are applicable to practical IDMA systems such that an IDMA receiver can be designed from the physical layer up. We summarise the key contributions made in this thesis in the Sections below.

9.1.1 System Model

In Chapter 2 we developed a general framework for an IDMA communication system. The basic model for iterative multiuser detection was first described. Interleave-division multiple-access was introduced and contrasted with the traditional multiuser DS/CDMA receiver technique. The receiver technique for IDMA was presented in detail. The FEC coding schemes utilised with IDMA in this thesis were described in detail. Finally, the performance results for an IDMA receiver utilising the afore-mentioned codes were presented.

9.1.2 Timing Acquisition

The timing of the received signal is the first parameter that needs to be estimated in any receiver. The task of estimating the initial timing point of a user's signal is termed timing acquisition. Efficient acquisition is necessary for good performance of a multiuser IDMA receiver. In Chapter 3 we investigated an acquisition technique for highly loaded systems which combined acquisition with interference cancellation for IDMA to achieve large improvements in performance.

We compared our new acquisition technique with a conventional correlator based acquisition method. We demonstrated that for high performance multiuser detection, information sharing between the acquisition unit and the receiver is essential to perform acquisition of new users. Depending on the reliability of the information from the IMUD, this technique improves the system capacity (in terms of user loading) by significantly reducing the likelihood of false alarms and missed detections in severe MAI scenarios.

9.1.3 Timing Tracking

After the initial timing point of a received signal has been acquired, it is necessary for the receiver to further refine the estimated timing points of subsequent chips. Timing tracking is the process of continually refining the estimates of the chip timing points. Tracking is a necessary process which is needed to compensate for timing drifts, which commonly occur in practise due to differences in frequencies between receive and transmit oscillators. In Chapter 4 we presented conventional and iterative approaches for timing tracking of an IDMA system. We showed that conventional timing recovery achieves sufficient performance for a fully loaded system subject to low timing drift. Operating under these conditions we showed that by using large spreading gains and a very low bandwidth loop filter the effects of MAI on the timing recovery loop can be mitigated. After this we compared the performance of the iterative timing recovery with conventional timing recovery for a fully loaded system subject to severe drift. Under these circumstances the receiver using iterative timing recovery showed a huge performance improvement for higher E_b/N_0 where the reliability of the data channel is increased. We also derived the lower bound of the timing error variance which depends on the reliability of the soft information from the previous iteration.

9.1.4 Asynchronous Detection

Most modern 3G spread spectrum systems do not support user synchronism in the uplink. Frame asynchronism in the uplink has a number of benefits over synchronous uplink communication. Most importantly asynchronism in the uplink reduces complexity of both the base station and terminal by removing the need for closed loop timing control. In Chapter 5 we developed an optimal asynchronous IDMA receiver. We compared the performance of the system with the conventional iterative receiver. Our results showed that the optimal

receiver for the repetition coded system outperforms the iterative approaches for higher E_b/N_0. For the very small block sizes that we considered in this Chapter the performance of the iterative receiver was compromised due to ineffective interleaving causing cross-correlation between user signals. When the ML receiver is across multiple blocks the receiver was able to cancel IBI. Therefore a significant performance improvement was achieved, albeit at the cost of exponential complexity.

9.1.5 Analysis and Power Optimisation

Analysis techniques for iterative receivers are necessary to understand the convergence behaviour as well as the achievable performance of such systems. Analytical tools are very useful in order to predict the performance of the system quickly without the need for time consuming simulations. EXIT charts have been shown to be the most powerful analytical tool for iterative receivers. Power optimisation for multiuser spread spectrum communications is necessary for a number of reasons. Firstly, it has been shown that multiuser receivers can only achieve capacity with power or rate allocation. Power allocation has a number of additional benefits for multicell systems since it lowers intercell interference, which in turn facilitates higher total cell throughput and increased cell coverage. In this thesis we present analysis and optimisation techniques for multiuser IDMA.

In Chapter 6 we investigated EXIT chart analysis for coded IDMA systems. The effect of the number of users, spreading factor and code rate were observed on the EXIT charts. A closed-form EXIT function for an IC was derived and the accuracy of the EXIT chart analysis of the IC was shown through simulations. In this Chapter tools for analysis of iterative receivers and decoders were described and developed.

In Chapter 7 we developed a new technique for the analysis of an unequal power allocated multiuser iterative detector using multi-dimensional EXIT analysis. We provided analysis which can be used to accurately predict the convergence behavior of such a system, and showed that our proposed analysis gives further insight into the convergence behavior of a multiuser receiver with multiple power levels. The multi-dimensional EXIT chart was presented as an engineering tool which can be used for improved power allocation and code selection of a multiuser receiver. We showed by simulation that the presented technique improved the sum rate capacity of a multiuser IDMA receiver over the averaged EXIT chart analysis in literature for heavily loaded systems.

9.1.6 Multicell Analysis

In Chapter 8 we proposed a multiuser multi-power cellular design, using power zones in order to reduce intercell interference. As a significant proportion of the interference in a cellular system comes from surrounding cells we investigated how a multi-power configuration using power zoning could reduce the effects of the intercell interference. The proposed scheme has a two fold advantage, firstly it improves performance of the iterative multiuser receivers by power leveling and secondly there is an increase in signal to interference ratio (SIR), due to the zoning technique. We observe significant gain in SIR for heavily loaded systems. Our results showed that using power allocation and power zoning along with soft handover can significantly increase the achievable cell loading over the conventional receiver techniques previously described.

9.2 Conclusions and Extensions

This thesis has presented techniques for practical acquisition, tracking, analysis and optimisation of multiuser IDMA receivers (in the uplink). We modeled an asynchronous IDMA system and developed an optimal receiver. Finally, we provided analysis and optimisation for coded multiuser IDMA systems in single and multi-cell environments. Simulations were used to demonstrate the accuracy of the techniques in all cases. We showed that highly loaded systems simply cannot operate in practice unless interference cancellation is used as part of the acquisition process. It reduces false alarms and missed detections to an acceptable level such that new users can be detected and added to the receiver for detection and decoding. As a consequence the throughput/performance of a base station can be greatly improved. We also showed a practical timing tracking algorithm for an IDMA receiver, this highlighted the benefits of integrating timing tracking with detection when the drift is large. We showed that multi-dimensional EXIT analysis for unequal power IDMA systems provides significant improvements in the accuracy of the modelling compared with the conventional 2D EXIT analysis. We defined a new power profile optimisation technique using the multidimensional analysis and showed how it can improve the performance of the power allocation. The power zoning technique for multi-cellular multiuser receivers was shown to have huge performance benefits over traditional multiuser receivers in terms of greater cell loading for a fixed signal to interference ratio, SIR. We showed an example where a system with multi-zone multi-power and soft-hand-over results

in a 50% increase in cell loading over a system with just soft hand over and multiuser receivers.

The work described in this thesis presents a framework for the acquisition, tracking, analysis, and optimisation of multiuser IDMA systems. The future work below describes how the results could be refined for specific applications, channels, and codes, on the path to potential standardisation of IDMA:

- Multipath fading channel in the system model
- Simulations of acquisition under Rayleigh fading channel
- Simulations of tracking under multipath Rayleigh fading channel
- Modelling of non-coherent tracking (where the channel information is unknown)
- Use a FEC code for the optimal receiver in Chapter 5
- Simulations using capacity achieving FEC codes
- Use of practical activation scheduling in the IDMA receiver, particulary in Chapter 7
- Use IDMA in combination with orthogonal frequency division multiple access (OFDMA).

Bibliography

[1] K. Kusume, G. Bauch, and W. Utschick, "IDMA vs. CDMA: Detectors, Performance and Complexity," in *IEEE Global Telecommunications Conference*, (Honolulu, Hawaii), pp. 1 –8, December 2009.

[2] S. Verdu, "Minimum probability of error for asynchronous Gaussian multiple-access channels," *IEEE Transactions on Information Theory*, vol. 32, pp. 85 – 96, January 1986.

[3] M. C. Reed, C. B. Schlegel, P. D. Alexander, and J. A. Asenstorfer, "Iterative Multiuser Detection for CDMA with FEC: Near single user performance," *IEEE Transactions on Communications*, vol. 46, pp. 1693–1699, December 1998.

[4] M. L. Moher, "An iterative multiuser decoder for near-capacity communications," *IEEE Transactions on Communications*, vol. 46, pp. 870–880, July 1998.

[5] X. Wang and H. V. Poor, "Iterative (turbo) soft interference cancellation and decoding for coded CDMA," *IEEE Transactions on Communications*, vol. 47, pp. 1046–1061, July 1999.

[6] P. Alexander, A. Grant, and M. Reed, "Iterative detection in code-division multiple-access with error control coding," *European Transactions on Telecommunications*, vol. 9, pp. 419–425, September 1998.

[7] M. L. Moher, "Turbo-based multiuser detection," in *IEEE International Symposium on Information Theory*, (Ulm, Germany), p. 195, June-July 1997.

[8] M. Moher, *Cross-Entropy and Iterative Detection*. PhD thesis, The University of Ottawa, Canada, May 1997.

[9] M. L. Moher, "An iterative multiuser decoder for asynchronous BPSK users," in *IEEE International Symposium on Information Theory*, (Cambridge, USA), p. 423, August 1998.

[10] L. Ping, L. Liu, K. Y. Wu, and W. K. Leung, "Interleave division multiple access (IDMA) communications," in *3rd International Symposium on Turbo Codes and Related Topics*, (Brest, France), pp. 173–180, September 2003.

[11] L. Ping, L. Lui, K. Wu, and W. Leung, "On Interleave-Division Multiple-Access," in *IEEE International Conference on Communication*, vol. 5, (Paris, France), pp. 2869–2873, June 2004.

[12] L. Ping, "Interleave-Division Multiple Access and chip-by-chip iterative multi-user detection," *IEEE Commun. Magazine*, vol. 43, pp. S19–S23, June 2005.

[13] L. Ping, L. Liu, K. Wu, and W. K. Leung, "Interleave Division Multiple-Access," *IEEE Transactions on Wireless Communications*, vol. 5, pp. 938–947, April 2006.

[14] X. Gui and T. S. Ng, "A novel chip-interleaving DS SS system," *IEEE Transactions on Vehicular Technology*, vol. 49, pp. 21 –27, January 2000.

[15] M. L. Moher and P. Guinand, "An iterative algorithm for asynchronous coded multi-user detection," *IEEE Communications Letters*, vol. 2, pp. 229–231, August 1998.

[16] R. H. Mahadevappa and J. G. Proakis, "Mitigating multiple access interference and intersymbol interference in uncoded CDMA systems with chip-level interleaving," *IEEE Transactions on Wireless Communications*, vol. 1, pp. 781 – 792, October 2002.

[17] P. Wang, J. Xiao, and L. Ping, "Comparison of orthogonal and non-orthogonal approaches to future wireless cellular systems," *IEEE Vehicular Technology Magazine*, vol. 1, pp. 4–11, September 2006.

[18] L. Liu, J. Tong, and L. Ping, "Analysis and optimization of CDMA systems with chip-level interleavers," *IEEE Journal on Selected Areas in Communications*, vol. 24, pp. 141 – 150, January 2006.

[19] P. A. Hoeher and W. Xu, "Multi-Layer Interleave-Division Multiple Access for 3GPP Long Term Evolution," in *IEEE Conference on Communications*, (Glasgow, Scotland), pp. 5508–5513, August 2007.

[20] P. A. Hoeher, H. Schoeneich, and J. C. Fricke, "Multi-layer Interleave-Division Multiple access: theory and practice," *Eur. Trans. Telecomm.*, vol. 19, pp. 523–536, January 2008.

[21] A. J. Viterbi, "Very Low Rate Convolutional Codes for Maximum Theoretical Performance of Spread-Spectrum Multiple-Access Channels," *IEEE Journal on Selected Areas in Communications*, vol. 8, pp. 641–649, May 1990.

[22] S. Verdu and S. Shamai, "Spectral efficiency of CDMA with random spreading," *IEEE Transactions on Information Theory*, vol. 47, pp. 622–640, March 2001.

[23] J. Hui, "Throughput analysis for code division multiple accessing of the spread spectrum channel," *IEEE Transactions on Vehicular Technology*, vol. 33, pp. 98 – 102, August 1984.

[24] F. Brännström, T. Aulin, and L. Rasmussen, "Iterative detectors for trellis-code multiple-access," *IEEE Transactions on Communications*, vol. 50, pp. 1478 – 1485, September 2002.

[25] S. Bruck, U. Sorger, S. Gligorevic, and N. Stolte, "Interleaving for outer convolutional codes in DS-CDMA systems," *IEEE Transactions on Communications*, vol. 48, pp. 1100 –1107, July 2000.

[26] A. Tarable, G. Montorsi, and S. Benedetto, "Analysis and design of interleavers for CDMA systems," *IEEE Communications Letters*, vol. 5, pp. 420 –422, October 2001.

[27] L. Ping, L. Liu, K. Wu, and W. K. Leung, "A unified approach to multiuser detection and space-time coding with low complexity and nearly optimal performance," in *40th Allerton Conference*, (Allerton House, USA), pp. 170–179, October 2002.

[28] L. Liu, W. K. Leung, and L. Ping, "Simple iterative chip-by-chip multiuser detection for CDMA systems," in *The 57th IEEE Semiannual Vehicular Technology Conference*, vol. 3, (Jeju, Korea), pp. 2157 – 2161, April 2003.

[29] L. Ping, L. Liu, K. Wu, and W. Leung, "Approaching the capacity of multiple access channels using interleaved low-rate codes," *IEEE Communications Letters*, vol. 8, pp. 4 – 6, January 2004.

[30] G. Sage, "Serial Synchronization of Pseudonoise Systems," *IEEE Transactions on Communication Technology*, vol. 12, pp. 123 –127, December 1964.

[31] A. Polydoros and C. Weber, "A Unified Approach to Serial Search Spread-Spectrum Code Acquisition–Part I: General Theory," *IEEE Transactions on Communications*, vol. 32, pp. 542 – 549, May 1984.

[32] A. Polydoros and C. Weber, "A Unified Approach to Serial Search Spread-Spectrum Code Acquisition–Part II: A Matched-Filter Receiver," *IEEE Transactions on Communications*, vol. 32, pp. 550 – 560, May 1984.

[33] R. Ward, "Acquisition of Pseudonoise Signals by Sequential Estimation," *IEEE Transactions on Communication Technology*, vol. 13, pp. 475 –483, December 1965.

[34] R. Ward and K. Yiu, "Acquisition of Pseudonoise Signals by Recursion-Aided Sequential Estimation," *IEEE Transactions on Communications*, vol. 25, pp. 784 – 794, August 1977.

[35] T. K. Moon, R. T. Short, and C. K. Rushforth, "A RASE approach to acquisition in SSMA systems," in *IEEE Military Communications Conference*, vol. 3, (McLean, VA, USA), pp. 1037 –1041, November 1991.

[36] C. Gumacos, "Analysis of an optimum sync search procedure," *IEEE Transactions on Communications Systems*, vol. 11, pp. 89 –99, March 1963.

[37] E. Posner, "Optimal search procedures," *IEEE Transactions on Information Theory*, vol. 9, pp. 157 – 160, July 1963.

[38] S. M. Stigler, "Thomas Bayes's Bayesian Inference," *Journal of the Royal Statistical Society. Series A (General)*, vol. 145, no. 2, pp. pp. 250–258, 1982.

[39] J. Neyman and E. S. Pearson, "On the problem of the most efficient tests of statistical hypotheses," *Philosophical Transactions of the Royal Society of London Series A Containing Papers of a Mathematical or Physical Character*, vol. 231, no. 1933, pp. 289–337, 1933.

[40] G. Corazza and V. Degli-Espoti, "Acquisition based capacity estimates for CDMA with imperfect power control," in *IEEE International Symposium on Spread Spectrum Techniques and Applications*, (Oulu, Finland), pp. 325–329, July 1994.

[41] U. Madhow and M. B. Pursley, "Acquisition in direct sequence spread spectrum communication networks: An asymptotic analysis," *IEEE Trans. Inform. Theory*, vol. 39, pp. 903–912, May 1993.

[42] E. G. Strom, S. Parkvall, S. Miller, and B. E. Ottersten, "Propagation delay estimation in asynchronous direct-sequence code-division multiple access systems," *IEEE Transactions on Communications*, vol. 44, pp. 84 –93, January 1996.

[43] P. Cheung and P. Rapajic, "CMA-based code acquisition scheme for DS-CDMA systems," *IEEE Transactions on Communications*, vol. 48, pp. 852 –862, May 2000.

[44] R. R. Rick and L. B. Milstein, "Parallel acquisition in mobile DS-CDMA systems," in *IEEE Military Communications Conference*, vol. 3, (San Diego, USA), pp. 1165 –1169, November 1995.

[45] S. Glisic, T. Poutanen, W. Wu, G. Petrovic, and Z. Stefanovic, "New PN code acquisition scheme for CDMA networks with low signal-to-noise

ratios," *IEEE Transactions on Communications*, vol. 47, pp. 300 –310, February 1999.

[46] M. C. Reed and L. W. Hanlen, "Return Link Code Acquisition for DS-CDMA in a High Capacity Multi-user Systems," in *IEEE International Symposium on Spread Spectrum Techniques and Applications*, (Sydney, Australia), pp. 218–222, August 2004.

[47] M. C. Reed, L. W. Hanlen, and G. E. Corazza, "Return-Link Code Acquisition for 1-D and 2-D With DS-CDMA for High-Capacity Multiuser Systems," *IEEE Transactions on Vehicular Technology*, vol. 57, pp. 324 –334, January 2008.

[48] B. Senanayake, M. C. Reed, and Z. Shi, "Timing Acquisition for Multi-User IDMA," in *IEEE International Conference on Communications*, (Beijing, China), pp. 5077 – 5081, May 2008.

[49] Z. Wang, J. Hu, and X. Xiong, "Effect of sample-timing error on performance of Interleave-Division Multiple Access systems," in *7th International Conference on Information, Communications and Signal Processing*, (Macau, China), pp. 1 –6, December 2009.

[50] A. J. Viterbi, *CDMA: Principles of Spread Spectrum Communication*. Addison-Wesley, 1995.

[51] U. Mengali and A. N. D'Andrea, *Synchronization techniques for digital receiver*. Springer, 1997.

[52] J. G. Proakis, *Communication Systems Engineering*. Prentice Hall, 2002.

[53] E. Ozturk, "Performance analysis of asynchronous direct sequence code division multiple access for general chip waveforms over multi-path Rayleigh fading channels," *IET Communications*, vol. 1, pp. 570–576, August 2007.

[54] "Technical specification 25.104: Radio transmission and reception, v3.2.0 (20002003)."

[55] H. Meyr, M. Moeneclaey, and S. A. Fechtel, *Digital Communication Receivers: Synchronization, Channel Estimation, and Signal Processing*. John Wiley & Sons, Inc., 1998.

[56] J. J. Spilker and D. T. Magill, "The Delay-Lock Discriminator-An Optimum Tracking Device," *Proceedings of the IRE*, vol. 49, pp. 1403 –1416, September 1961.

[57] M. R. O'Sullivan, "Tracking Systems Employing the Delay-Lock Discriminator," *IRE Transactions on Space Electronics and Telemetry*, vol. SET-8, pp. 1 –7, March 1962.

[58] J. J. Spilker, "Delay-Lock Tracking of Binary Signals," *IEEE Transactions on Space Electronics and Telemetry*, vol. 9, pp. 1 –8, March 1963.

[59] F. M. Gardner, "Demodulator reference recovery techniques suited for digital implementation," Final Report ESTEC Contract No. 6847/86/NL/DG, European Space Agency, August 1988.

[60] K. Mueller and M. Muller, "Timing Recovery in Digital Synchronous Data Receivers," *IEEE Transactions on Communications*, vol. 24, pp. 516 – 531, May 1976.

[61] W.-H. Sheen and C.-H. Tai, "A Noncoherent Tracking Loop with Diversity and Multipath Interference Cancellation for Direct-Sequence Spread-Spectrum Systems," *IEEE Transactions on Communications*, vol. 46, pp. 1516–1524, November 1998.

[62] N. Noels, H. Steendam, and M. Moeneclaey, "Carrier phase tracking from turbo and LDPC coded signals affected by a frequency offset," *IEEE Communications Letters*, vol. 9, pp. 915 – 917, October 2005.

[63] N. Noels, V. Lottici, and A. Dejonghe, "A Theoretical Framework for Soft-Information-Based Synchronization in Iterative (Turbo) Receivers," *EURASIP Journal on Wireless Communications and Networking*, vol. 2005, pp. 117–129, September 2005.

[64] A. G. Burr and L. Zhang, "Iterative joint synchronisation and turbo-decoding," in *IEEE International Symposium on Information Theory*, (Laussane, Switzerland), p. 414, June-July 2002.

[65] R. Nuriyev and A. Anastasopoulos, "Analysis of joint iterative decoding and phase estimation for the noncoherent AWGN channel, using density evolution," in *IEEE International Symposium on Information Theory*, (Laussane, Switzerland), p. 168, June-July 2002.

[66] A. Nayak, J. Barry, and S. McLaughlin, "Joint timing recovery and turbo equalization for coded partial response channels," *IEEE Transactions on Magnetics*, vol. 38, pp. 2295 – 2297, September 2002.

[67] V. Lottici and M. Luise, "Carrier phase recovery for turbo-coded linear modulations," in *IEEE International Conference on Communications*, vol. 3, (New York city, USA), pp. 1541 – 1545, April-May 2002.

[68] X. Jin and A. Kavcic, "Cycle-slip-detector-aided iterative timing recovery," *IEEE Transactions on Magnetics*, vol. 38, pp. 2292 – 2294, September 2002.

[69] J. Barry, A. Kavcic, S. LcLaughlin, A. Nayak, and W. Z., "Iterative timing recovery," *IEEE Signal Processing Magazine*, vol. 21, pp. 89 – 102, January 2004.

[70] N. Noels, H. Steendam, M. Moeneclaey, and H. Bruneel, "A maximum-likelihood based feedback carrier synchronizer for turbo-coded systems," in *IEEE 61st Vehicular Technology Conference*, vol. 5, (Stockholm, Sweden), pp. 3014 – 3018, May-June 2005.

[71] N. Noels and M. Moeneclaey, "Iterative Carrier Synchronization Techniques in Transmission Systems Protected by a Powerful Error-Correcting Code," in *The Forty-First Asilomar Conference on Signals, Systems and Computers*, (Pacific Grove, CA, USA), pp. 1913 –1917, November 2007.

[72] N. Noels, H. Steendam, and M. Moeneclaey, "Performance Analysis of ML-Based Feedback Carrier Phase Synchronizers for Coded Signals," *IEEE Transactions on Signal Processing*, vol. 55, pp. 1129 –1136, March 2007.

[73] B. Senanayake, M. C. Reed, and Z. Shi, "Iterative timing recovery for IDMA receivers operating under severe timing drift," in *Australian Communications Theory Workshop*, (Canberra, Australia), pp. 71 –76, February 2010.

[74] J. Hagenauer and P. A. Hoeher, "Concatenated Viterbi-Decoding," in *The Fourth Joint Swedish-Soviet International Workshop on Information Theory*, (Gotland, Sweden), pp. 29–33, August 1989.

[75] Z. Shi and C. B. Schlegel, "Joint iterative decoding of serially concatenated cancellation and decoding for coded CDMA," *IEEE Journal on Selected Areas in Communications*, vol. 19, pp. 1646–1653, August 2001.

[76] Z. Shi and C. B. Schlegel, "Performance Analysis of Iterative Detection for Unequal Power Coded CDMA Systems," in *IEEE Global Telecommunications Conference*, vol. 3, (San Francisco, USA), pp. 1537–1542, December 2003.

[77] H. El Gamal and J. Hammons, A.R., "Analyzing the turbo decoder using the Gaussian approximation," *IEEE Transactions on Information Theory*, vol. 47, pp. 671 –686, February 2001.

[78] H. El Gamal and J. Hammons, A.R., "Analyzing the turbo decoder using the Gaussian approximation," in *IEEE International Symposium on Information Theory*, (Sorrento , Italy), p. 319, June 2000.

[79] D. Divsalar, S. Dolinar, and F. Pollara, "Iterative turbo decoder analysis based on density evolution," *IEEE Journal on Selected Areas in Communications*, vol. 19, pp. 891 –907, May 2001.

[80] T. J. Richardson and R. L. Urbanke, "The capacity of low-density parity-check codes under message-passing decoding," *IEEE Transactions on Information Theory*, vol. 47, pp. 599 –618, February 2001.

[81] T. J. Richardson, M. A. Shokrollahi, and R. L. Urbanke, "Design of capacity-approaching irregular low-density parity-check codes," *IEEE Transactions on Information Theory*, vol. 47, pp. 619 –637, February 2001.

[82] S. ten Brink, "Convergence of iterative decoding," *Electron. Lett.*, vol. 35, pp. 806–808, May 1999.

[83] S. ten Brink, "Convergance behaviour of iteratively decoded parallel concatenated codes," *IEEE Transactions on Communications*, vol. 49, pp. 1727–1737, October 2001.

[84] M. Tüchler, S. T. Brink, and J. Hagenauer, "Measures for Tracing Convergence of Iterative Decoding Algorithms," in *in Proc. 4th IEEE/ITG Conference on Source and Channel Coding*, (Berlin, Germany), pp. 53–60, January 2002.

[85] A. Ashikhmin, G. Kramer, and S. ten Brink, "Code rate and the area under extrinsic information transfer curves," in *IEEE International Symposium on Information Theory*, (Laussane, Switzerland), p. 115, June-July 2002.

[86] A. Ashikhmin, G. Kramer, and S. ten Brink, "Extrinsic Information Transfer Functions: Model and Erasure Channel Properties," *IEEE Transactions on Information Theory*, vol. 50, pp. 2657–2673, November 2004.

[87] S. ten Brink, G. Kramer, and A. Ashikhmin, "Design of Low-Density Parity-Check Codes for Modulation and Detection," *IEEE Transcations on Communications*, vol. 52, pp. 670–678, April 2004.

[88] C. Measson and R. Urbanke, "Further analytic properties of EXIT-like curves and applications," in *IEEE International Symposium on Information Theory*, (Yokohama, Japan), p. 266, June-July 2003.

[89] C. Masson, R. Urbanke, and et al., "Life above threshold: From list decoding to area theorem and MSE," in *IEEE Information Theory Workshop*, (San Antonio, TX, USA), October 2004.

[90] S. ten Brink, "Convergence of multidimensional iterative decoding schemes," in *The Thirty-Fifth Asilomar Conference on Signals, Systems and Computers*, vol. 1, (Pacific Grove, CA, USA), pp. 270 –274 vol.1, November 2001.

[91] F. Brännström, L. K. Rassmussen, and A. J. Grant, "Convergence analysis and optimal scheduling for multiple concatenated codes," *IEEE Transactions on Information Theory*, vol. 51, pp. 3354–3364, September 2005.

[92] J. Boutros and G. Caire, "Iterative multiuser joint decoding: Unified framework and asymptotic analysis," *IEEE Transactions on Information Theory*, vol. 48, pp. 1772–1793, July 2002.

[93] J. Boutros and G. Caire, "Iterative multiuser joint decoding: unified framework and asymptotic analysis," in *IEEE International Symposium on Information Theory*, (Washington, DC , USA), p. 317, June 2001.

[94] J. W. Lee and R. E. Blahut, "Bit error rate estimate of finite length codes," in *IEEE International Conference on Communications*, vol. 4, (Alaska, USA), pp. 2728 – 2732, May 2003.

[95] J. W. Lee and R. E. Blahut, "A note on the analysis of finite length turbo decoding," in *IEEE International Symposium on Information Theory*, (Lausanne, Switzerland), p. 83, June-July 2002.

[96] J. W. Lee and R. E. Blahut, "Convergence Analysis and BER Performance of Finite-Length Turbo Codes," *IEEE Transactions on Communications*, vol. 55, pp. 1033 –1043, May 2007.

[97] J. W. Lee and R. E. Blahut, "Generalized EXIT chart and BER analysis of finite-length turbo codes," in *IEEE Global Telecommunications Conference*, vol. 4, (San Francisco, USA), pp. 2067 – 2072, December 2003.

[98] D. Tse and P. Viswanath, *Fundamentals of Wireless Communication*. Cambridge Unversity Press, 2005.

[99] T. M. Cover, *Elements of Information Theory*. Wiley-Interscience, 1991.

[100] G. Caire, S. Guemghar, A. Roumy, and S. Verdu, "Maximizing the spectral efficiency of coded CDMA under successive decoding," *IEEE Transactions on Information Theory*, vol. 50, pp. 152–164, January 2004.

[101] T. Yang, J. Yuan, and Z. Shi, "Rate Optimization for IDMA Systems with Iterative Joint Multi-User Decoding," *IEEE Transactions on Wireless Communications*, vol. 8, pp. 1148 – 1153, March 2009.

[102] K. Li, X. Wang, and L. Ping, "Analysis and Optimization of Interleave-Division Multiple-Access Communication Systems," *IEEE Transactions on Wireless Communications*, vol. 6, pp. 1973 –1983, May 2007.

[103] C. B. Schlegel and Z. Shi, "Optimal Power/Rate Allocation and Code Selection for Iterative Joint Detection of Coded Random CDMA," *IEEE Transactions on Information Theory*, vol. 52, pp. 4286–4294, September 2006.

[104] D. P. Shepherd, Z. Shi, M. C. Reed, and F. Schreckenbach, "Optimization of Unequal Power Coded Multiuser DS-CDMA using Extrinsic Information Transfer Charts," in *Conference on Information Sciences and Systems*, (Princeton, New Jersey, USA), pp. 1435–1439, April 2006.

[105] D. P. Shepherd, F. Brännström, Z. Shi, F. Schreckenbach, and M. C. Reed, "Adaptive Optimization of an Iterative Multi-User Detector for Turbo-coded CDMA," *IEEE Transactions on Wireless Communications*, vol. 7, pp. 4284 – 4293, November 2008.

[106] P. Newson and M. R. Heath, "The Capacity of a Spread Spectrum CDMA System for Cellular Mobile Radio with Consideration of System Imperfections," *IEEE Journal on Selected Areas in Communications*, vol. 12, pp. 673–684, May 1994.

[107] P. D. Alexander, "Multiuser receivers in cellular CDMA," in *5th International Symposium on Spread Spectrum Techniques and Aplications*, vol. 2, (Sun city, South Africa), pp. 668–670, September 1998.

[108] A. J. Viterbi, A. M. Viterbi, K. S. Gilhousen, and E. Zehavi, "Soft Handoff Extends CDMA Cell Coverage and Increases Reverse Link Capacity," *IEEE Journal on Selected Areas in Communications*, vol. 12, pp. 1281–1288, October 1994.

[109] Z. Dawy, S. Davidovic, and I. Oikonomidis, "Coverage and Capacity Enhancement of CDMA Cellular Systems via Multihop Transmission," in *IEEE Global Telecommunications Conference*, vol. 2, (San Fransisco), pp. 1147 – 1151, December 2003.

[110] Z. Dawy and A. Seeger, "Coverage and Capacity Enhancement of Multiservice WCDMA Cellular Systems via Serial Interference Cancellation," in *IEEE International Conference on Communicaitons*, vol. 6, (Paris, France), pp. 3121 – 3127, June 2004.

[111] K. Kusume and G. Bauch, "CDMA and IDMA: Iterative Multiuser Detections for Near-Far Asynchronous Communications," in *IEEE 16th International Symposium on Personal, Indoor and Mobile Radio Communications*, (Berlin, Germany), pp. 426 – 431, September 2005.

[112] K. Kusume and G. Bauch, "Some aspects of Interleave Division Multiple Access in Ad Hoc networks," in *4th International Symposium on Turbo Codes & Related Topics in Connection with International ITG Conference on Source and Channel Coding*, (Munich, Germany), April 2006.

[113] W. K. Leung, L. Liu, and L. Ping, "A Simple Approach to Near-Optimal Multiuser Detection: Interleave-Division Multiple-Access," in *IEEE Wireless Communications and Networking Conference*, vol. 1, (New Orleans, USA), pp. S391–S396, March 2003.

[114] H. Schoeneich and P. A. Hoeher, "Adaptive interleave-division multiple access–a potential air interface for 4G bearer services and wireless LANs," in *First IFIP International Conference on Wireless and Optical Communications and Networks*, (Muscat, Oman), pp. 179–182, June 2004.

[115] I. Mahafeno, C. Langlais, and C. Jego, "OFDM-IDMA versus IDMA with ISI cancellation for quasi-static Rayleigh fading multipath channels," in *4th International Symposium on Turbo Codes & Related Topics in Connection with International ITG Conference on Source and Channel Coding*, (Munich, Germany), April 2006.

[116] S. Zhou, Y. Li, M. Zhao, X. Xu, J. Wang, and Y. Yao, "Novel techniques to improve downlink multiple access capacity for Beyond 3G," *IEEE Communications Magazine*, vol. 43, pp. 61 –69, January 2005.

[117] Q. Bui, S. Houcke, and M. Debbah, "A Suitable Multiple Access Scheme for Self-Organizing Networks: Unique Interleaver IDMA," *under revision, IEEE Transactions on Communications*, 2011.

[118] S. M. Perlaza, L. Cottatellucci, and M. Debbah, "A game theoretic framework for decentralized power allocation in IDMA systems," in *IEEE 19th International Symposium on Personal, Indoor and Mobile Radio Communications*, (Cannes, France), pp. 1 –5, September 2008.

[119] V. Chandrasekhar, J. Andrews, and A. Gatherer, "Femtocell networks: a survey," *IEEE Communications Magazine*, vol. 46, pp. 59 –67, September 2008.

[120] B. Senanayake, M. C. Reed, and Z. Shi, "An Optimal Asynchronous IDMA Receiver," in *Australian Communications Theory Workshop*, (Sydney, Australia), pp. 28 –32, February 2009.

[121] B. Senanayake and M. C. Reed, "Multi-dimensional EXIT analysis for iterative multi-user detection with unequal power allocation," in *6th International Symposium on Turbo Codes and Iterative Information Processing*, (Brest, France), pp. 409 –413, September 2010.

[122] B. Senanayake and M. C. Reed, "Multi-Dimensional EXIT Analysis and Optimization for Multi-User Receivers," *conditionally accepted by IEEE Transactions on Wireless Communications*, December 2011.

[123] B. Senanayake and M. C. Reed, "Analysis of the Capacity Enhancement of Cellular Systems using Multiuser Receivers and Multiple Power Zones," in *the 7th IEEE Workshop on Broadband Wireless Access*, (Houston, United States of America), pp. 1490–1494, December 2011.

[124] C. Berrou, A. Glavieux, and P. Thitimajshima, "Near Shannon limit error-correcting coding and decoding: turbo-codes," in *IEEE International Conference on Communications*, (Geneva, Switzerland), May 1993.

[125] C. Berrou and A. Glavieux, "Near Optimum Error Correcting Coding and Decoding: Turbo-Codes," *IEEE Transactions on Communications*, vol. 44, pp. 1261–1271, October 1996.

[126] J. Hagenauer, "The turbo principle: Tutorial introduction and state of the art," in *International Symposium on Turbo Codes and Related Topics*, (Brest, France), pp. 1–11, September 1997.

[127] C. Douillard, M. Jzquel, and C. Berrou, "Iterative Correction of Intersymbol Interference: Turbo Equalization," *European Transactions on Telecommunications*, vol. 6, pp. 507–511, September-October 1995.

[128] M. C. Reed, *Iterative Receiver Techniques for Coded Multiple Access Communication Systems*. PhD thesis, The University of South Australia, 1999.

[129] P. Alexander, M. Reed, J. Asenstorfer, and C. Schlegel, "Iterative Multiuser Interference Reduction: Turbo CDMA," *IEEE Transactions on Communications*, vol. 47, pp. 1008–1014, July 1999.

[130] M. C. Reed and P. D. Alexander, "Iterative multi-user detection using antenna arrays and FEC on multipath channels," *IEEE Journal on Selected Areas in Communications*, vol. 17, pp. 2082–2089, December 1999.

[131] M. Honig and R. Ratasuk, "Large-system performance of iterative multiuser decision-feedback detection," *IEEE Transactions on Communications*, vol. 51, pp. 1368 – 1377, August 2003.

[132] A. Al Rustamani, A. Damnjanovic, and B. Vojcic, "Turbo greedy multiuser detection," *IEEE Journal on Selected Areas in Communications*, vol. 19, pp. 1638 –1645, August 2001.

[133] A. Al Rustamani and B. Vojcic, "A new approach to greedy multiuser detection," *IEEE Transactions on Communications*, vol. 50, pp. 1326 – 1336, August 2002.

[134] T. Giallorenzi and S. Wilson, "Multiuser ML sequence estimator for convolutionally coded asynchronous DS-CDMA systems," *IEEE Transactions on Communications*, vol. 44, pp. 997 –1008, August 1996.

[135] A. Damnjanovic and B. Vojcic, "Iterative multiuser detection/decoding for turbo coded CDMA systems," *IEEE Communications Letters*, vol. 5, pp. 104 –106, March 2001.

[136] H. Holma and A. Toskala, *WCDMA for UMTS*. West Sussex, England:Wiley, 2002.

[137] L. Ping, W. Peng, and W. Xiaodong, "Recent Progress in Interleave-Division Multiple-Access (IDMA)," in *IEEE Military Communications Conference*, (Orlando, USA), pp. 1 –7, October 2007.

[138] X. Ma and L. Ping, "Coded modulation using superimposed binary codes," *IEEE Transactions on Information Theory*, vol. 50, pp. 3331 – 3343, December 2004.

[139] L. Duan, B. Rimoldi, and R. Urbanke, "Approaching the AWGN channel capacity without active shaping," in *IEEE International Symposium on Information Theory*, (Ulm, Germany), p. 374, June/July 1997.

[140] J. Tong, *Superposition coded modulation.* PhD thesis, City University of Hong Kong, May 2009.

[141] J. C. Fricke, H. Schoeneich, and P. A. Hoeher, "An Interleave-division multiple access based system proposal for the 4G uplink," in *IST Mobile & Wireless Communications Summit 2005*, (Dresden, Germany), 2005.

[142] J. C. Fricke, P. A. Hoeher, and H. Schoeneich, "An uplink proposal based on adaptive interleave-division multiple access," in *14th Wireless World Research Forum Meeting (WWRF14)*, (San Diego, California), pp. 1–7, July 2005.

[143] H. Schoeneich and P. A. Hoeher, "Iterative pilot-layer aided channel estimation with emphasis on interleave-division multiple access systems," *EURASIP J. Appl. Signal Process.*, vol. 2006, pp. 250–250, January 2006.

[144] X. Zhou, Z. Shi, and M. C. Reed, "Iterative Channel Estimation for IDMA Systems in Time-Varying Channels," in *IEEE Global Telecommunications Conference*, (Washington DC, USA), pp. 4020 – 4024, November 2007.

[145] L. Ping, W. K. Leung, and K. Y. Wu, "Low-Rate Turbo-Hadamard Codes," *IEEE Transactions on Information Theory*, vol. 49, pp. 3213–3224, December 2003.

[146] M. Eroz and L.-N. Lee, "Low Rate Coded Interleave Division Multiple Access on Rician Fading Channels," in *IEEE Global Telecommunications Conference*, (Washington DC, USA), pp. 1488 – 1491, November 2007.

[147] C. B. Schlegel and M. Burnashev, "Optimal error control coding for iterative cancellation systems," in *IEEE International Symposium on Information Theory*, (Austin, Texas, USA), pp. 1993 –1997, June 2010.

[148] C. B. Schlegel and M. Burnashev, "Optimal Error Control Coding for Iterative Cancellation Systems," in *Proceedings of the 6th International Symposium on Turbo Codes & Iterative Information Processing*, (Brest, France), pp. 434–438, September 2010.

[149] M. Eroz and L.-N. Lee, "On FEC Design for Interleave Division Multiple Access," in *71st Vehicular Technology Conference*, (Taipei, Taiwan), pp. 1 –4, May 2010.

[150] L. Linton, P. Conder, and M. Faulkner, "Improved Interleave-Division Multiple Access (IDMA) Performance Using Dynamic FEC Code

Allocation," in *IEEE Wireless Communications and Networking Conference*, (Sydney, Australia), pp. 1 –6, April 2010.

[151] L. Ping and L. Liu, "Analysis and Design of IDMA Systems Based on SNR Evolution and Power Allocation," in *IEEE 60th Vehicular Technology Conference*, vol. 2, (Los Angeles, California, USA), pp. 1068 – 1072, September 2004.

[152] D. P. Shepherd, *Optimisation of Iterative Multi-User Receivers using Analytical Tools*. PhD thesis, Research School of Information Sciences and Engineering, The Australian National University, September 2008.

[153] C. E. Shannon, "A mathematical theory of communications," *Bell Systems Technical Journal*, vol. 27, pp. 379–423,623–656, 1948.

[154] S. Benedetto and G. Montorsi, "Unveiling Turbo Codes: Some Results on Parallel Concatenated Coding Schemes," *IEEE Transactions on Information Theory*, vol. 42, pp. 409–428, March 1996.

[155] S. Benedetto and G. Montorsi, "Serial Concatenation of Interleaved Codes: Performance Analysis, Design, and Iterative Decoding," *IEEE Transactions on Information Theory*, vol. 44, pp. 909–926, May 1998.

[156] S. Benedetto and G. Montorsi, "Iterative decoding of serially concatenated convolutional codes," *Electronics Letters*, vol. 32, pp. 1186 –1188, June 1996.

[157] L. R. Bahl, J. Cocke, F. Jelinek, and J. Raviv, "Optimal decoding of linear codes for minimising symbol error rate," *IEEE Transactions on Information Theory*, vol. 20, pp. 284–287, March 1974.

[158] A. Viterbi, "Error bounds for convolutional codes and an asymptotically optimum decoding algorithm," *IEEE Transactions on Information Theory*, vol. 13, pp. 260 – 269, April 1967.

[159] Z. Rosberg, "Optimal transmitter power control in interleave division multiple access (IDMA) spread spectrum uplink channels," *IEEE Transactions on Wireless Communications*, vol. 6, pp. 192 –201, January 2007.

[160] R. L. Pickholtz, D. L. Schilling, and L. Milstein, "Theory of spread spectrum communications-a tutorial," *IEEE Transactions on Communications*, vol. 30, pp. 855–884, May 1982.

[161] J. G. Proakis, *Digital Communications*. McGraw-Hill, 3 ed., 1995.

[162] H. Meyr, M. Moeneclaey, and S. A. Fechtel, *Digital Communication Receivers: Synchronization, Channel Estimation and Signal Processing*. Wiley, 1998.

[163] E. I. Jury, *Theory and Application of the z-transform method.* John Wiley & Sons, Inc., 1964.

[164] O. Nagy, M. C. Reed, and Z. Shi, "Optimal Detection of IDMA Signals," in *IEEE Wireless Communications and Networking Conference*, (Hong Kong), pp. 1236 – 1240, March 2007.

[165] O. Nagy, "Performance analysis of a generic system model for uncoded IDMA using serial and parallel interference cancellation," *European Transactions on Telecommunications*, vol. 19, pp. 511–522, August 2008.

[166] S. Verdu, *Multiuser Detection.* Cambridge University Press, 1998.

[167] J. A. Nelder and R. Mead, "A simplex method for function minimization," *The Computer Journal*, vol. 7, pp. 308–313, 1965.

[168] K. Narayanan, "Effect of precoding on the convergence of turbo equalization for partial response channels," *IEEE Journal on Selected Areas in Communications*, vol. 19, pp. 686–698, April 2001.

[169] J. Hagenauer, "The EXIT Chart - introduction to extrinsic information transfer in iterative process," in *12th European Signal Processing Conference*, (Vienna, Austria), pp. 1541–1548, September 2004.

[170] D. P. Shepherd, F. Brännström, and M. C. Reed, "Fidelity charts and stopping/termination criteria for iterative multiuser detection," in *4th International Symposium on Turbo Codes & Related Topics in Connection with International ITG Conference on Source and Channel Coding*, (Munich, Germany), pp. 3–7, April 2006.

[171] C. E. Shannon, "The zero error capacity of a noisy channel," *IRE Transactions on Information Theory*, vol. IT-2, pp. 8–19, September 1956.

[172] R. Storn and K. Price, "Differential Evolution A Simple and Efficient Heuristic for Global Optimization over Continuous Spaces," *J. of Global Optimization*, vol. 11, pp. 341–359, December 1997.